Hydrographic Conditions of a Continental Shelf Region in the Northwest African Upwelling System from In-situ Data

Paul Juby

Supervised By

Dr France Floc'h (Laboratoire Domaines océaniques, France)

Dr Thomas Meunier (Laboratoire de Physique des océans, France)

Dr Anne Deschamps (Laboratoire Domaines océaniques, France)

Professor Marcello Vichi (University of Cape Town, South Africa)

Minor dissertation submitted in partial fulfillment of the requirement for the degree of Master of Science in Applied Marine Science

Department of Biological Sciences

University of Cape Town

March 2015

Plagiarism Declaration

I know the meaning of Plagiarism and declare that all of the work in the document, save for that which is properly acknowledged, is my own.

Table of Contents

Abstract

This study investigates the hydrographic and dynamic properties of the continental shelf region between Cape Juby (28.5 °N) and Agadir (30.4 °N) within the Moroccan Sub-region of the North West African Upwelling System. Data came from two cruises conducted in June (beginning of summer) and November (end of autumn) 2013. Coastal upwelling was obvious in both cruises in the in-situ temperature and salinity data as well as in remotely sensed sea surface temperature maps. ADCP data showed the presence of a strong jet like current associated with enhanced upwelling off Cape Juby. This strong quasi-permanent upwelling center was observed during both cruises. It results from the orientation of this portion of coast which is aligned with the dominant wind direction, as well as a wind intensification near the cape. The presence of a secondary upwelling front was also observed near the shelf break. It was accompanied by an intense baroclinic jet. The EK60 data showed evidence of internal waves as well as small and mesoscale turbulence that were probably strongly interacting with the mean upwelling circulation and made a straightforward interpretation of the data quite challenging. However, this study revealed the main physical processes of this poorly studied region, as well as their seasonal variability.

Acknowledgements

I would like to thank my supervisors for their continued support and assistance throughout this project. Without their technical skills, connections and patience I would have never been able to complete this on my own. Thanks to France Floc'h and Thomas Meunier for making me feel welcome to the IUEM and continued guidance on the project through difficult times. Thanks to Guillaume Fromant for his time and technical assistance. I would also like to thank Anne and Julien Vignier for introducing me to French culture and making me feel at home in a foreign country.

Thank you to the Black family who gave me a place to stay in Cape Town for six months, without them I would not have been able to take this opportunity. In addition I also thank the Cavanagh family for their good food and letting me live with them in the south of France.

The presence AMS class of 2014 has been hugely beneficial towards my studies through their support and openness when it comes to facing new challenges. Special mention to Christopher Waspe and Ben Brooker for their flaming style and influence. I would like to thank my parents who have provided me with continued support and given me so many opportunities throughout my life.

Thanks to the sponsors ICEMASA, Campus France and Ma-Re who worked swiftly and diligently throughout my trip and allowed me a fantastic time in Brest. I would also like to thank Marcello Vichi who provided assistance when I really needed it.

We also acknowledge Anne Deschamps who tragically passed away in late 2014. Her presence will be sorely missed by many in the IUEM. Her dedication to the Epure Project laid the foundation my own work as well as the work of numerous other scientists and students. We are incredibly grateful for her contribution to our work and our lives.

Chapter One: Literature Review

1.1. Eastern Boundary Upwelling Systems

Throughout the world's oceans there are four regions considered to be eastern boundary upwelling systems (EBUS). These EBUS (Figure 1) are the Peru-Chilean (0 – 20 °S), Californian (45 – 30 °N), Northwest African (30 – 10 °N) and Benguela (15 – 35 °S) (Reid and Schwartloze, 1962; Mittelstaedt *et al.,* 1975; Siesser, 1980; Alheit and Bernal, 1993; Chavez and Messié, 2009). Figure 1 shows the location of the four EBUS, dominant wind direction and mean sea surface temperature. EBUS were often associated with the easternmost, near-coastal extent of the Pacific and Atlantic subtropical gyres (Chavez and Messié, 2009).

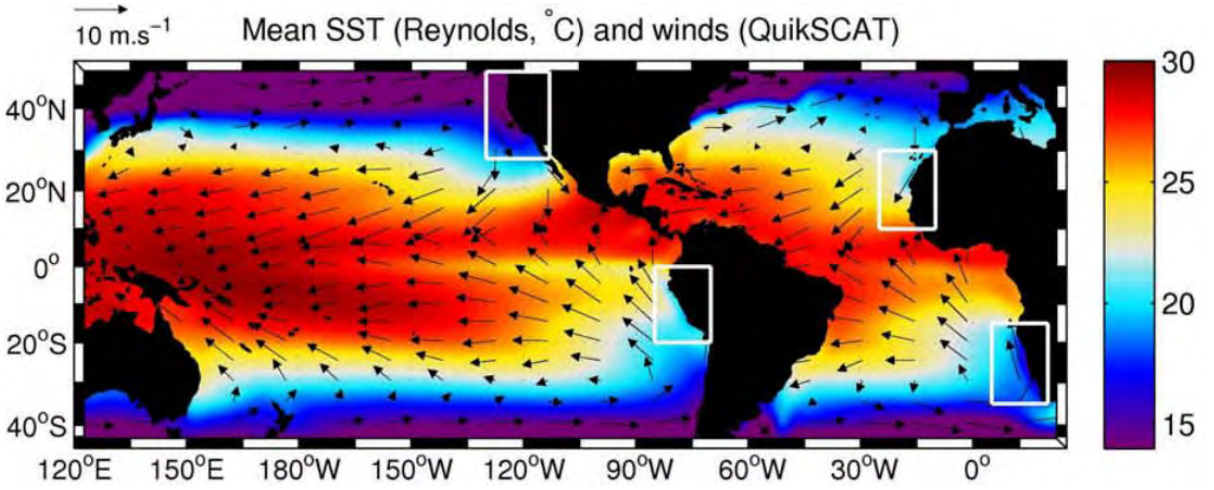

Figure 1: Basin-scale map of SST (°C) and winds from QuickSCAT (Chavez and Messié, 2009).

Coastal upwelling occurs in response to the divergence of the horizontal transport near the coast, when the wind has a sufficient alongshore component: In the ocean, the wind stress effect is confined to a thin surface layer (0 to 15 m), called the Ekman layer. Within this Ekman layer, the horizontal momentum is dominated by a balance between the wind stress and the Coriolis force. It results in a horizontal velocity field with a spiral-like vertical distribution, known as

the Ekman spiral. The transport integrated over the Ekman layer thickness is shifted 90° to the right (left) in the northern (southern) hemisphere (Ekman, 1905).

Along most subtropical eastern boundaries, the coastline is mostly parallel to the dominant winds, resulting in an offshore Ekman transport. This causes a divergence of the Ekman transport between the coast, where the cross-shore transport must vanish and offshore, where it can be fully developed. According to the continuity equation, an upward vertical velocity must then appear to balance this horizontal divergence and is called coastal upwelling (McEwen, 1912; Sverdrup 1938).

Coastal water is replaced by cold nutrient rich water that is advected into the euphotic zone. If the wind is sufficiently strong and blows for a sufficient period of time the thermocline will eventually break the surface. This cold water along the coast is separated by a sharp front from the warmer water offshore. This is often corroborated by images of Sea Surface Temperature (SST) where such a front is apparent (Figure 1). The cold water is nutrient rich and associated with phytoplankton blooms. Therefore Maps of Sea Surface Colour (SSC) that show chlorophyll-a concentration have similar frontal patterns to that of SST maps (Gordon and Clark, 1981; Abbott and Zion, 1985).

The advection of cooler denser water near the coast results in a cross-shore horizontal free-surface gradient as the sea surface height is lowered. As a result of this surface pressure gradient and the Coriolis force, an equatorward along shore coastal current appears near the upwelling front. The sub-surface horizontal density gradient results in a strong baroclinic vertical shear of the surface jet (Charney, 1947; Eady, 1949, James, 1987).

Early satellite images showed the existence of intense mesoscale to sub-mesoscale activity along the upwelling front (Traganza *et al.,* 1980). These structures are obvious as tongues of cold water, sometimes extending hundreds of kilometers offshore and are known as upwelling

filaments (Brink, 1983; Flament *et al.,* 1985). Their dynamics were often associated with the interaction of the upwelling current and major topographic features such as capes or promontories (Batteen, 1997; Meunier *et al.,* 2010) but can also result from the destabilization of the current (Ikeda *et al.*, 1989; Haidvogel *et al.*, 1991). In general, the interaction of any eddy with an upwelling front is able to generate those sub-mesoscale features. (Meunier *et al.*, 2012). Upwelling regions can therefore become areas of complex dynamics with the interaction of many structures of different scales.

Associated with each EBUS is a poleward undercurrent that flows along the continental slope. The characteristics and dynamics of the poleward undercurrent vary between different EBUS. However in each EBUS the poleward undercurrent has an along shore orientation that is opposite to the flow of the surface currents. Typical velocity ranges from 0.1 to 0.3 $m.s^{-1}$ in a flow between 100 to 300 m deep along the continental slope (Neshyba *et al*., 1989; Warren, 1990).

EBUS are among the richest eco-systems in the ocean because of the amount of productivity they sustain. EBUS "support a rate of fish harvest nearly 100 times the global mean and account for >20% of the world's marine fish catch" (Rykaczewski and Checkley, 2008). The fisheries that EBUS support therefore have a major social and economic importance to adjacent nations.

1.2. The Northwest African Upwelling System

1.2.1. Main Characteristics

The Northwest African Upwelling System (NWAUS) stretches from 12 – 43 °N it its broadest sense but is subject to seasonal shifts on both the northern and southern limits (Arístegui *et al*., 2009). It is characterized by strong geographic diversity, unique upwelling responses and high seasonal variability (Arístegui *et al*., 2009).

The NWAUS is considered to be the coastal extent of the Canary current system (CanC). The CanC flows southward down the African coast with a poleward under-current and marks the eastern boundary of the North Atlantic Subtropical Gyre (Knoll *et al*., 2002; Batteen *et al*., 2007). Mason *et al.* (2011) have noted the presence of a broad seasonal cycle but the path and variability of the CanC and interactions with the upwelling region remaining uncertain. Seasonal variability is strong; in winter the CanC moves offshore near Madeira where it

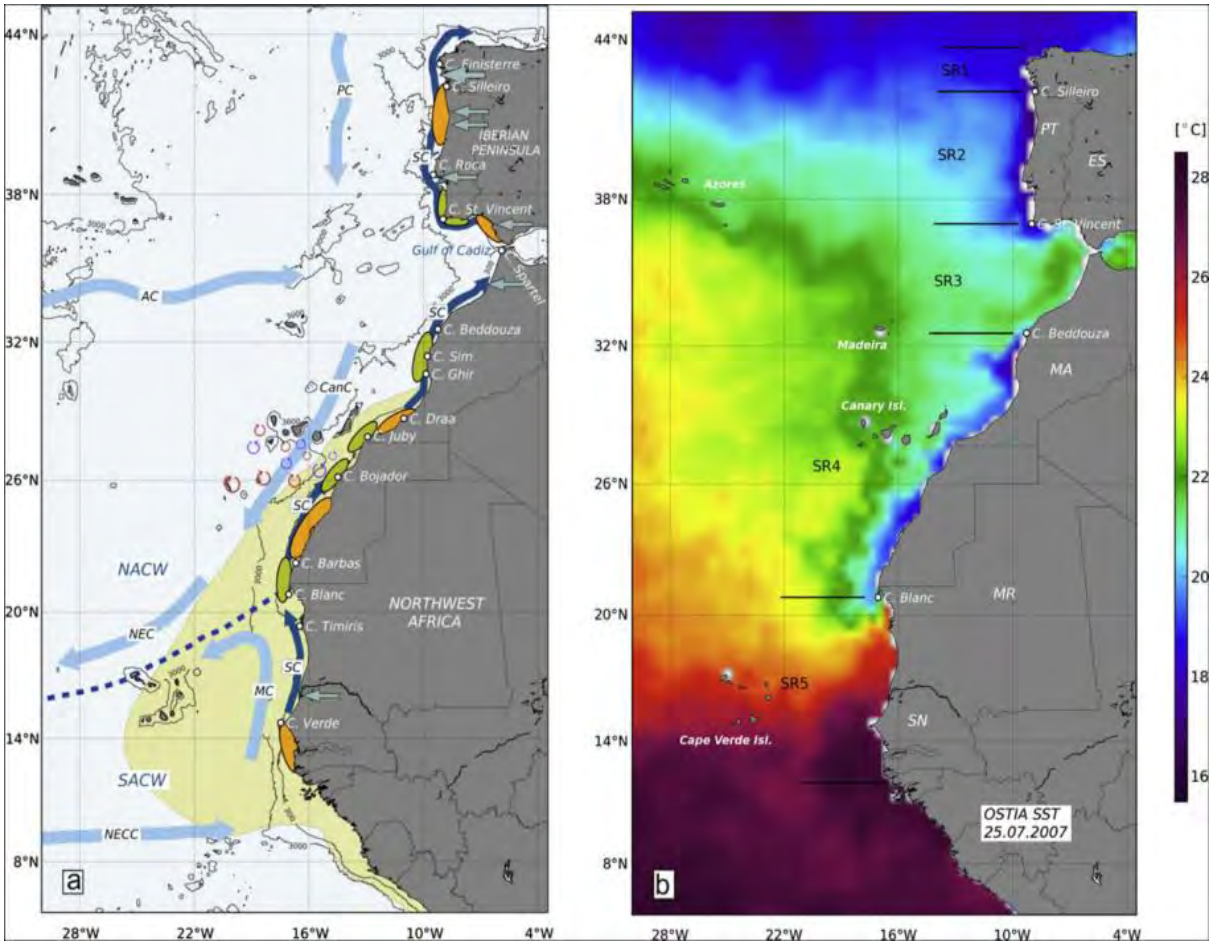

Figure 2: The Northwest African Upwelling Ecosystem. (a) Schematic map showing capes and fresh water inputs (horizontal light blue arrows), major surface currents (light blue), slope currents (dark blue), dust inputs (shaded yellow), eddies (blue: cyclonic, red: anticyclonic) and water masses (NACW and SACW). (b) SST from 25 July 2007 with demarcations for the five sub-regions (SR1 – SR5) (Stark et al., 2007; Arístegui et al., 2009). PC: Portuguese Current, AC: Azores Current, CanC: Canary Current, NEC: North Equatorial Current, NECC: North Equatorial Countercurrent, MC: Mauritanian Current, NACW: North Atlantic Central Water, SACW: South Atlantic Central Water.

weakens and then later strengthens in the summer months to occupy a central flow between the African coast and Madeira (Stramma and Siedler, 1988).

The capes along the African coastline and presence of the Canary Islands causes mesoscale turbulence which exhibits strong temperature and chlorophyll gradients (Knoll *et al*., 2002; Nieto *et al*., 2012). Following this the CanC then joins the North Equatorial Current (NEC) where it leaves the coast and heads southwest to the Atlantic (Barton, 1987).

The NW African upwelling system presents all the features of typical EBUS: Cold water along the coast separated by a sharp temperature front, a surface intensified baroclinic equatorward jet and a poleward undercurrent. The upwelling and associated surface jet are driven by the northeast trade winds occurring in these latitudes (Mittelstaedt, 1991). Trade winds are strongest in summer and strongly influenced by the seasonal shift of the Azores high-pressure cell (Mittelstaedt, 1991). The variability of the trade winds and impact of the Azores high-pressure cell is varied between regions of the NWAUS. Due to the seasonal shifting of the trade winds upwelling is strongest in summer and autumn north of 25°N (Knoll *et al*., 2002).

From 28 °N the poleward undercurrent has been observed to occur in all seasons with a mean speed of 12 $cm.s^{-1}$ and maximum velocities in the upper 500m (Knoll *et al*., 2002). Largely confined to the continental slope, it is known to have a 30 to 60 km width and depth of several hundred meters (Barton, 1989; Knoll *et al*., 2002).

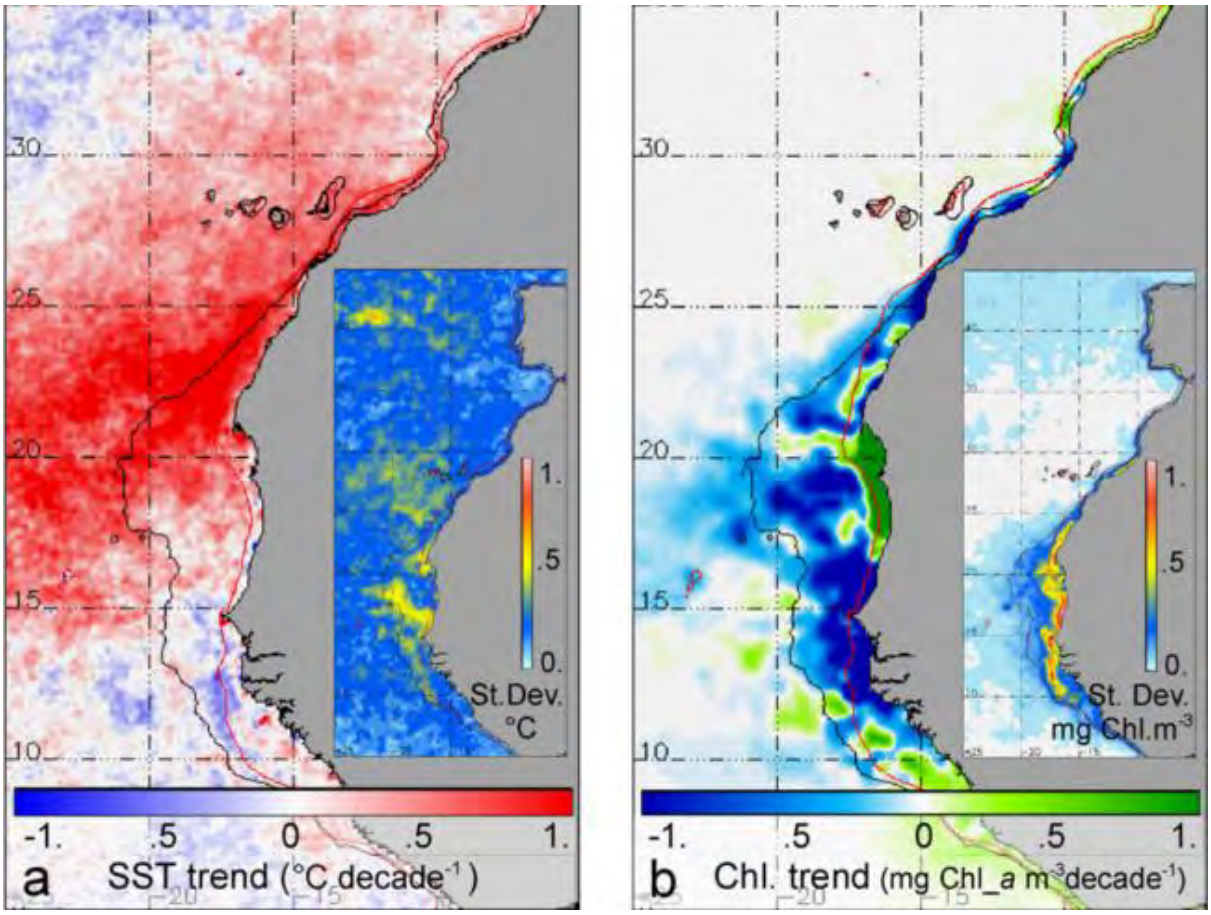

Figure 3: Decadal trends between 1998 and 2007 from AVHRR and SeaWiFS data. (a) SST (°C). (b) Surface chlorophyll-a (Chl a, mg.m-3). Standard deviations are shown as inserts (Arístegui et al., 2009).

1.2.2. Mesoscale Features

Strong mesoscale and submesoscale activity has been observed in the NWAUS with the presence of recurrent filaments near every major cape (Kostianoy and Zatsepin, 1996); Cape Ghir (Barton *et al*., 1998; Pelegrí *et al*., 2005), Cape Juby (Barton *et al.,* 2004; Arístegui *et al.,* 2004) and Cape Blanc (Meunier *et al.,* 2012). Numerous mechanisms have been proposed for generation of these filaments which include wind influence, eddy interaction, meandering of the equatorward jet, baroclinic instability and interaction of upwelling jet with the topography (Ikeda and Emery, 1984; Strub *et al*., 1991; Mooers and Robinson, 1984; Kelly, 1986). In any case, those filaments are related to eddy entrainment (Meunier *et al*., 2010, Meunier *et al.*,

2012). They have a strong impact on the offshore export of nutrients and plankton from the coastal rich water and the oligotrophic ocean interior.

Barton *et al*. (2004) also describe the CanC as "unique amongst the subtropical eastern boundary currents in that it flows through an archipelago of islands extending from near coast to open ocean". The island topography creates perturbations in the flow of the CanC that results in the formation of eddies that, as mentioned previously, exhibit strong temperature and chlorophyll gradients (Knoll *et al*., 2002; Barton *et al.,* 2004; Nieto *et al*., 2012).

In addition to this, eddies that interact with the coast and islands increase mesoscale turbulence in the region and draw cool, nutrient rich filaments away from the coast for up to several hundred kilometers (Arístegui *et al*., 1997; Barton *et al.,* 2004).

Flow perturbation appears to be strongest in summer but there is possibly bias in this observation as most data is collected in the summer months (Barton *et al.,* 2004). Rodríguez *et al.* (1999) have found that eddies are frequent in winter months during weaker flow which potentially indicates that eddies may be a result of current flow disturbance. From observations in 1999, Barton *et al*. (2004) found a dozen eddies downstream of the Canary Islands, half of these were cyclonic (up to 50km diameter) and half anticyclonic that increased in size (up to 100km diameter) as they moved further downstream.

Constantly recurring filaments starting near Cape Juby (28.5 °N) appear to be related to the semi-permanent eddy in the Fuerteventura-Africa channel (Barton *et al*., 2004). Barton *et al*. (2004) state that "filaments would form whenever coastal upwelling is strong enough for the upwelling front and associated current jet to expand beyond the shelf to be entrained around the eddy". Filaments are usually located next to coastal irregularities (such as capes) and tend to appear in the same coastal locations like Cape Blanc, Cape Juby and Cape Ghir which has been corroborated by satellite observations (Stevens and Johnson, 2003; Troupin *et al*., 2012).

1.2.3. Internal Waves

Internal waves are found throughout the world's oceans and have been extensively studied because of their ability to "influence oceanic current measurements, undersea navigation, antisubmarine warfare operations and even the feeding habits of marine animals" (Osborne and Burch, 1980).

Jackson *et al.* (2012) provide a brief description; "internal waves propagate along a pycnocline in the ocean, the portion of the water associated with a sharp change in density, typically the result of differences in temperature or salinity". There are various ways in which internal waves can be generated. Typically they are produced through the interaction of the current and the topography. As the current encounters a topographic anomaly it is diverted upward generating a density anomaly that will then freely propagate as a gravity wave (Rattray, 1960).

It has long been recognized that the heterogeneous nature of the northwestern African coastline possesses morphological structure that interacts with the CanC which is one of the drivers of the various processes in the region (Cruzado and Salat, 1981). The presence of internal waves has been documented although relatively few studies have been conducted on these phenomena. Internal waves have been recorded near the shelf break but seldom appear over the shelf (Salat and Font, 1977; Cruzado and Salat, 1981).

Observations from Woods (1968) show that mixing of the thermocline can be influenced by breaking of internal waves as they move inshore over a continental shelf. There has been speculation on the dynamics of these breaking internal waves but due to lack of information on the time scale of these mixing events the dynamics of internal wave breaking and thermocline mixing are largely unresolved (Gregg *et al*., 1985). A simple and commonly accepted hypothesis is that the random superposition of internal waves achieves sufficient amplitude and

disturbance at the thermocline to influence mixing (Stommel and Fedrov, 1967; Garrett and Munk, 1972; Desaubies and Smith, 1982).

When internal waves, propagating shoreward from the deep ocean over a continental shelf their characteristics become dependent on the surrounding shelf region. Observations have found "the wavelengths are longer at the front than near the back of the wave packets and that the wavelengths are at least as long as or longer than the fluid depth above the shelf" (Djordjevic and Redekopp, 1978).

Internal waves are challenging to record because they propagate in various directions, have different generation processes and may be in superposition (Jackson *et al*., 2012). To measure internal waves scientists usually require several stationary points of measurements in a given area and a composite understanding of the local hydrography and topography. Moving vessels are also able to measure internal waves but have greater difficulty in resolving these processes because of the inherent spatial variability of the vessel.

1.2.4. Spatial and Seasonal Variability

Due to the strong geographic diversity, unique upwelling responses and high seasonal variability the NWAUS has been split into five sub-regions (SR) (Figure 2b). Sub-region one to five are respectively; Galician (42-44°N), Portuguese (37-42°N), Gulf of Cadiz (33-37°N), Moroccan (33-37°N) and Mauritanian-Senegalese (12-21°N).

Arístegui *et al*. (2009) provide a brief summary of the various sub-regions in terms of their ecosystem characteristics. The Galician and Portuguese sub-regions have summer upwelling of NACW with the presence of filaments. Additionally it has a narrow shelf with many capes and rivers inputting fresh water. The Gulf of Cadiz sub-region has intermittent peroids of no upwelling and is prone to coastal retention of water.

The Moroccan sub-region (MSR) is very geographically varied with a narrow shelf, capes and offshore islands. There is all year upwelling of either NACW or SACW that is seasonally varied. There is also dust that is inputted into the region that blows off the Sahara Desert. Finally the Mauritanian-Senegalese SR has input from freshwater rivers and dust from the Sahara desert. It has winter upwelling in an offshore poleward regime and upwells mainly SACW.

The ecosystem characteristics of these regions illustrate the sheer diversity of the NWAUS. Figure 4 represents the differences between regions in terms of Ekman transport ($-Q_x$). Most experience summer upwelling with the exception of the Mauritanian-Senegalese that experiences upwelling peaks in winter (Arístegui *et al*., 2009). The varied nature of the NWAUS often calls for research to be conducted on a zonal basis so that research can be manageable and within time and budget constraints.

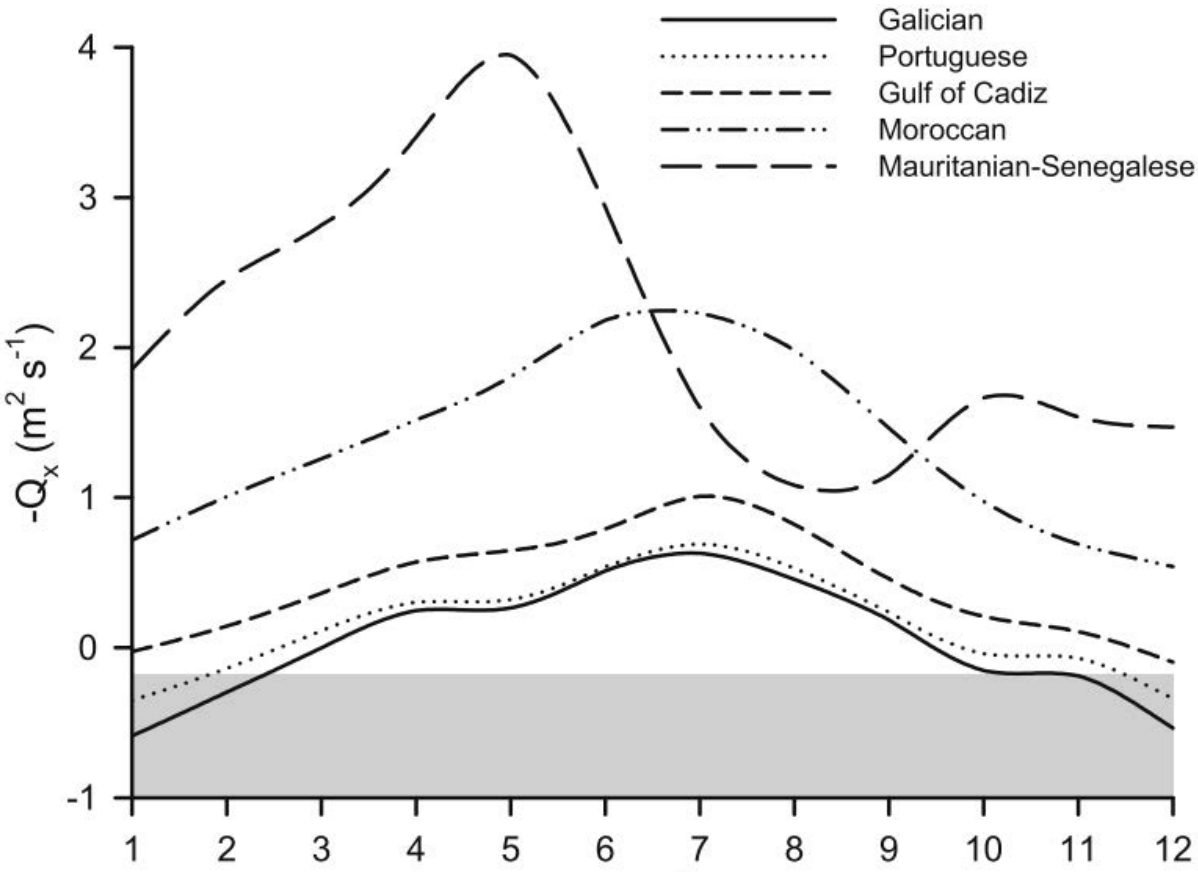

Figure 4: Long-term average seasonal cycle of the offshore Ekman transport calculated at the different sub-regions of the CanC upwelling (Arístegui et al., 2009).

1.2.5. Long Term Temporal Variability

There has been speculation that in the face of climate change eastern boundaries of temperate and subtropical oceans may experience intensified upwelling via increased alongshore winds (Bakun, 1990; Barton *et al*., 2013). Previous studies have indicated reduced nocturnal cooling on land overnight would increase pressure gradients across land and sea resulting in increased equatorward wind and thus upwelling along Californian, Iberian, Moroccan and Peruvian coastlines (Bakun, 1990). More recent work has supported this theory through core analysis of Cape Ghir using an SST-alkenone proxy showed a 1.2°C reduction that correlated with increased CO_2 levels since 1950 (McGregor *et al*., 2007). Additionally wind records from COADS (Comprehensive Ocean-Atmosphere Data Set) since 1950 have lent credence to this hypothesis (Barton *et al*., 2013).

According to Barton *et al*. (2007) general cooling is not the long term trend. Firstly, there is no correlation with the northward movement of sub-tropical fish species as these fish would not prefer cooler waters. Secondly, these findings are inconsistent with warming of coastal regions and other studies finding reduced upwelling along the Moroccan coastline (Quéro *et al*., 1998; Belkin, 2009; Narayan *et al*., 2010; Pardo *et al*., 2011). Barton *et al*. (2007) conclude that coastal sea temperature is slowly increasing, wind estimates show differences in trends and variability and importantly that there is no substantial evidence for a general upwelling intensification. These data indicate that there is variability present that is both inter- and intra-seasonal (Lathuilière *et al*., 2008).

Figure 3 shows decadal trends in the NWAUS in SST and chlorophyll-a between 1998 and 2007. Aristeguí *et al*. (2009) show a gradual warming of the surface water of 1 °C that is concentrated between 15 and 30 °N. There has been a decrease in chlorophyll-a production between 15 and 25 °N by 1 $mg.m^{-3}$. There has been a sharp increase in chlorophyll-a by 1

mg.m^{-3} between 17 and 21 °N that is confined to the coast. This is potentially due added nitrates from dust that has been blown westwards from the Sahara desert and therefore not directly related to SST.

1.2.6. The Moroccan Sub-region

The MSR stretches from Cape Beddouza (33°N) down to Cape Blanc (21°N) and is characterized by a narrow shelf, capes and the presence of the offshore Canary Islands which cause extended filaments and island eddies (Arístegui *et al*., 2009). There is an all year upwelling with seasonal variation that is stronger in the summer months (Wooster *et al.,* 1976; Arístegui *et al*., 2009). An interesting feature is dust input from the Sahara desert that increases primary production via dissolving nitrates. The main pelagic resources are Horse mackerel and Sardine with the main demersal resources being Blue Whiting, Sparids and Cephalapods (Arístegui *et al*., 2009).

The heterogeneity of the MSR causes varied responses from the coastal processes in the region. Firstly, in addition to the island induced eddies, filament formation is prominent along Capes Ghir (~30 °N) and Juby (28.5 °N) (Arístegui *et al*., 2009). As shown in Figure 2 there is a

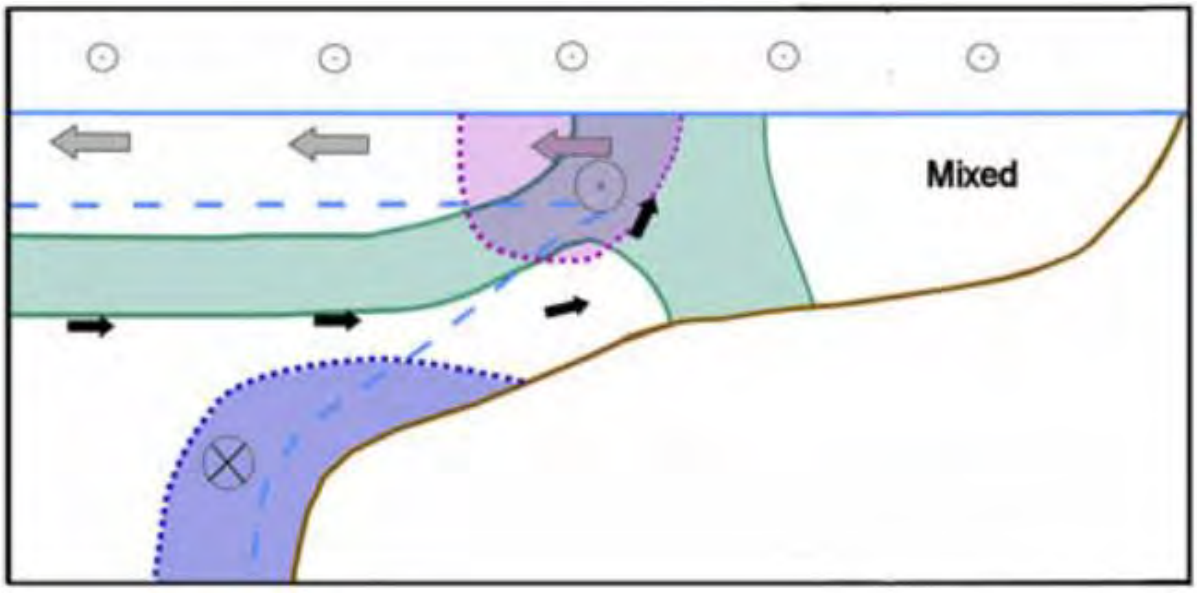

Figure 5: Schematic cross-section of upwelling in the Moroccan sub-region (Arístegui et al., 2009).

poleward undercurrent that persist year-round that is usually 100 km wide and about 300 m deep (Arístegui *et al*., 2009). At times this may interact with the surface current as the CanC has been known to reverse in late fall and winter, specifically between Cape Juby and the Canary Islands (Navarro-Pérez and Barton, 2001; Hernández-Guerra *et al*., 2002). The cause of the CanC reversal is potentially due to a weakening of trade winds during this time (Navarro-Pérez and Barton, 2001; Hernández-Guerra *et al*., 2002). Due to the wide shelf there is evidence that near-shore counter currents are present but there have been few studies on the phenomenon (Mittelstaedt, 1991).

The peak of the Ekman transport for the Moroccan Sub-region (MSR) is in June/July. Figure 4 also shows that the MSR has the second highest level of transport of all sub-regions.

Figure 5 shows a schematic cross-section of the upwelling in the MSR. The small circles show the equatorial wind stress that drive Ekman transport of water offshore represented by the grey arrows. The surface layer is replaced by onshore flow (black arrows) that upwells the pycnocline (green) that may separate from the coast due to the width of the shelf. Upwelling in this region is not confined to the coast with a large mixed region inshore of the outcropped isopycnals. The area in pink represents the surface intensified jet while the blue region denotes the poleward undercurrent that is trapped to the continental slope.

1.3. Introduction

The dynamics and processes of EBUS are not yet fully understood and there is still room for future research to deepen our understanding of these ecosystems. There is a growing need for research in these regions so that policy makers are able to make informed decisions about how to manage these dynamic resources in the face of increasing human population and climate change (Strub *et al*., 2013). The NWAUS is well studied and the coastal dynamics of this region

are largely understood at the main capes such as Cape Ghir, Cape Bojador and Cape Blanc. However the shelf region near Cape Juby (28.5 °N) (Figure 2) remains largely unstudied.

Cape Juby is a unique point along the NWAUS because of the presence of the Canary Islands directly offshore that greatly influence mesoscale variability (Barton *et al.,* 1998). Cape Juby therefore delimits a narrow canal between the African coast and the Canary Islands. It is known to be a place of filament development and an upwelling cell with enhanced upwelling near the Cape (Barton *et al.,* 1998; Hernández-León *et al.*, 2002; Arístegui *et al.,* 2004).

The Epure Project has run from January 2012 to December 2015. Its purpose is to further understand upwelling, seasonality and the presence of metal trace elements and their impacts on the fishing industry (Epure, 2015). The data considered in this report comes from two cruises performed in July and November 2013 aboard the IRD research vessel Antea. The cruises were conducted in the vicinity of the Moroccan coastline between Cape Juby (28.5 °N) and Agadir (30.4 °N) to further elucidate the processes that occur in this region.

This report aims to a better description and understanding of the latter processes by the processing analysis of the EPURE data. The main question we intend to answer are:

- What are the hydrographic conditions of the Cape Juby continental shelf area?
    - What are the dominant processes in this region?
    - What is their seasonal variability?

The report is organized as follows. Chapter 1 provides a brief literature review and introduction to the project. The literature review discusses the main characteristics of EBUS with a focus on the NWAUS, particularly the Moroccan sub-region. Chapter 2 describes the data and methods used while chapter 3 presents the results and interpretations of the study. Finally, a brief summary of the main results and concluding remarks are proposed in chapter 4.

Chapter Two: Data and Methods

2.1. Methods

The EPURE Project consisted of four cruises between June and December of 2013. Data relevant to this study were collected during cruise 1 and cruise 3 (also referred to as E1 and E3). E1 lasted from 27 June until 7 July and E3 lasted from 7 to 17 November. The data were collected on the continental shelf between Cape Juby (28.5° N) and Agadir (30.4 °N). The two cruises mainly followed a similar course track with differences occurring in the length of the transects due to ship time limitation. E3 aimed to increase the sampled area and increase the data set with information that might give insights to seasonality. E3 also increased the number of sections while resampling several sections from E1.

Cross-shore sections were measured from the coast to the shelf break between depths of 20 and 100m. Currents, bathymetry and fish and plankton distribution were measured throughout the EPURE campaign with acoustic instruments (EK60 and ADCP). Physical parameters (temperature, salinity and density) were measured at different stations along the various sections.

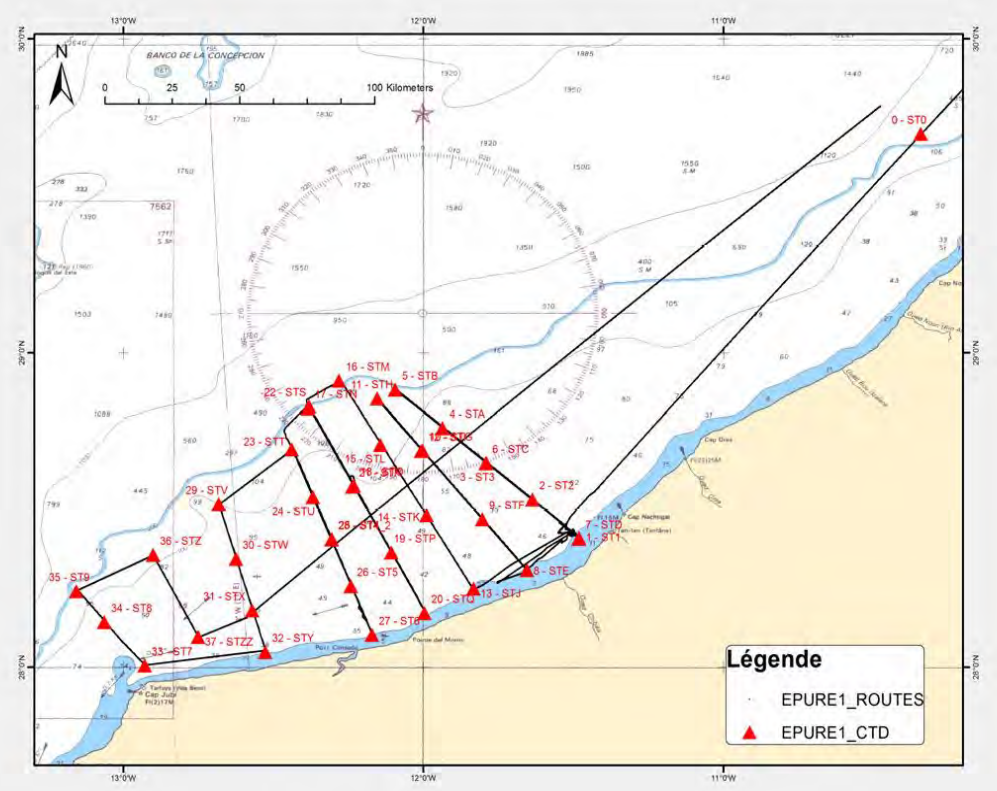

Figure 6: Epure 1 cruise track showing cross-shore sections with red triangles representing CTD stations.

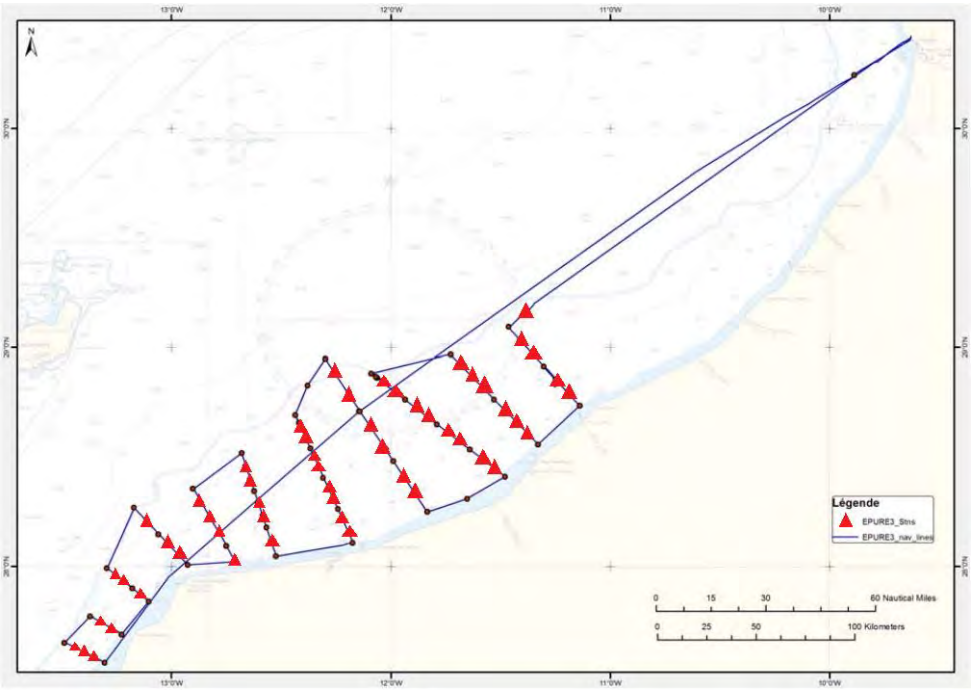

Figure 7: Epure 3 cruise track showing cross-shore sections with red triangles representing CTD stations.

Figures 6 and 7 show the original cruise tracks of the E1 and E3. Other stations are marked for measurements that are outside the scope of this study and have therefore been excluded from this description. CTD stations are shown as red triangles.

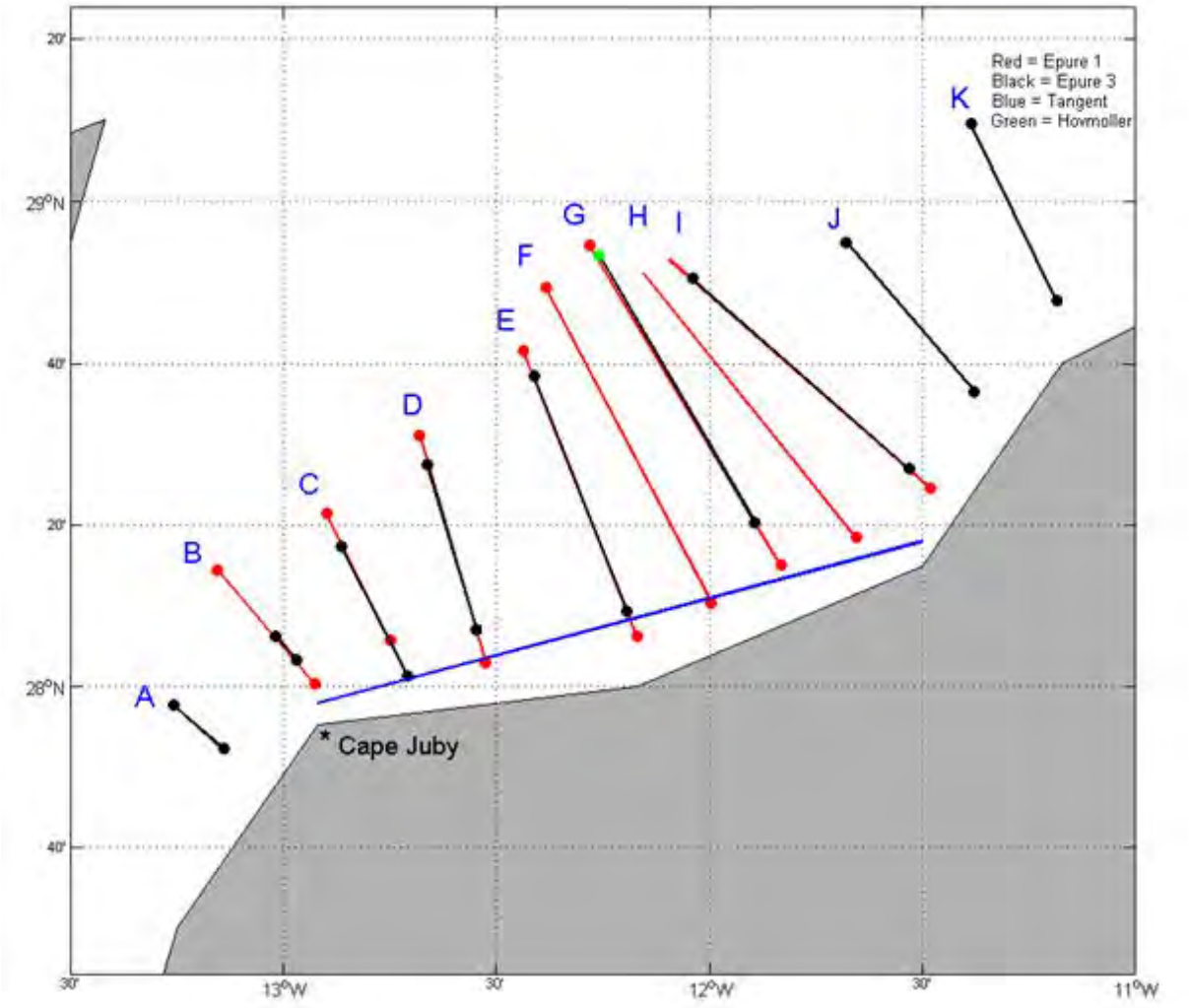

Figure 8: Epure 1 sections (red) Epure 3 sections (black) over 13 locations (A - K).

E1 (Figure 6) consisted of 8 sections that began near Agadir and moved in a south easterly direction toward Cape Juby. E3 (Figure 7) consisted of 11 section of which only 9 yielded usable data. The cruise (E3) started at Cape Juby and moved in a north westerly direction. To account the opposing cruise trajectories sections have been assimilated into 13 locations (blue) from A to K. 'Locations' allow for easier comparison of sections that occupy the same space.

There are only 6 locations (B, C, D, G, E & I) that have been sampled by each cruise. These locations are ideal for comparison across time intervals.

2.1.1. Data Acquisition

A variety of instruments were used throughout all the EPURE legs. For the purpose of this report only the relevant instruments are listed and briefly described.

2.1.1.1. CTD

A Seabird CTD 911 with sensors for temperature, conductivity, pressure, turbidity, oxygen, and fluorescence was attached to a rosette and was used for the vertical profiles (Figures 6 and 7). The rosette also allowed collection of water samples at various depths (Figure 9). Complete with attachments, it is a large device and so a Seabird CTD SBE19 with sensors for temperature, conductivity, pressure, turbidity, oxygen, fluorescence and was used in conjunction with a CTD 911 for E3. The smaller Seabird CTD SBE19 was able to perform vertical profiles directly from the deck without using a rosette. This dramatically increased the number of possible stations for E3.

During E1, certain locations were sampled twice within eight hours of each other to examine temporal changes over short periods and day/night changes. The direction of the sections were either coast-ward or ocean-ward and usually alternated throughout each leg.

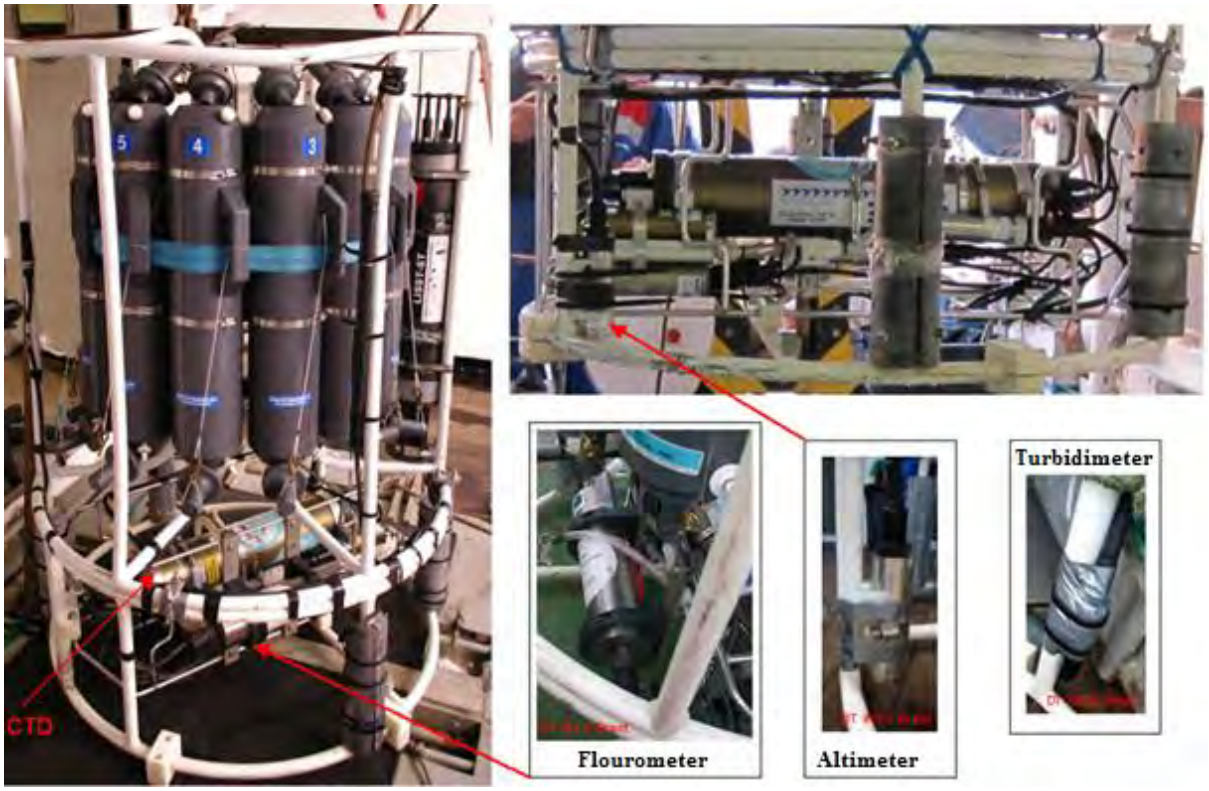

Figure 9: Implementation of the Seabird CTD 911 on the rosette with sensors for temperature, conductivity, pressure, turbidity, oxygen and fluorescence.

The average descent speed of the CTD was 1 m/s. During E3 a specific location (28°53,29'N ; 12°15,52'W) was repeatedly resampled 32 times (over 3 hours) to test for the presence of solitons. This is marked on Figure 8 as the green dot on Location G. Each descent took on average a total of seven minutes.

For analysis, sections from Locations I, G and E were chosen for comparisons with sections from the same locations from E3. Locations I, G and E are favourable for E1 because of their length (Figure 8) as well as the number of vertical profiles per section (Table 1).

Table 1: Epure 1 brief summary of sections

Section	Location	Start		End		# Profiles	Direction
		Time	*GPS*	*Time*	*GPS*		
1	I	02h31 (29-06)	28.414 °N 11.480 °W	19h45 (29-06)	28.883 °N 12.092 °W	5	Offshore
2	H	12h11 (30-06)	28.311 °N 11.656 °W	23h23 (30-06)	28.853 °N 12.157 °W	4	Offshore
3	G	17h55 (01-07)	28.250 °N 11.836 °W	06h00 (02-07)	28.914 °N 12.282 °W	4	Offshore
4	F	08h13 (02-07)	28.174 ° N 11.996 °W	22h45 (02-07)	28.815 °N 12.382 °W	4	Inshore
5	E	12h12 (03-07)	28.101 °N 12.171 °W	22h51 (03-07)	28.693 °N 12.439 °W	5	Offshore
6	D	10h43 (04-07)	28.048 °N 12.527 °W	18h45 (04-07)	28.513 °N 12.679 °W	4	Offshore
7	C	23h15 (04-07)	28.006 °N 12.926 °W	04h34 (05-07)	28.242 °N 13.160 °W	3	Offshore
8	B	08h00 (05-07)	28.094 °N 12.748 °W	12h42 (05-07)	28.361 °N 12.897 °W	2	Inshore

For E3 the sections chosen from Locations I, G and E have 8, 6 and 7 vertical profiles respectively (Table 2), making them good candidates for analysis. The sections at these locations are also the three longest of the E3 cruise.

Table 2: Epure 3 brief summary of sections

Section	Location	Start		End		# Profiles	Direction
		Time	*GPS*	*Time*	*GPS*		
1	A	07h45 (10-11)	27.872 °N 13.137 °W	10h18 (10-11)	27.956 °N 13.252 °W	3	Offshore
2	B	18h58 (10-11)	28.051 °N 12.970 °W	20h00 (10-11)	28.101 °N 13.019 °W	2	Inshore
3	C	23h33 (10-11)	28.025 °N 12.714 °W	04h23 (11-11)	28.296 °N 12.870 °W	4	Offshore
4	D	10h35 (11-11)	28.116 °N 12.546 °W	16h37 (11-11)	28.460 °N 12.660 °W	5	Inshore
5	E	23h04 (11-11)	28.155 ° N 12.195 °W	09h01 (12-11)	28.639 °N 12.412 °W	7	Offshore
Hov.	G	17h35 (12-11)	28.888 °N 12.259 °W	22h00 (12-11)	28.888 °N 12.259 °W	32	Stationary
6	G	00h05 (13-11)	28.342 °N 11.893 °W	11h22 (13-11)	28.887 °N 12.260 °W	6	Offshore
7	I	20h17 (13-11)	28.449 °N 11.531 °W	06h38 (14-11)	28.838 °N 12.038 °W	8	Offshore
8	J	16h45 (14-11)	28.609 °N 11.378 °W	23h21 (14-11)	28.918 °N 11.679 °W	6	Inshore
9	K	05h05 (15-11)	28.792 °N 11.183 °W	18h43 (15-11)	29.158 °N 11.386 °W	4	Offshore

2.1.1.2. ADCP

An Acoustic Doppler Current Profiler (ADCP) was used to determine the velocity at different depths of the water column. An ADCP can be placed on a fixed point such as the sea floor or a river bed. In this case it was placed on the bottom of the vessel to measure the velocity field during the cruise. Using the Doppler effect it transmits ‘pings’ at a fixed frequency and records the backscatter as the sound waves bounce off particles that are suspended in the water column. When the sound waves return, particles travelling towards the ADCP will have a different

frequency depending on the velocity of the reflector and thus of the surrounding current. (Ocean Instruments, 2015).

The 150 kHz ADCP calculated velocity over 16 m cells. For the depth range we explored, an additional 600 kHz RDI workhorse ADCP was used. This ADCP calculated the velocity over 1 m cell, which is more relevant for the purpose of our cruise. Unfortunately, its scope is only about 50 m. During E1 there were electrical difficulties with the ADCP. These problems were soon resolved but as a consequence there is no data for the first two sections of Epure 1 (locations I and H).

The ADCP data was cleaned and processed by the Laboratoire Domaine Océanique at the Insititut Universitaire Européen de la Mer (France Floc'h, pers. comm. August 2014).

The third ADCP (75 kHz) was used to gauge the current velocities at depth intervals of 4 to 9 m, 9 to 14 m, 14 to 19 m and 24 to 29 m. For each of these cross-shore sections the along shore component was also calculated and represented with the vertical maps for locations I, G and H. The along shore current was calculated using the same equations for along and cross-shore wind (section 2.1.3).

2.1.1.3. EK60

A SIMRAD EK60 echo sounder is normally used for fish stock assessment. It is an acoustic instrument that transmits 'pings' at various frequencies and records the backscattered data. It uses four quadrats that are excited in parallel (split-beam nature) which allows for tracking of particles that are in suspension. For this application the EK60 locates the position of plankton and necton and therefore estimates the position of the thermocline through a biological proxy.

The EK60 transmitted at 38, 70, 120 and 200 kHz giving a slightly different image of the water for each frequency. The transducer was placed 3 m below the surface of the water on the ship's hull. For location of the thermocline the most accurate frequency was 120 kHz which would

pulse every 256 microseconds with a 64 microsecond sample rate. Data was then processed with Echopen 1.6 using algorithms for 120 kHz. Echopen 1.6 was compiled in MATLAB ® and is provided by SIMRAD.

2.1.2. Hydrographic Data Processing

Information was extracted from the CTD and checked against manually recorded time stamps for CTD stations. Several errors were found relating to GPS locations of CTD profiles. These were corrected except for one location on Epure 3 Section 2 (location B) and this was removed from the study. This explains why the Epure 3 Section 2 is very short at location B.

Vertical and horizontal maps were interpolated from the original vertical profiles (CTD stations). Several interpolation schemes were tested until a linear interpolation scheme was chosen. The Barnes Algorithm (Barnes, 1973) was also tested but not used due to initial erratic results and time constraints. Individual temperature, salinity and density profiles were examined in vertical and isopycnic contours, in order to validate the interpolation and to help further interpretation. In E1, several of the CTD stations were sampled twice with a 12 hour gap to examine day-night temperature oscillations.

Horizontal maps were created at each depth (every 1m) for density, salinity and temperature on both cruises. The final depths used were 6, 21, 41 and 61m. The longitudinal gridstep was used for interpolation was 5.5 km and the vertical girdstep was 1 m.

Temperature-Salinity Plot

A standard TS plot was created for the identification of water masses. A standard routine from the Woods Hole Science Centre (1998) was downloaded and applied for this calculation.

Position of the Front and Depth of Mixed Layer

The position of the front was defined as the location of strongest temperature gradient along the cross-shore direction. The interpolated data from the horizontal maps was used for this application. The gradient was computed using a centred 6-grid point finite difference scheme. The mixed layer depth was computed using the same method among a vertical profile.

Climatological Data

Horizontal sections of temperature and salinity from the World Ocean Atlas (WOA13) compiled by the National Oceanic and Atmospheric Administration (World Ocean Atlas, 2013) were also used. WOA13 "is a set of objectively analysed (0.25° grid) climatological fields of in-situ temperature, salinity, dissolved oxygen, Apparent Oxygen Utilization (AOU), percent oxygen saturation, phosphate, silicate, and nitrate at standard depth levels for annual, seasonal, and monthly compositing periods for the World Ocean. It also includes associated statistical fields of observed oceanographic profile data interpolated to standard depth levels on 5°, 1°, and 0.25° grids" (Levitus *et al.,* 2005; Levitus *et al.,* 2009; World Ocean Atlas, 2013).

2.1.3. Wind Data

Data were obtained from MyOcean online-catalogue where the specific product consisted of a 0.125° resolution ASCAT level 3 ocean wind surface product compiled from QuickScat sensor on Aqua. According to MyOcean (2015); "the L3 global wind product of MyOcean is composed of daily gridded observations of the scatterometer on a regular lat-lon grid, using Gouraud shading interpolation technique. Data from ascending and descending passes are gridded into separate files". These data were extracted for the period of the cruises as well as one week before.

Along and Cross-shore Wind

Figure 8 shows a blue line indicating an alongshore tangent. The QuickScat data were recorded as north-east positive, in this study the data was transformed to be alongshore and south-west positive. Firstly the north and east wind components were projected on the along and cross-shore direction.

If we considered the ends of the tangent to be X1, X2 and Y1, Y2 we first need to find the angle of the tangent to the coast, θ.

$$\theta = tan^{-1}\frac{(Y2 - Y1)}{(X2 - X1)}$$

Following this we then project the northward and eastward components onto this angle to find the alongshore (U_a) wind.

$$U_a = U.cos\theta + V.sin\theta$$

Cross-shore (U_c) wind was also calculated

$$U_C = -U.sin\theta + V.cos\theta$$

Internal Waves

A total of 32 vertical profiles were recorded (28.888 °N 12.259 °W) during E3 (Figure 8) over 3 hours. Each profile descent took 7 minutes. These vertical profiles were assimilated into a Hövmoller plot. This was a fixed location which indicated the presence of internal waves or solitons.

EK60 data was examined in MATLAB where perturbations of the thermocline were considered to show the presence of internal waves. In this study the two snapshots were chosen for each cruise and the amplitude of the internal waves were recorded.

Chapter Three: Results and Interpretation

3.1. Results

3.1.1. Epure 1

3.1.1.1. Context

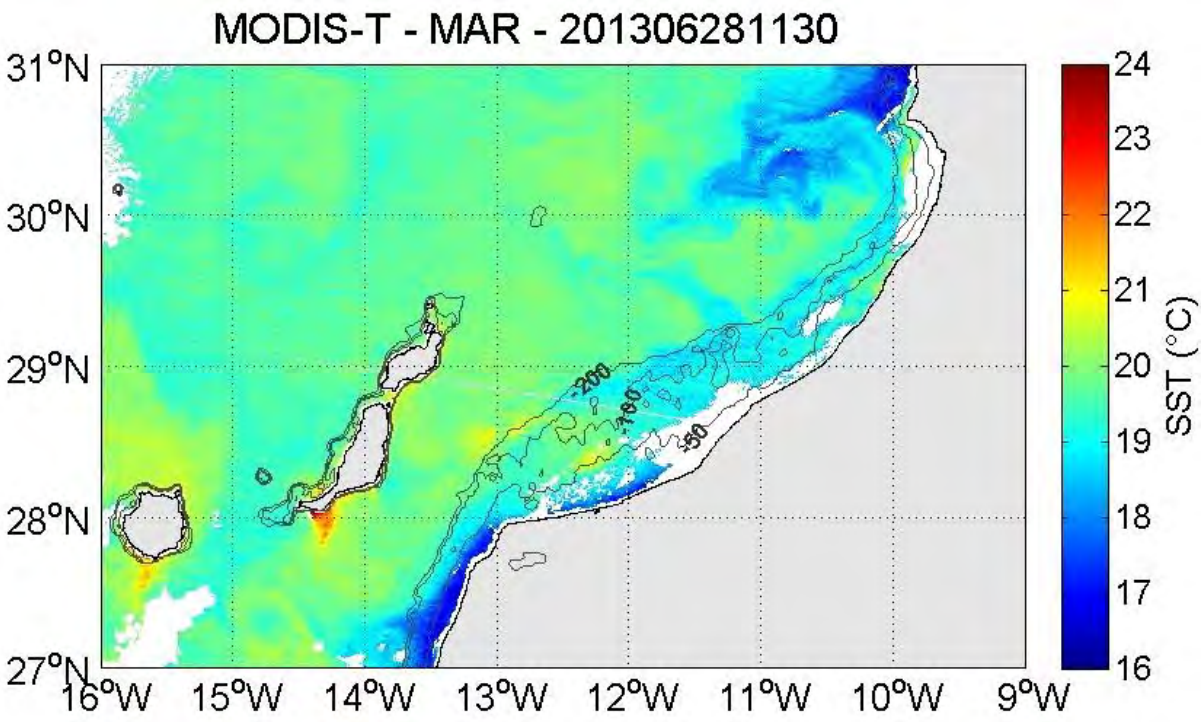

Figure 10: SST on 28 June at 11h30.

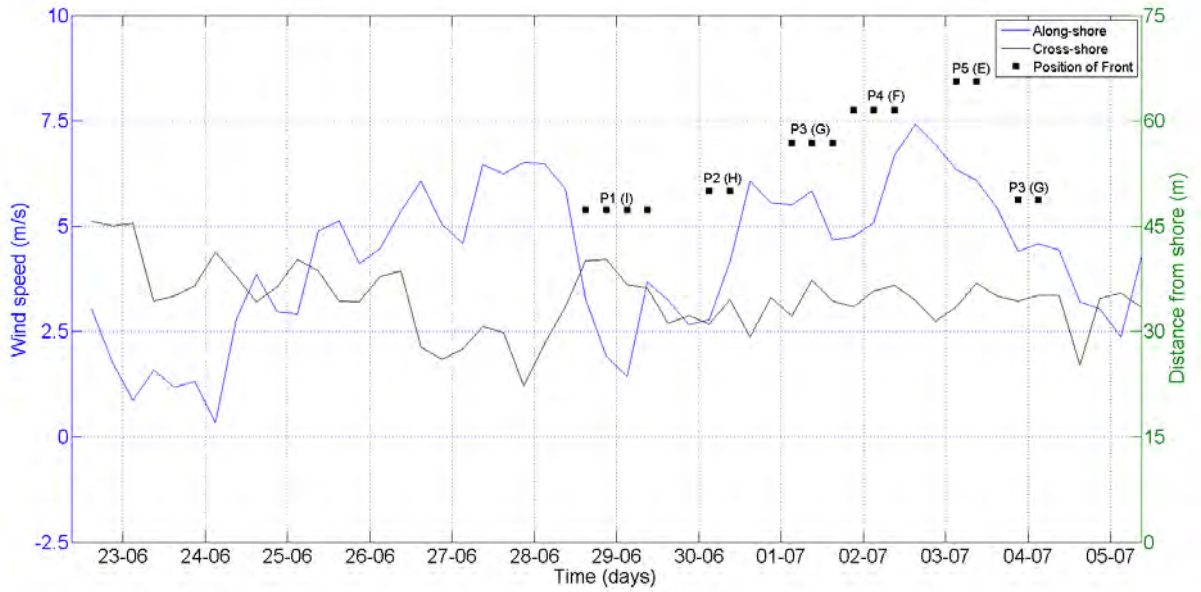

Figure 11: Position of the front in relation to along and cross-shore wind before and throughout the Epure 1 cruise.

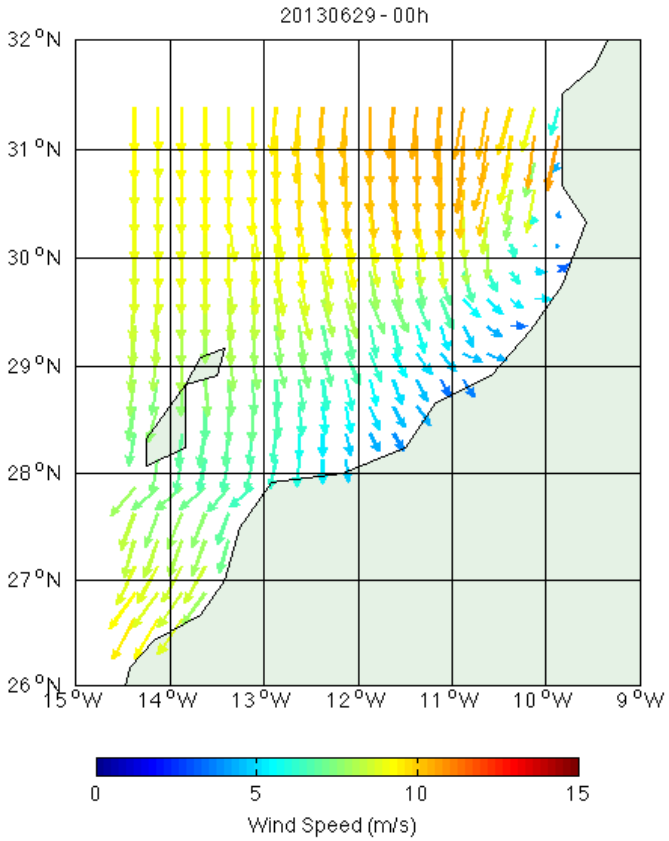

Figure 12: Surface wind speed on 29 June 2013 at 00h00.

Figure 10 shows SST acquired from MODIS on 28 June at 11h30. The area shown in the map is the MSR of the NWAUS. These data show the conditions 3 hours before the first CTD cast from E1. Two distinct zones of upwelling are discernible in our survey area. Along the coast south-west of Cape Juby (27.95°N 13°W to 27°N 13.5°W) there is cool water close to the coast (approximately 17 °C). This cool water extends offshore to the edge of the shelf break at the 200 m isobath. Between 28°N 12.6°W and 28.25°N 11.7°W there is a small strip of upwelling with coastal water around 18 °C. This upwelling is much less intense and remains close to the coast within the 50 m contour. It is possible that the gaps of information on the graph are a result of fog and that some low intensity coastal upwelling is present between 28.25°N 11.7°W and 28.9°N 11°W.

From 28.8 °N 12.5°N to 29.5 °N 11.5°W there appears to be a secondary upwelling close to the 200 m isobath. It is weaker than the other upwelling regions and the front is disturbed by

the presence of mesoscale activity. Moving directly inshore from 28.8 °N 12.5°N there is a patch of warm water at 28.35 °N 12.25 °W (21 °C) and then cooler water closer to the coast.

Figure 11 shows the intensity of along and cross-shore wind stress for the duration of the E1 (28 June – 4 July) and six days prior to the start of the field work (22 – 27 June). The cross-shore wind in this figure is calculated from a line drawn parallel to the shore that is shown in Figure 8. The wind is positive (south westward) throughout the sampling period which means it is therefore upwelling favourable. Prior to the 24th there was little or no along shore wind. From the 24th the along shore wind builds from 0.2 m.s^{-1} to a peak of 6.8 m.s^{-1} on the 28th but then suddenly decreases during the next 24 hours. Just after midnight on the 29th the wind has fallen to 1.8 m.s^{-1} and then rises somewhat erratically to 7.5 m.s^{-1} at noon on the 2nd. Between the 29th and the 2nd there is a peak during the afternoon of the 30th (6.25 m.s^{-1}) and two drops in wind speed at midnight of the 30th (2.6 m.s^{-1}) and early afternoon on the 1st (4.85 m.s^{-1}). From noon of the 2nd the wind uniformly decreases over the next two and half days until it reaches 2.5 m.s^{-1} at midnight of the 5th.

A snapshot of the surface wind velocity 12 hours prior to the start of field work is shown in Figure 12. At 30 °N 10 °W there is a patch of wind stress curl that is a quasi-permanent or recurrent feature in this particular area. Directly north-east of Cape Juby (28 °N 13 °W) the wind is blowing towards the coast, meaning that it is more cross-shore than along shore and therefore less upwelling favourable. This corresponds to Figure 10 at 29-06.

3.1.1.2. Hydrography

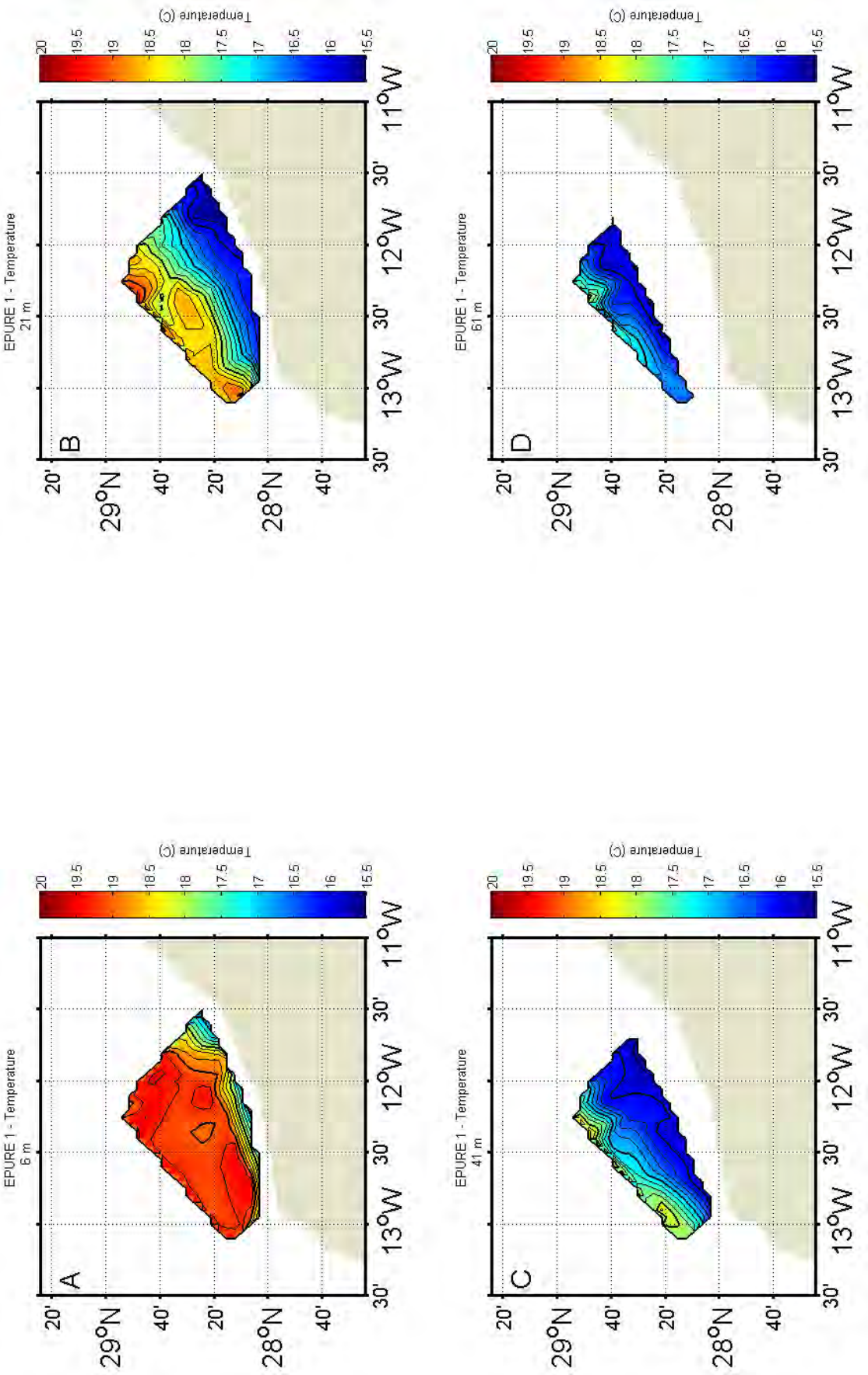

Figure 13: Temperature horizontal maps for Epure 1 cruise from 37 CTD stations. Thick contours represent 1 °C intervals and thin contours represent 0.25 °C intervals.

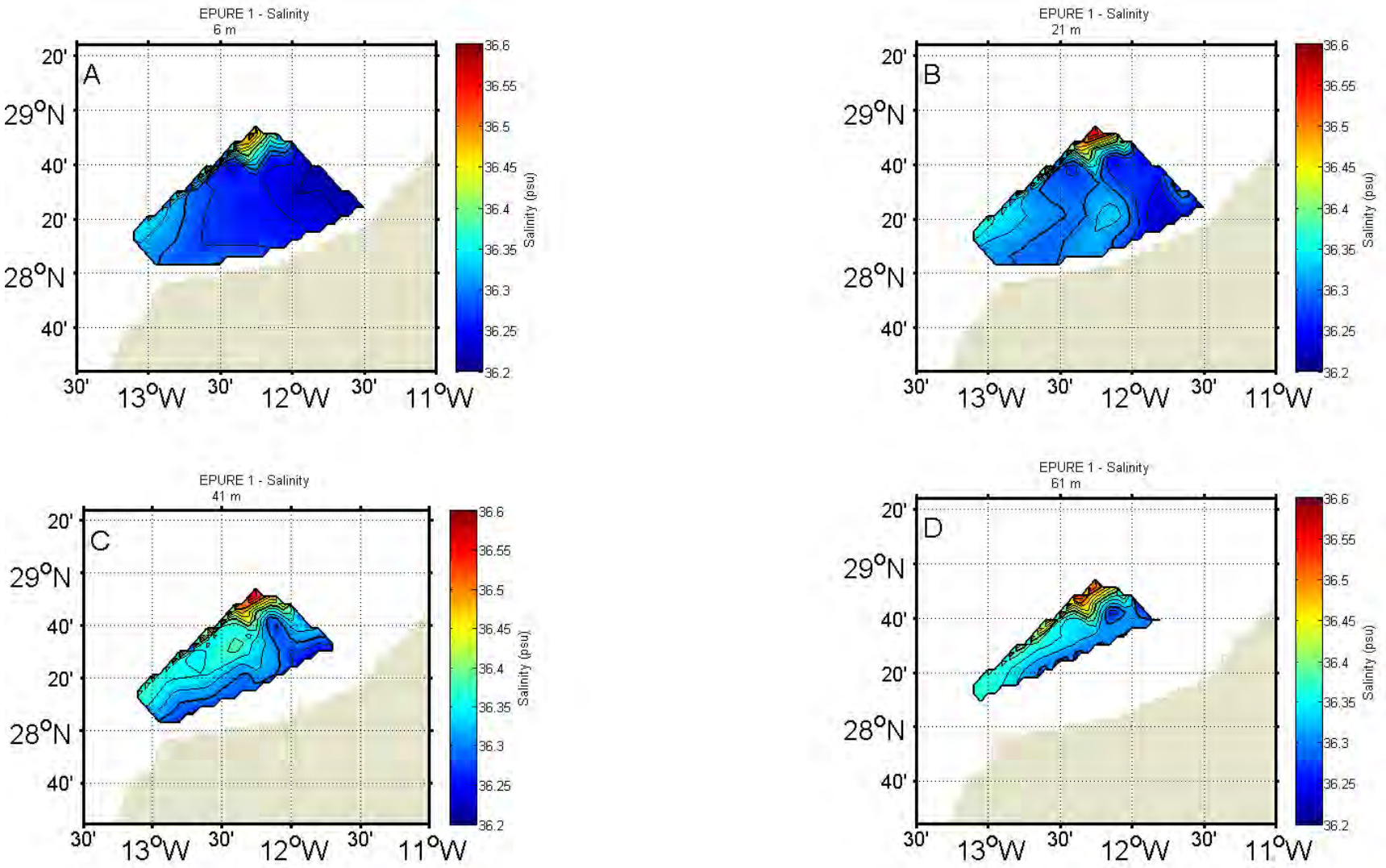

Figure 14: Salinity horizontal maps for Epure 1 cruise from 37 CTD stations. Thick contours represent 0.1 psu intervals and thin contours represent 0.025 psu intervals.

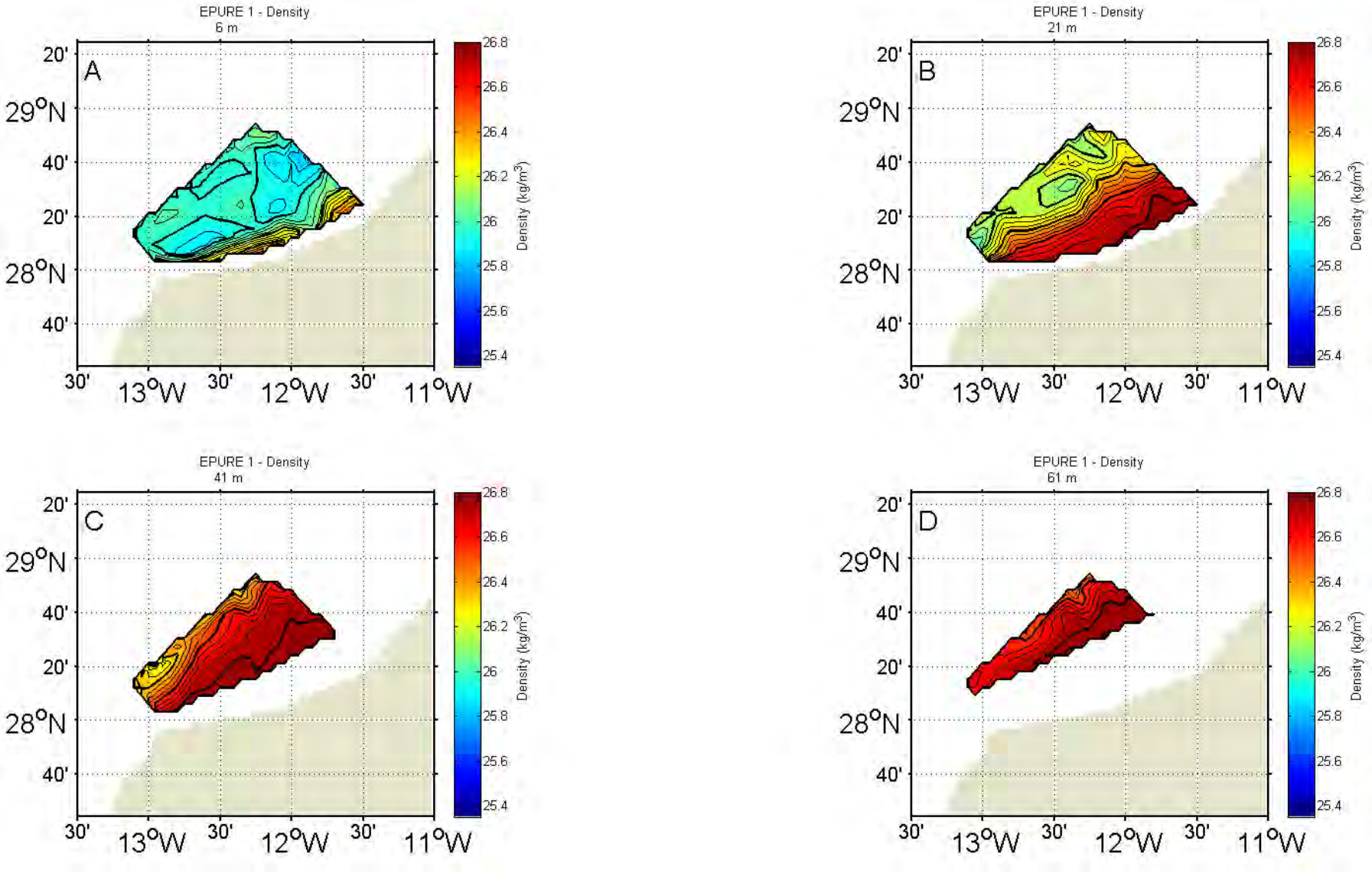

Figure 15: Density horizontal maps for Epure 1 cruise from 37 CTD stations. Thick contours represent 0.2 kg.m-3 intervals and thin contours represent 0.05 kg.m-3 intervals.

Figure 13 (a,b,c,d) shows horizontal maps of temperature at respectively 6, 21, 41 and 61 m. At 6 m, a sharp front separates coastal cold water (about 17.5°C) to warmer offshore water (over 19°C). The front enters the surveyed area from the north (28.1°N 13°W) with a significant cross-shore component and then meanders near 28.3°N 11.8°W and aligns with the coastline between 28.3°N 11.75°W and 28.4°N 11.6°W. The temperature front is still obvious at 21 m and has an along shore orientation within the whole surveyed area. It is defined by a strong gradient between the 16 to 18 °C isotherms. A circular patch of warmer water within the enclosed 18.8 °C isotherm is evident near 28.5°N 12.45°W, just offshore of the upwelling front.

At greater depths (41 and 61 m), the front is still discernible but broadens and is centred near the shelf break. It still has an alongshore orientation. The water temperature ranges from 16°C near the coast to 18°C offshore.

Horizontal maps of salinity at 6, 21, 41 and 61 m are shown in Figure 14 (a,b,c,d). At 6 m there is no clear front and the main feature is a zone of high salinity (36.5 psu) at the northern extent of the surveyed area (28.8°N 12.25°W). At 21 m there is high spatial variability with a patch of slightly less saline water enclosed within the 36.275 psu isohaline near 28.35°N 12.2°W.

At 41 m, smooth front between the 36.275 and 36.35 psu isohalines is observed and has a clear alongshore orientation. The front enters the surveyed zone at 28.1°N 12.95°W, briefly meanders offshore near 28.65°N 12.15°W and then re-aligns with the coast between 28.5°N 12°W and 28.55°N 11.75°W. At 61 m the front is still present with a similar pattern to 41 m with a corresponding patch of slightly less saline water (36.275 psu) at 28.65°N 12.15°W.

Figure 15 (a,b,c,d) shows horizontal maps of density at respectively 6, 21, 41 and 61 m. The pattern of density shows an important similarity with temperature. Denser water corresponds with cooler temperatures and the fronts can be found in the same positions (Figure 13).

At 6 m, a sharp front separates dense coastal water (26.4 $kg.m^{-3}$) to less dense offshore water (less than 25.9 $kg.m^{-3}$). The front enters the surveyed area (28.1°N 13°W) with a significant cross-shore component and then meanders towards the coast near 28.3°N 11.9°W and aligns with the coastline between 28.3°N 11.75°W and 28.4°N 11.6°W. At 21 m the front becomes more obvious, retaining an along shore orientation throughout with a slight offshore meander (at the point 28.45°N 11.75°W) and then returning to its along shore position along the 26.6 $kg.m^{-3}$ isopycnal.

At 41 m the front is still present with an along shore orientation. There is a slightly less dense patch of water found at 28.32°N 12.95°W within the 26.4 $kg.m^{-3}$ isopycnal. At 61 m the front is present with the same orientation as before.

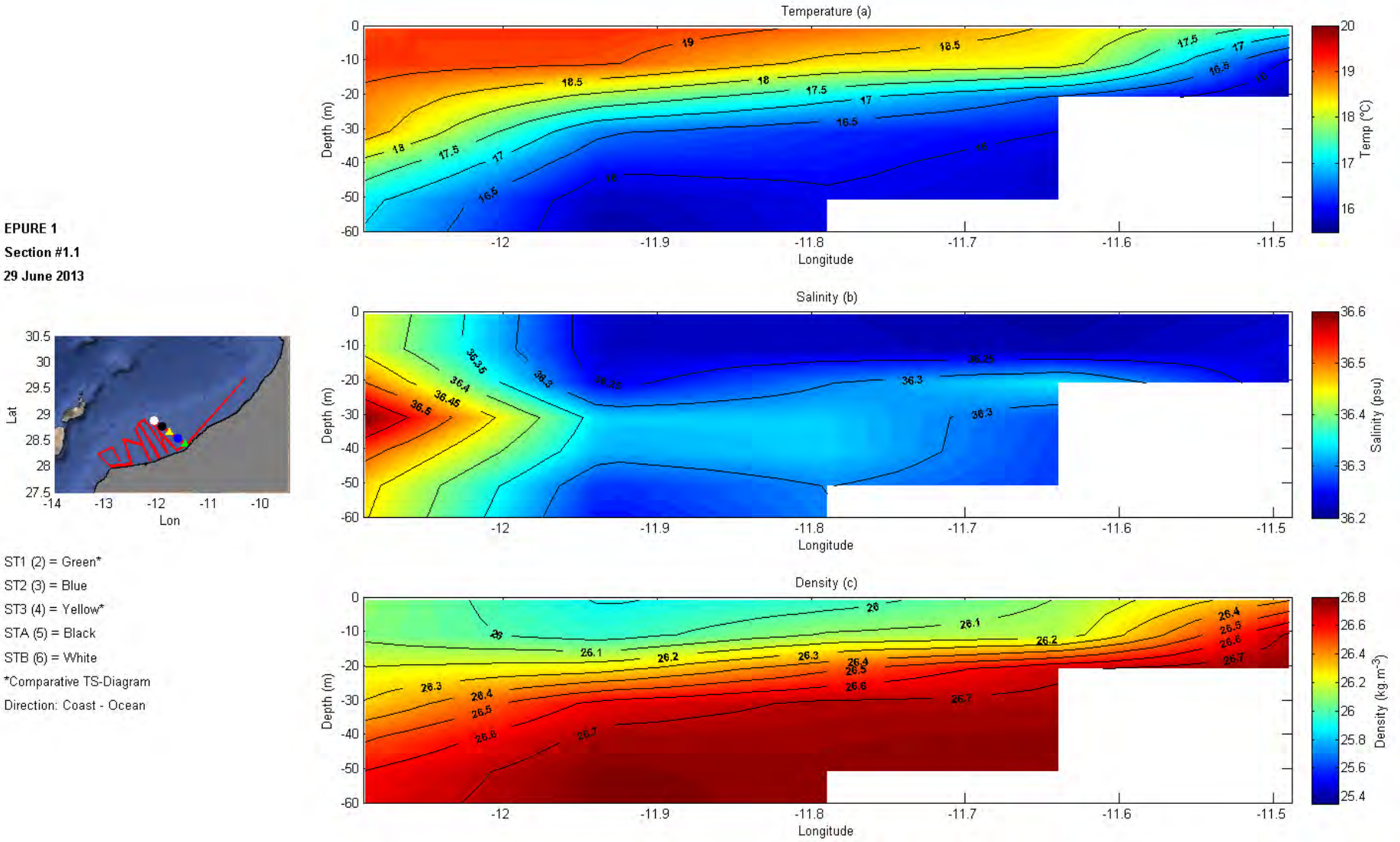

Figure 16: Vertical profiles for temperature, salinity and density at location I. ADCP data was not available for this profile

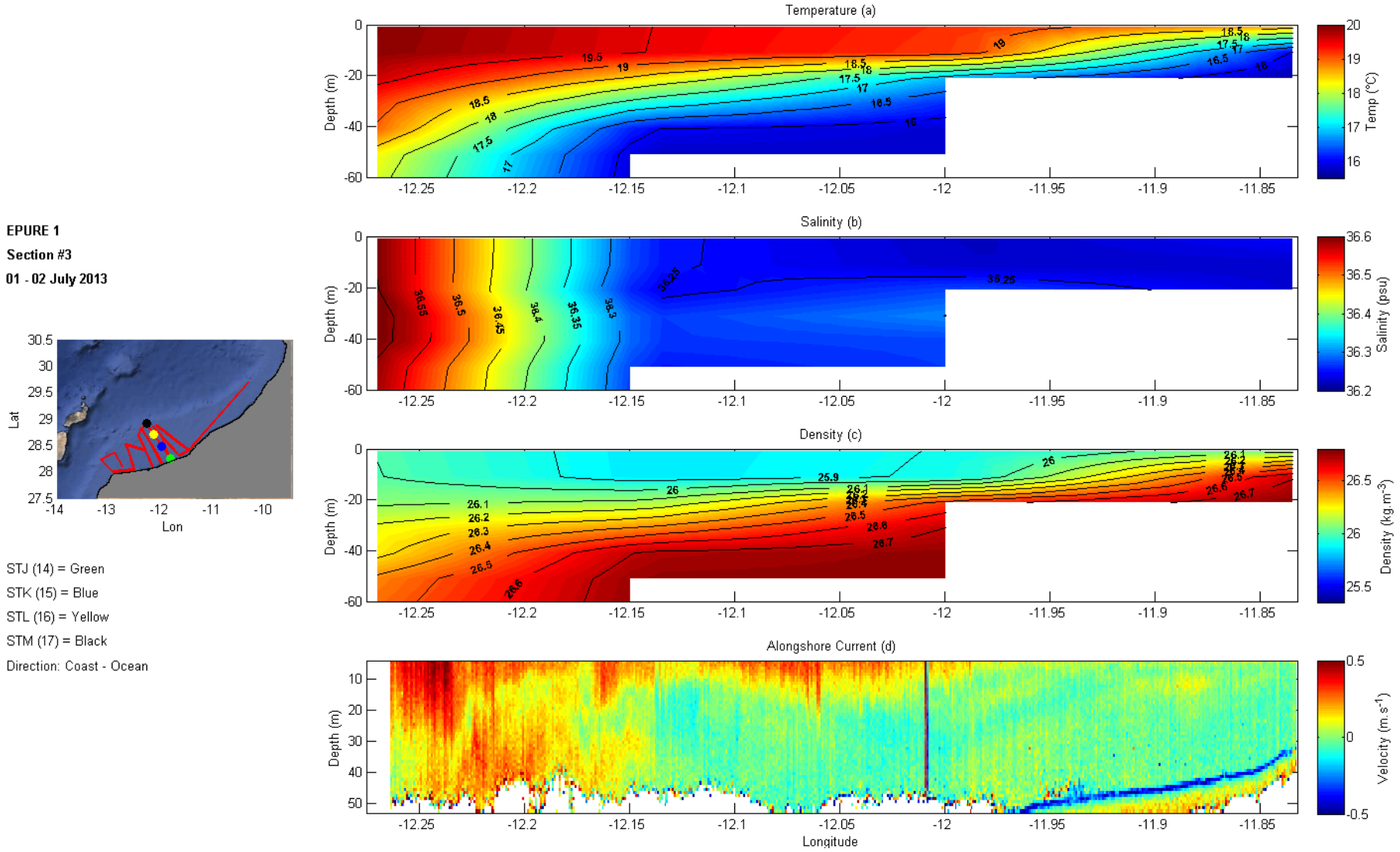

Figure 17: Vertical profiles for temperature, salinity, density and velocity at location G.

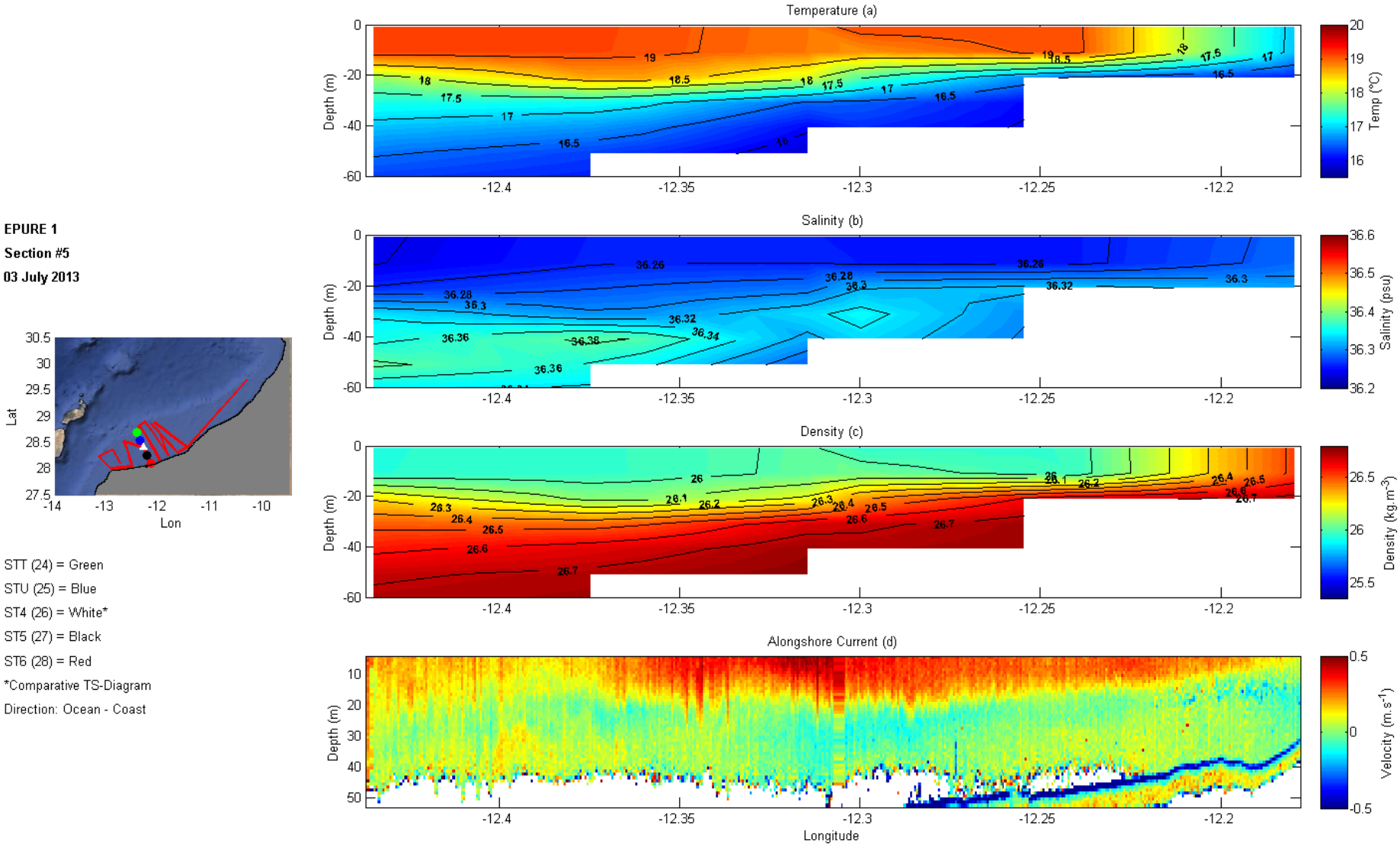

Figure 18: Vertical profiles for temperature, salinity, density and velocity at location E.

The vertical structure of the temperature, salinity and density fields along three Locations (I, G and E) are shown in Figures 16, 17 and 18.

The temperature at section I (Figure 16a), upwelling is evident within the whole map with all isotherms rising towards the coast between 11.92°W and 11.52°W. The thermocline outcrops near the coast (11.51°W) and is centred around the 17.5°C isotherm which is 45 m deep near 12.1°W. Between 12.1°W and 11.92°W the isotherms are more evenly spaced where their slope increases with depth.

There are clear signs of upwelling in the salinity field (Figure 16b). Between 11.92°W and 11.52°W there is a salinity inversion with a tongue of saltier water (36.3 psu) protruding inshore that is surrounded above and below by fresher water (36.25 psu). Between 12.1°W and 11.92°W the front is obvious between the 36.55 and 36.3 psu isohalines, which extend into an inshore salty tongue.

The density structure (Figure 16c) is similar to that of temperature and the pycnocline is at the same position as the thermocline along the 26.3 $kg.m^{-3}$ isopycnal. The 26 $kg.m^{-3}$ isopycnal outcrops at 12°W and 11.75°W.

Upwelling is evident throughout the temperature at location G (Figure 17a). Between 12.15°W and 11.84°W the thermocline is particularly sharp and centred around the 17.5 °C isotherm which is about 35m deep at 12.15°W and outcrops near the coast. Isotherms are gently sloping from 12.15°W to 11.95°W but the slope increases towards the coast eastward of 11.95°W. Between 12.27°W and 12.15°W the isotherms are more evenly spaced with flatter isotherms near the surface (19.5 °C at 20 m) and steeper isotherms at greater depths.

Salinity (Figure 17b) has no clear upwelling signal near the coast. Between 12.15°W and 11.84°W we observe saltier water (36.3 psu) deeper than 20m and fresher water (36.25 psu)

between the surface and 20 m. Between 12.27°W and 12.15°W there is a strong horizontal gradient between the 36.6 and 36.3 psu isohalines, approximatively over the shelf break.

The density field (Figure 17c) shows similar patterns as the temperature field: the pyncocline is located at the same depth as the thermocline. Between 12.27°W and 11.95°W the isopycnals have a slight positive slope with this slope increasing eastwards of 11.95°W towards the coast.

For temperature at location E (Figure 18a), the thermocline (centred around the 17.5 °C isotherm) remains horizontal between 12.45°W and 12.25°W at approximately 25 m depth. Eastward of 12.25°W the isotherms' slope increases until the thermocline outcrops near 12.2°W. East of 12.25°W there is also a strong horizontal gradient between the surface and 20 m depth with a weak localized upwelling. The 19 °C isotherm outcrops at 12.3°W and 12.24°W.

The salinity distribution along this location is shown on figure 18b. The salinity gradient near the coast is weak but discernible. Between 12.45°W and 12.25°W the most striking features are the tongues of salinity inversion. The first one is a patch of saltier water at 40 m depth (12.3°W) within the 13.34 psu isohaline. This patch corresponds to the circular patch on Figure 14c at 28.5°N 12.4°W. The strongest centre of inversion is at 50m between 12.45°W and 13.35°W that is delineated by the 36.34 psu isohaline with the centre of the patch reaching a salinity of 36.38 psu. This inversion also corresponds to Figure 17c.

Density (Figure 18c) and temperature (Figure 18a) show similar patterns. The pycnocline (centred around the 26.3 $kg.m^{-3}$ isopycnal) and the thermocline lies approximatively at the same depth. We observe the same flatness of isopycnals between 12.45°W and 12.25°W. East of 12.25°W there is a vertical horizontal gradient as well as the outcropping of the 26 $kg.m^{-3}$ isopycnal between 12.3°W and 12.24°W.

3.1.1.3. Velocity Field

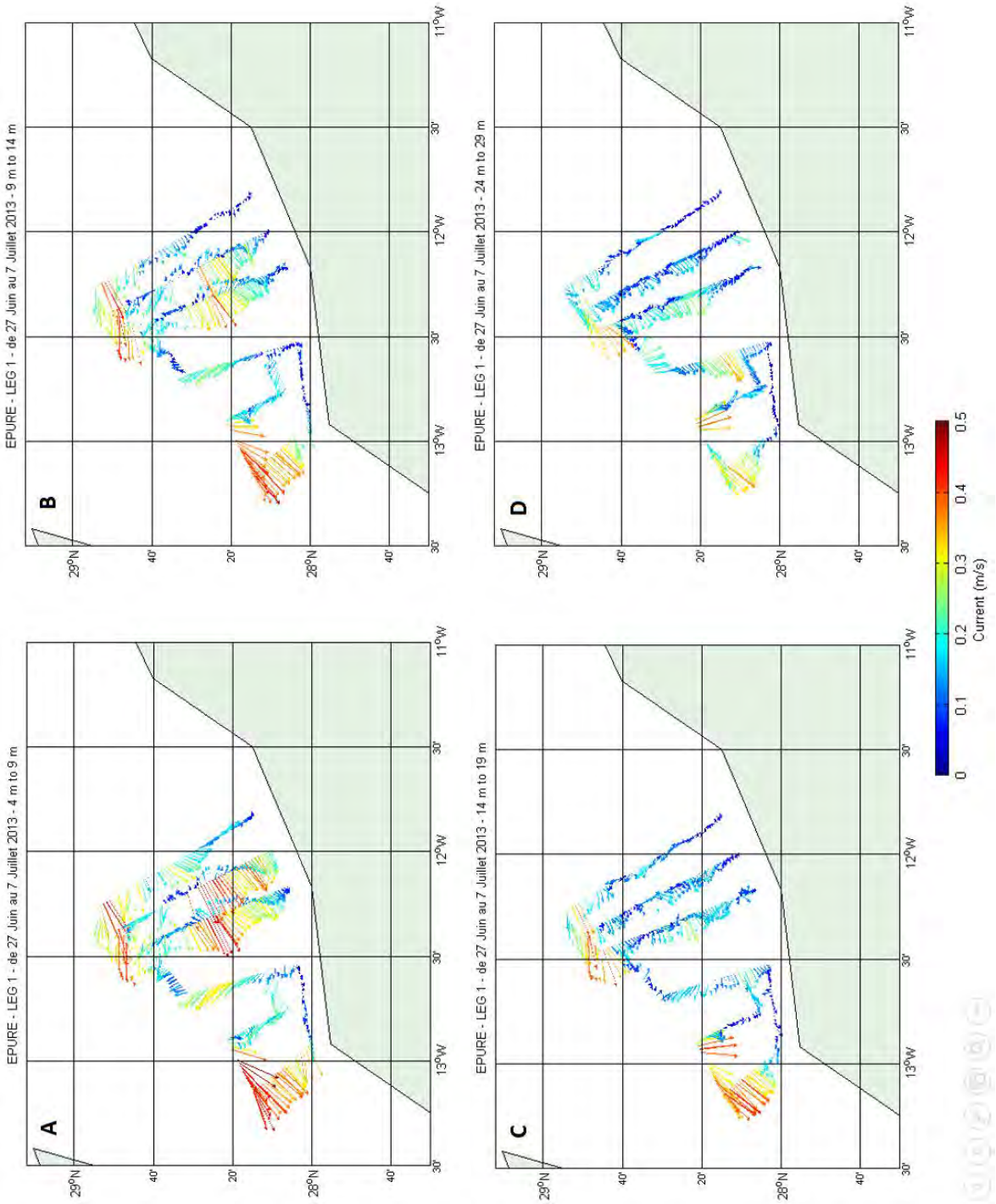

Figure 19: Velocity field for Epure 1. Two profiles are excluded due to ADCP malfunction.

The vertical structure of the along shore current at location G is shown in Figure 17d. Between 12.125°W and 12°W there is a strong vertical shear between 10 and 20 m with a maximum surface velocity of 0.5 $m.s^{-1}$ that decreases with depth to 0 $m.s^{-1}$ below 20m. West of 12.125°W (near the salinity front described in the previous map), the flow is less intense and appears to be more barotropic.

Along location E (Figure 18d), the along shore current is strongly vertically sheared. Between 12.375°W and 12.2°W there is a very strong along shore current between the surface and 20 m depth reaching velocities of 0.5 $m.s^{-1}$ at the centre of the jet.

Figure 19 shows the velocity field at 4 depth levels (a: 4 to 9 m, b: 9 to 14 m, c: 14 to 19 m, d: 24 to 29 m) recorded over the six days of Epure 1. One striking feature of the velocity field is the presence of several zones of strong convergence and divergence.

A strong jet-like current is present near Cape Juby (28.25°N 13.15°W). It is surface intensified with velocities reaching 0.5 $m.s^{-1}$ near the surface, and decreasing to 0.35 $m.s^{-1}$ between 24 and 29m. At the northern extent of the surveyed area (28.85°N 12.35°W) there is a slightly surface intensified current that reaches velocities of over 0.4 $m.s^{-1}$ near the surface, and decreasing to approximately 0.35 $m.s^{-1}$ between 24 and 29 m. This current then exits the surveyed area in a westerly direction. It is possible that this current then meanders in a south westerly direction around the edge of the surveyed zone and connects to the Cape Juby current at 28.25°N 13.15°W.

There is another current with a strong surface velocity that is observed at 28.35°N 12.18°W and 28.35°N 12.28°W. This current is strongly vertically sheared with surface velocities reaching 0.5 $m.s^{-1}$ and then rapidly decreasing to less than 0.2 $m.s^{-1}$ between 14 to 19 m. It is possible that this current continues its westerly trajectory and then meanders in a north westerly direction at 28.45°N 12.7°W. Following this it may connect with the proposed trajectory of the

current described at the northern extent (28.8°N 12.35°W) and also connect to the Cape Juby current at 13.15°W 28.25°N.

3.1.1.4. Internal Waves

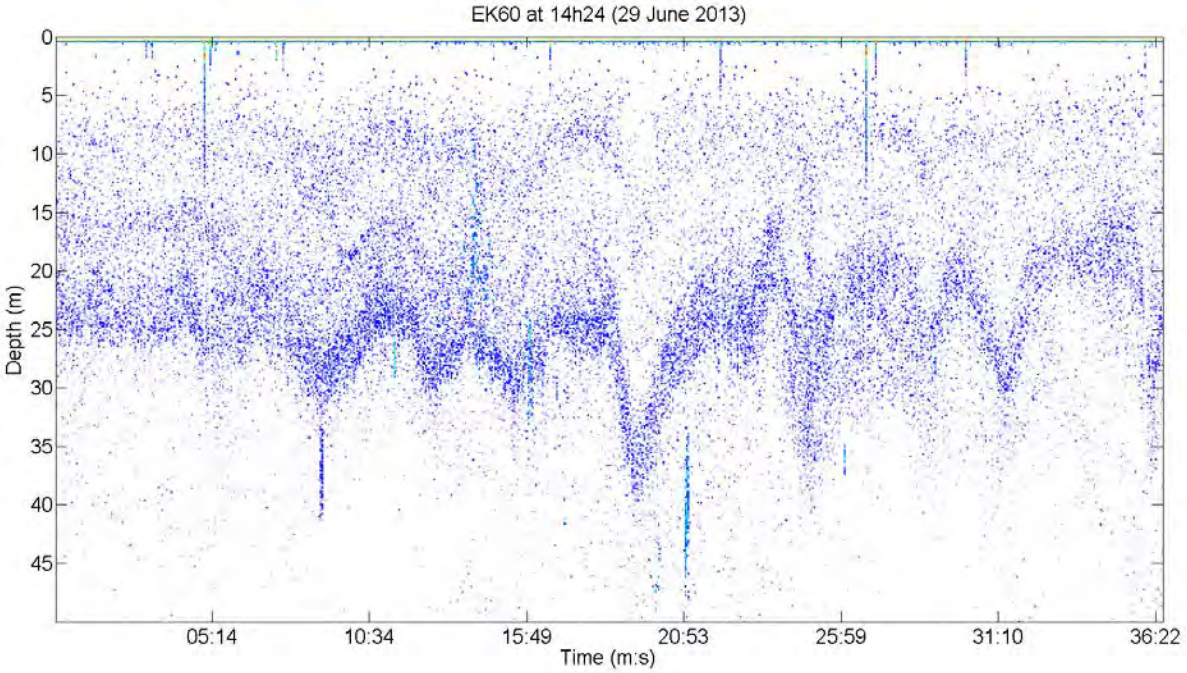

Figure 20: EK60 snapshot from E1 at Location I.

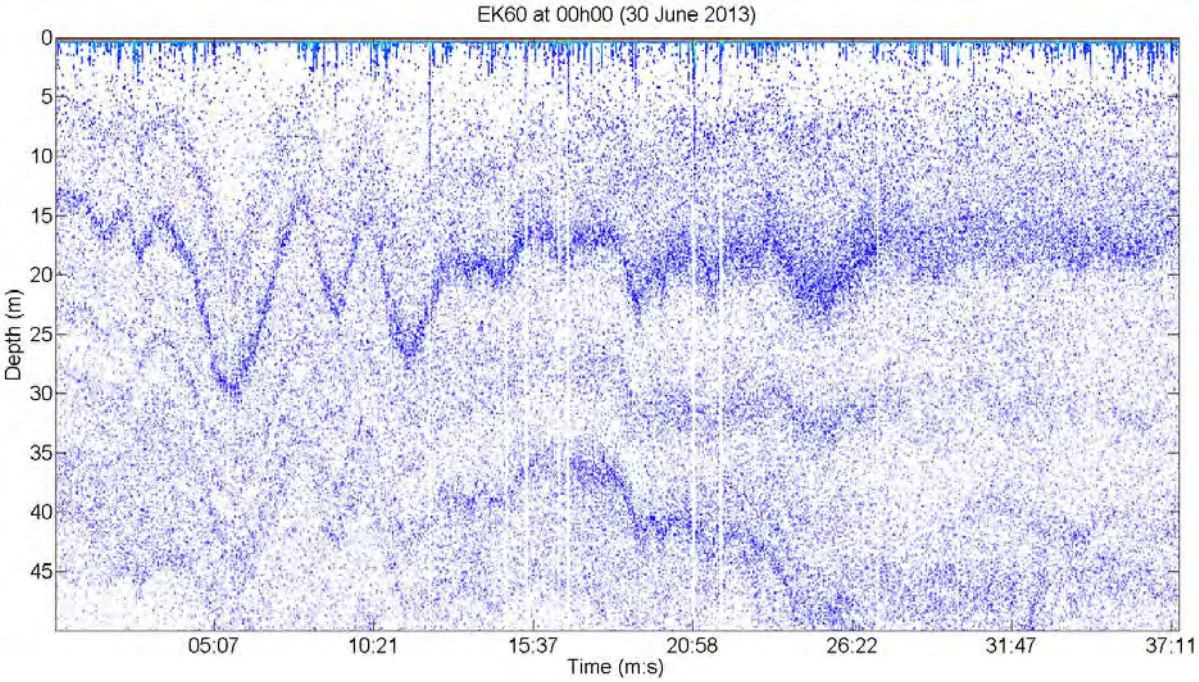

Figure 21: EK60 snapshot of E1 at Location G.

The acoustic data from the EK60 shows perturbations of the pycnocline (thick central line) for locations I and G in Figures 20 and 21 respectively. Over approximately 37 minutes, 700 pings were transmitted and received with each ping taking 3 to 4 seconds.

Figure 20 was recorded between 14:24:09 and 15:00:43 on the 29th of June 2013 over 36 minutes and 34 seconds (34 min 36 s). After 20 min 08 s, there is a vertical excursion of the pycnocline from 15 to 40 m deep. This is possibly a soliton or several internal waves in superposition. There are also six smaller deviations of the pycnocline between 20 and 30 m.

In Figure 21 the measurement started at 00:00:22 on 2nd July 2013 end at 00:37:46 on the same day with a duration of 37 min 24 s. There is a large displacement of the pycnocline after 05 min 07s where the pycnocline dips from 15 to 30 m. Between 07 min 43s and 12 min 58s there appear to be two smaller waves between 15 and 25 m.

3.2.2. Epure 3

3.2.2.1. Context

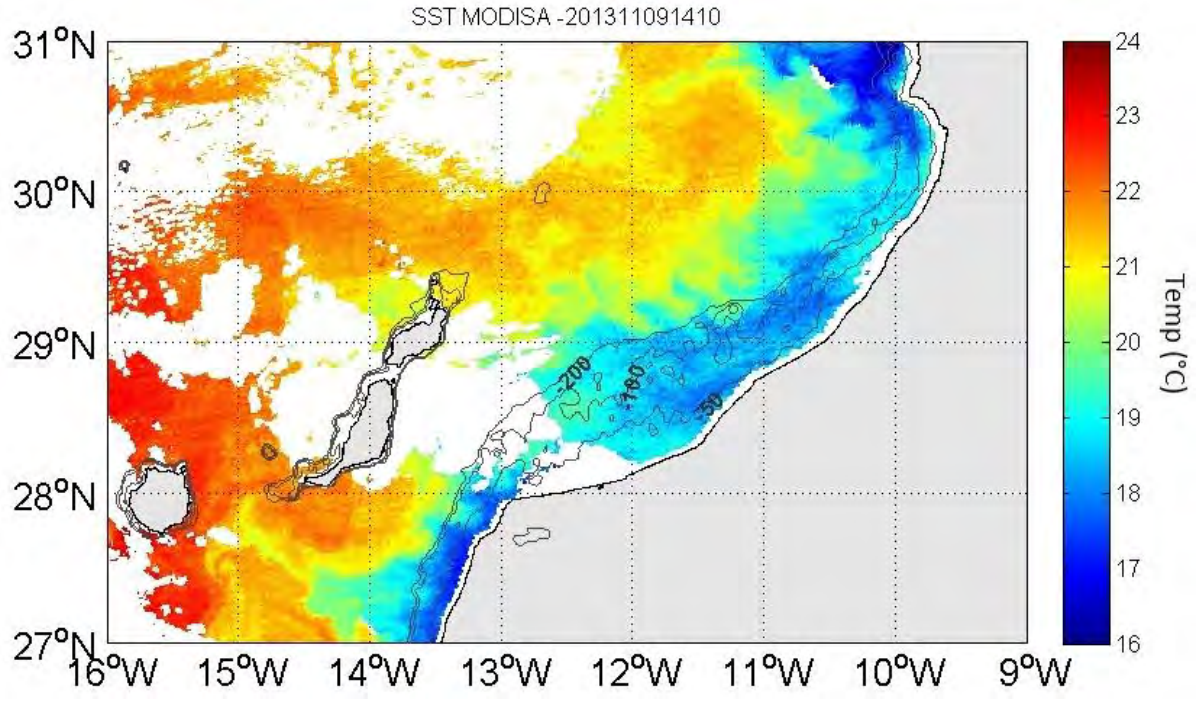

Figure 22: SST on 9 November 2013 at 14h10.

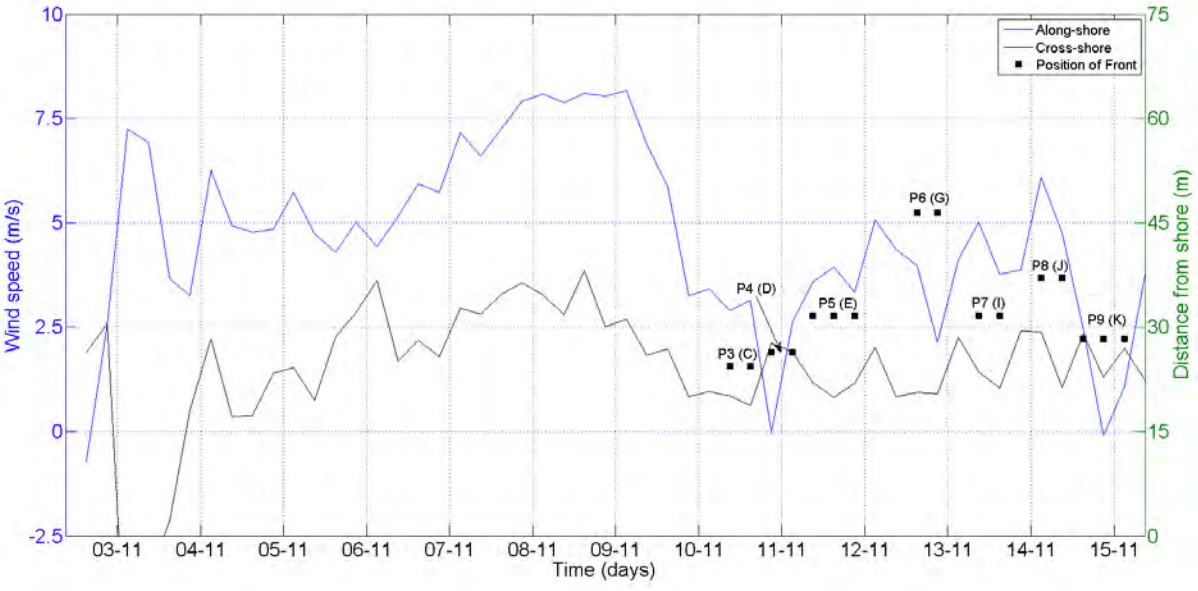

Figure 23: Position of the front in relation to along and cross-shore wind before and throughout E3.

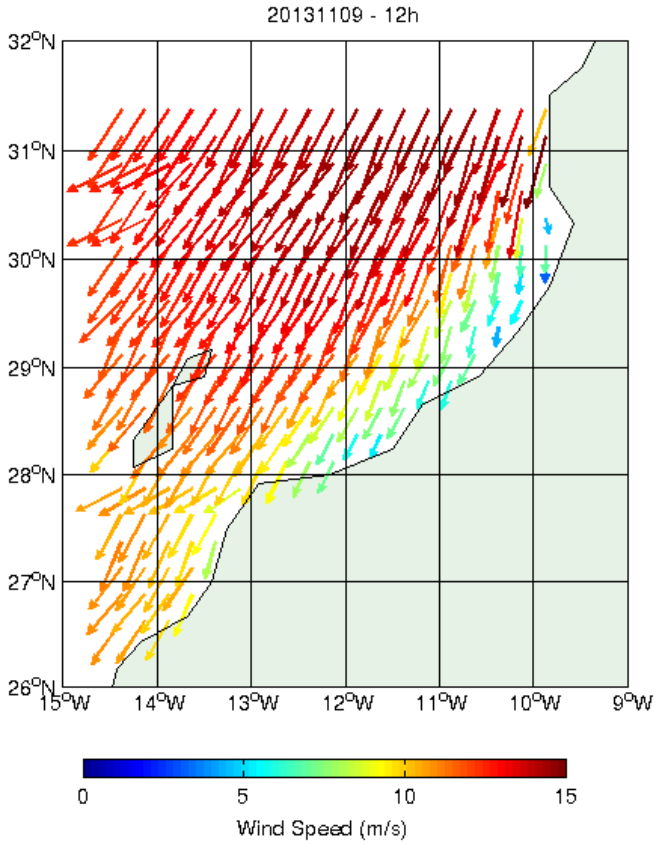

Figure 24: Surface wind speed on 9 November 2013 at 12h00.

Figure 22 shows the sea surface temperature on 9 November 2013 at 14h10, roughly 24 hours before the E3 cruise. Three zones of enhanced upwelling are obvious on the map : a large patch centred near 30.5 °N 10°W , the region just south of Cape Juby from 27.95°N 13°W to 27°N 13.5°W and the coastal region near 29.5°N 11.7°W with coastal temperatures ranging between 17 and 18 °C inshore of the 200 m isobath. Mesoscale activity, obvious as complex eddy and filament-like SST patterns are obvious near 28.4°N 12.3°W. A filament extends from 27.45°N 14.5°W to 27.8°N 15.1°W with a surface temperature of approximately 21 °C. There are warm and cool patches of water just offshore of the upwelling regions that are likely to be eddies.

The intensity of along and cross-shore wind stress for the duration of E3 (10 – 15 November) and eight days prior to the survey (3 – 9 November) is shown on Figure 23. The long period of sustained positive along shore wind indicates favourable conditions for strong upwelling to develop although the wind eventually became erratic and varied between individual locations.

Early on the 3rd the along shore wind is 7.4 $m.s^{-1}$ and falls over the next few days until it then increases from the 6th to reach 7.4 $m.s^{-1}$ again on the 7th, 3 days before sampling begins. Over the next 48 hours the along shore wind further increases to 7.6 $m.s^{-1}$ on the 9th, 24 hours before recording begins. At noon on the 10th the wind is 2.65 $m.s^{-1}$ and then falls to 0 $m.s^{-1}$ just before midnight of the 11th. For the rest of the recording period the along shore wind becomes very erratic. For the next 26 hours it increases to 5 $m.s^{-1}$ just after midnight of the 12th and then drops to 2.4 $m.s^{-1}$ just before midnight of the 13th. The 13th then sees a rise to 5 $m.s^{-1}$ at noon. In the early hours of the 14th the along shore wind is approximately 6.2 $m.s^{-1}$ and then rapidly falls to 0 $m.s^{-1}$ in very late evening of the same day. From the late hours of the 14th the along shore wind rises to 2.5 $m.s^{-1}$ at the beginning of the 15th.

Figure 24 shows a wind velocity map of the 9th November 2013 at 12h00 which is around 2 hours before Figure 22 was taken. There is strong wind offshore while the wind is weaker near the coast. Near Cape Juby (28 °N 13 °W) the wind appears to be slightly more along shore consistent with the stronger upwelling as inferred from SST in Figure 22 at 27.95°N 13°W to 27°N 13.5°W.

3.2.2.2. Hydrography

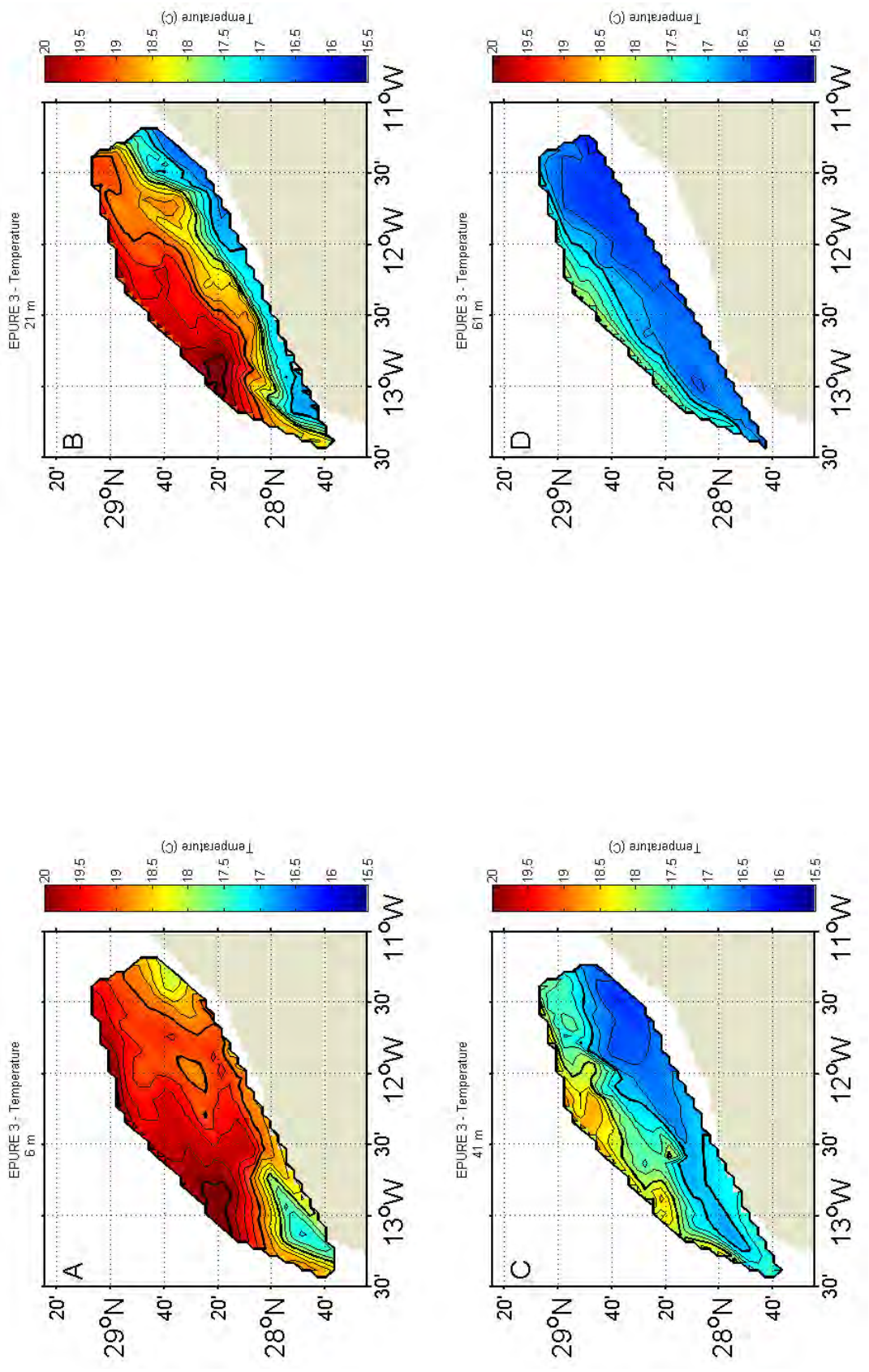

Figure 25: Temperature horizontal maps for Epure 3 cruise from 87 CTD stations. Thick contours represent 1 °C intervals and thin contours represent 0.25 °C intervals.

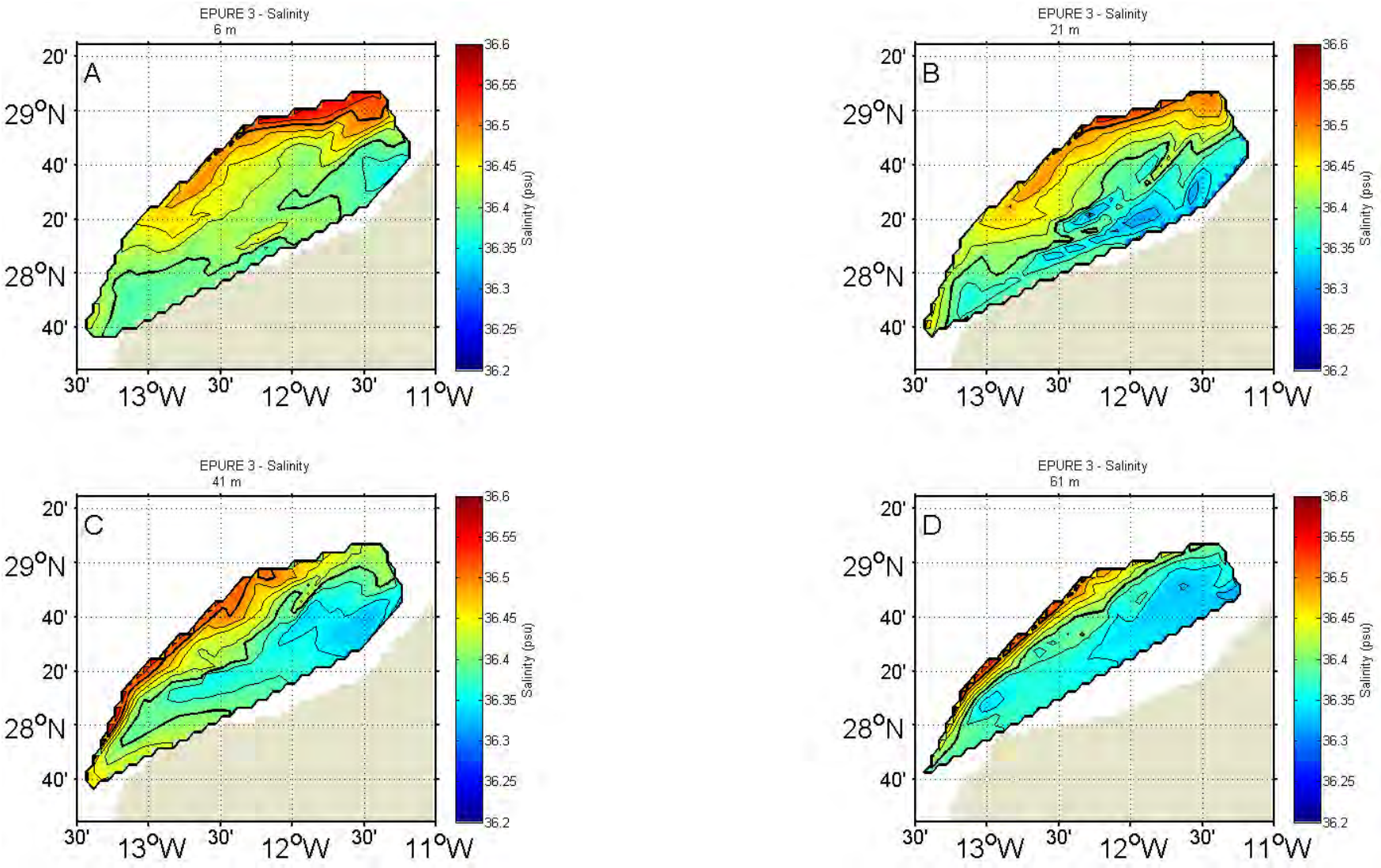

Figure 26: Salinity horizontal maps for Epure 3 cruise from 87 CTD stations. Thick contours represent 0.1 psu intervals and thin contours represent 0.025 psu intervals.

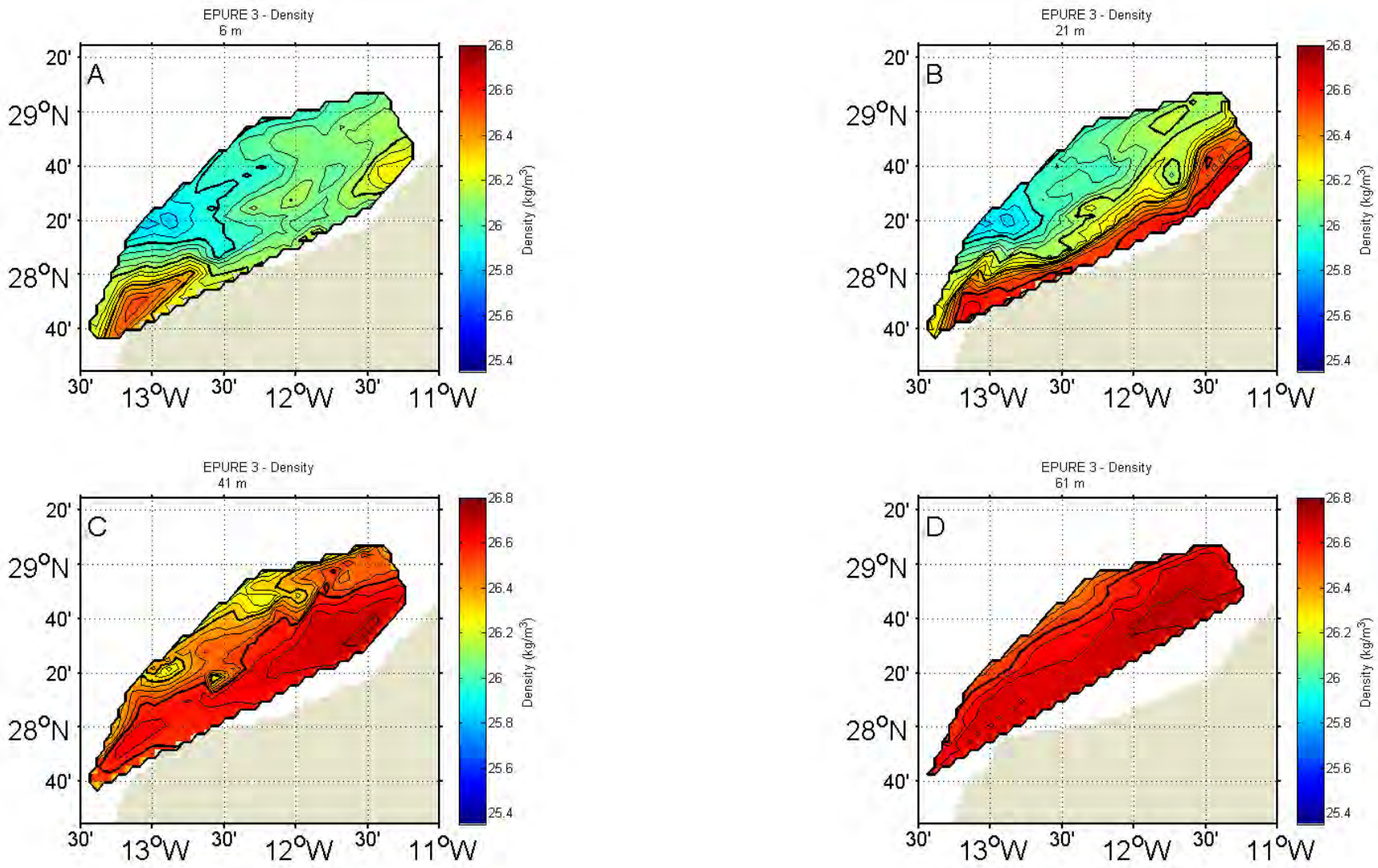

Figure 27: Density horizontal maps for Epure 3 cruise from 87 CTD stations. Thick contours represent 0.2 kg.m-3 intervals and thin contours represent 0.05 kg.m-3 intervals.

Figure 25 (a,b,c,d) shows horizontal maps of temperature at respectively 6, 21, 41 and 61 m. At 6 m, despite a high spatial variability, there is evidence of localized upwelling at the southern extent of the surveyed area just offshore of Cape Juby (27.8°N 13.15°W) where there is a small patch of cold water delimited by the 17.125 °C isotherm between 28°N 13.25°N and 28°N 12.5°W. North of the Cape Juby upwelling cell there is an area of warm water (near 28.35°N 12.95°W) enclosed within the 20 °C isotherm. There is also a second zone of less intense upwelling at the eastern extent of the surveyed area within the 19 °C isotherm (28.9°N 11.35°N to 28.35°N 11.65°W). The centre of this zone has a temperature of 18.125 °C (28.65°N 11.4°W).

At 21 m there appears to be a well-defined upwelling front with a significant along shore orientation that is centred around the 18 °C isotherm. The front enters the surveyed area at 28.65°N 13. 4°W and meanders towards an along shore orientation to 28.9°N 11.35°W. Near 27.8°N 13.15°W, a patch of cooler water is obvious inshore of the 17 °C isotherm. Between 28.35°N 11.75°W and 28.65°N 11.25°W there is an elongated patch of cooler upwelled water within the 16.75 °C isotherm. Around 28.35°N 12.95°N, a patch of warm water is enclosed within the 20 °C isotherm.

At 41 m the front becomes less obvious with more mesoscale and sub-mesoscale structures. However, there is a large cool patch of water enclosed within the 16.5 °C isotherm near 28.5°N 11.7°W. At the northern extent of the surveyed area (28.9°N 12.25°W) there is a zone of warmer water offshore of the 18 °C isotherm. At 61 m the along shore front broadens but is still discernible and centred around the 17 °C isotherm between 27.8°N 13.35°W and 29.1°N 11.55°W.

Figure 26 (a,b,c,d) shows horizontal maps of salinity at respectively 6, 21, 41 and 61 m. The distribution at 6 m shows high spatial variability. There is a narrow strip of saline water (36.5

psu) at the northern extent of the surveyed area (28.95°N 12.25°W to 29.1°N 11.45°W). A patch of less saline water is delineated by the 36.375 psu isohaline at 28.65°N 11.4°W. There is also a small patch of slightly more saline water is observed near the coast (28.28°N 12.25°).

At 21 m there are three patches of less saline water of approximately 36.35 psu (28.35°N 12.35°W, 28.3°N 11.95°W and 28.5°N 11.1°W). The most saline of these patches (observed at 28.28°N 12.25 at 6 m) is smaller but visible within the 36.4 psu isohaline. At the northern extent of the surveyed area there is a strip of more saline water (28.9°N 12.35°W to 29.1°N 11.75°W) with salinity greater than 35.5 psu.

At 41 m there appears to be a salinity front with an along shore orientation that separates saline water offshore (over 36.5 psu) along the north eastern boundary of the surveyed region with less saline water inshore. The front is centred along the 36.425 psu isohaline which starts near 27.8°N 13.35°W and runs to 29.1°N 11.5°W. There is a large patch of less saline water centred at 28.5°N 11.6°W that is delineated by the 36.35 psu isohaline.

At 61 m the front becomes more obvious. The front retains its along shore orientation and is now centred around the 36.4 psu isohaline, just over the shelf break.

Horizontal maps of density at respectively 6, 21, 41 and 61 m are shown on Figure 27 (a,b,c,d). Temperature and density have a similar distribution at all given depths with a sharp front offshore of Cape Juby (27.8°N 13.15°W) at 6 m. At 21, 41 and 61 m the along shore front holds the same positions for density and temperature. Salinity and density patterns show similarity at 41 and 61 m with a front located on the off shore extent of the surveyed region. This pattern is very similar to E1.

At 6 m there is a mass of dense water found south of the 26.2 $kg.m^{-3}$ isopycnal between 28°N 13.25°N and 28°N 12.35°W. At the centre of this delineation water density is 26.45 $kg.m^{-3}$ just offshore of Cape Juby at 27.8°N 13.15°W. North of Cape Juby there is a patch of less dense

water (28.35°N 12.95°W) enclosed within the 25.9 $kg.m^{-3}$ isopycnal. A small region of more dense water at the eastern extent of the surveyed area (28.9°N 11.4°N to 28.35°N 11.65°W) is delineated by the bold 26.2 $kg.m^{-3}$ isopycnal.

At 21 m there is strong front with a significant along shore component that is centred between the 26.2 and 26.6 $kg.m^{-3}$ isopycnals. The front enters the surveyed area at 28.65°N 13.4°W and meanders with an along shore orientation to 28.9°N 11.3°W. At 28.35°N 12.95°N there is a patch of less dense water within the 26 $kg.m^{-3}$ isopycnal.

At 41 m the front becomes less obvious but is still present with an along shore orientation. At 41 m there are three patches (two small and one large) of lighter water (28.35°N 12.95°W, 28.3°N 12.55°W and 28.85°N 12.25°W) that are all below 26.4 $kg.m^{-3}$. There is a patch of very dense water at 28.6°N 11.55°W shown within the 26.75 $kg.m^{-3}$ isopycnal.

At 61 m the orientation of the front is weak but discernible and retains an along shore orientation.

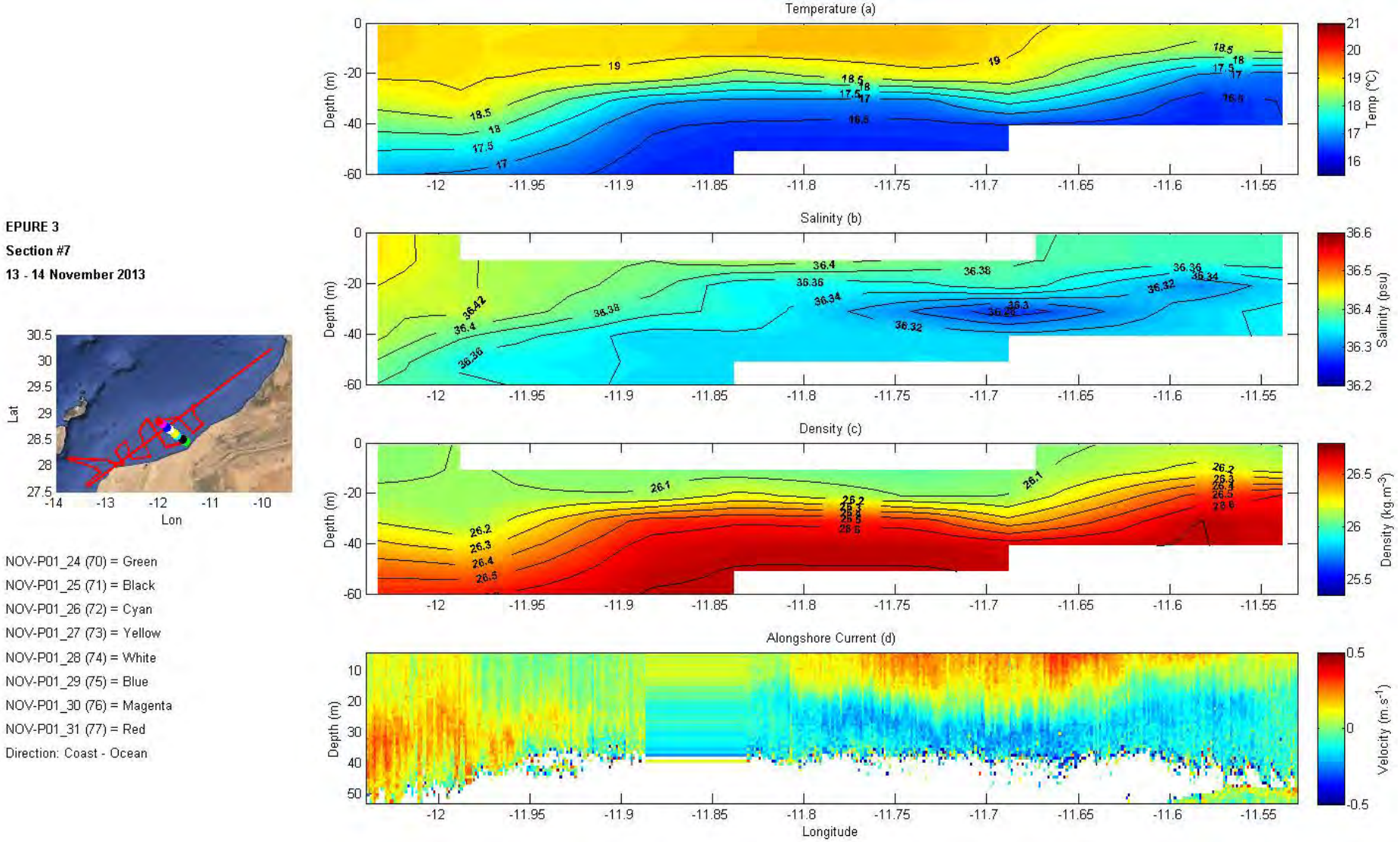

Figure 28: Vertical profiles for temperature, salinity, density and velocity at location I.

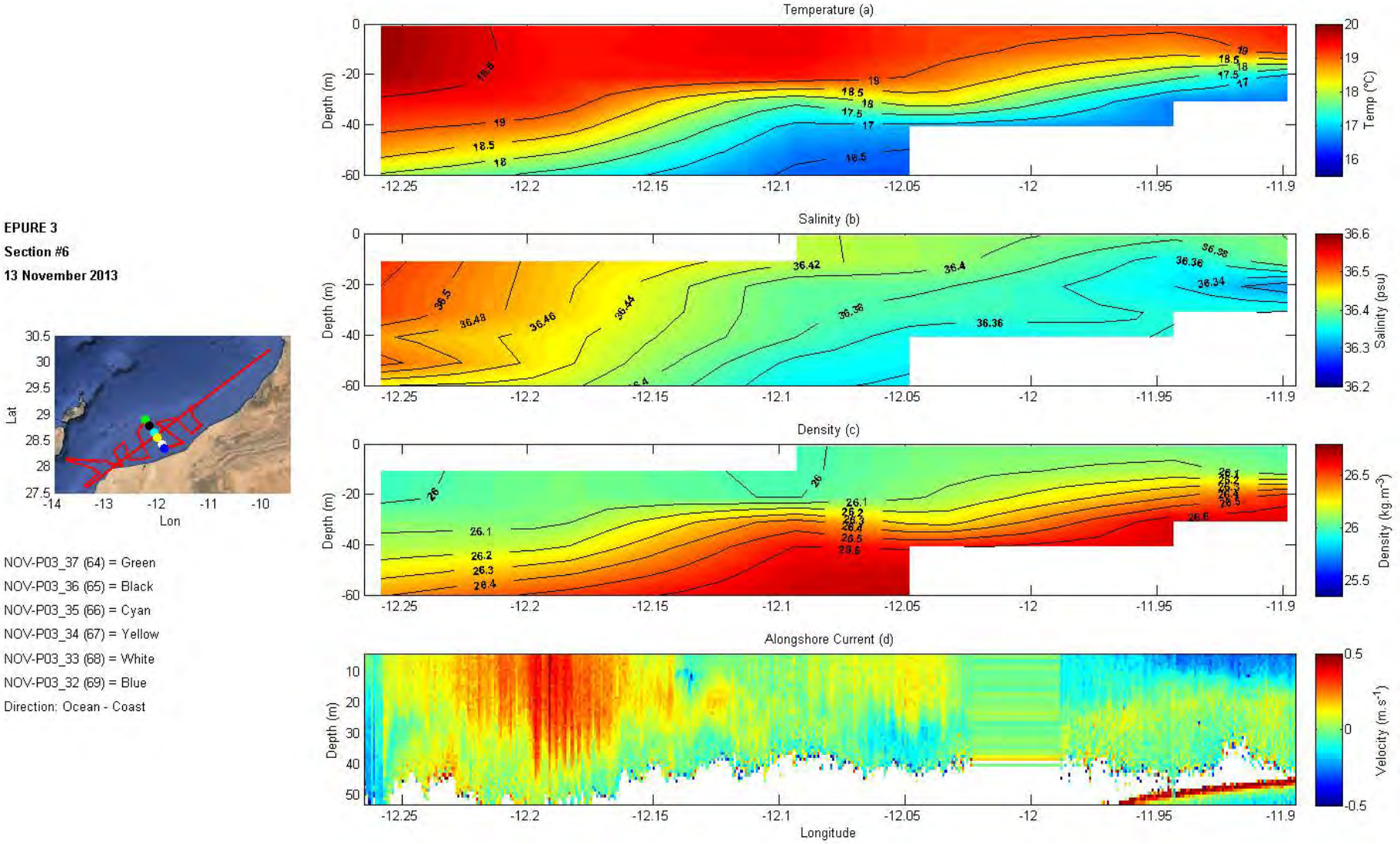

Figure 29: Vertical profiles for temperature, salinity, density and velocity at location G.

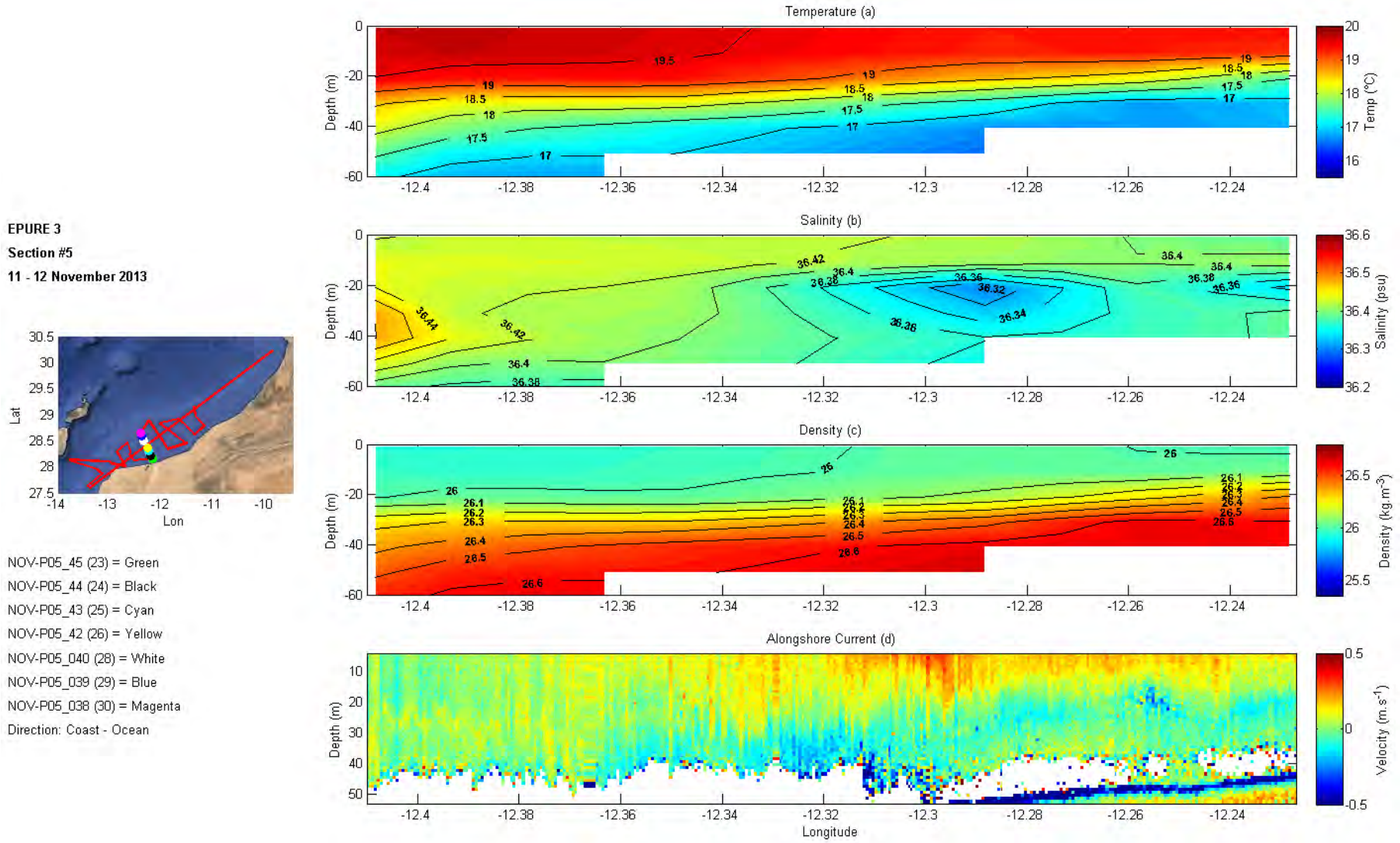

Figure 30: Vertical profiles for temperature, salinity, density and velocity at location E.

A more detailed view of the vertical distribution of temperature, salinity and density can be found in the vertical maps in Figures 28, 29 and 30.

Temperature in location I (Figure 28a) shows a net upward slope of the isotherms between 12.05°W and 11.55°W. The thermocline appears to be centred around the 18 °C isotherm. At 11.95°W the thermocline rises from about 45 m with sloping isotherms towards the coast up to a depth of 30 m at 11.9°W. Between 11.9°W and 11.75°W the isotherms are almost flat until 11.725°W. The isopycnals then take a negative slope and the thermocline drops to 40 m at 11.7°W. Eastward of 11.7°W the thermocline gradually rises to a depth of 20 m near the shore. The 19 °C isotherm also outcrops at 11.66°W.

The salinity map (Figure 28b) shows some anomalous points within the first few metres. These anomalies were likely caused by an increase in bubbles and were then removed from three of the CTD stations. Starting offshore (12.05°W) towards the coast (11.55°W) there is an overall decrease in salinity that follows no clear frontal pattern. The 36.38 psu isohaline outcrops at 11.68°W.The salinity map shows some high spatial variability and perhaps the most striking feature is the salinity inversion at 20 to 40 m between 11.775°W and 11.55°W. This tongue of fresher water is delineated by the 36.32 psu isohaline with the lowest salinity (36.28 psu) at 11.69°W at a depth of 35 m.

Density (Figure 28c) yielded some anomalous data at the same locations as salinity and this data was removed from three CTD stations. Density follows a very similar pattern to temperature with the same wavy orientation of the isopycnals. The pycnocline is centred along the 26.4 $kg.m^{-3}$ isopycnal. The 26.1 $kg.m^{-3}$ isopycnal outcrops at 11.64°W and 12°W.

The temperature map in location G (Figure 29a) is characterized by wavy isotherms that have a net positive in slope towards the coast (11.9°W). The 19.5 °C isotherm outcrops at 12.21 °C. The thermocline is centred around the 18 °C isotherm. The isotherms have a positive slope

between 12.25°W and 12.15°W. From 12.15°W to 12.05°W the isotherms flatten and become slightly negatively sloped. From 12.05°W to 11.9°W the isotherms become positively sloped again with the 19 °C isotherm nearly outcropping near 11.96°W.

Some data for the salinity map (Figure 29b) were anomalous and removed from one CTD station. The salinity distribution shows strong spatial variability with a weak horizontal gradient between 12.25°W and 12.1°W between the 36.52 and 36.4 psu isohalines. Between 12.1°W and 11.9°W there is a vertical salinity gradient between the 36.36 and 36.4 psu isohalines with the 36.4 psu isohaline outcropping at 12°W. Between 11.95°W and 11.9°W at 12 m deep there is a patch of low salinity within the 36.34 psu isohaline.

The salinity data error resulted in some anomalous density data which were removed from one CTD station. Density (Figure 29c) mainly behaves like temperature (Figure 29a). The pycnocline is centred around the 26.3 $kg.m^{-3}$ isopycnal. The 26 $kg.m^{-3}$ isopycnal outcrops at 12.08°W. The isopycnals have a positive slope between 12.25°W and 12.15°W. From 12.15°W to 12.05°W the isopycnals flatten and become slightly negatively sloped. From 12.05°W to 11.9°W the isopycnals slope upward towards the coast and then flatten eastwards of 11.95°W towards the coast.

At location E, the temperature map (Figure 30a) is very uniform with the thermocline centred around the 18 °C isotherm. The 18 °C isotherm is at 43 m deep at 12.41 °W and is slightly upwardly sloped moving east to the coast where it lies at 21 m deep at 12.23 °W. Most isotherms follow this sloping pattern with the exception of the 19.5 °C isotherm that outcrops at 12.33°W.

The salinity map (Figure 30b) is highly spatially variable with a patch of less saline water between 12.32°W and 12.27°W between 18 and 40 m deep within the 36.38 psu isohaline. This patch corresponds to Figure 26b at 13.25°N 12.29°W. At the western extent (12.41°W) there

is a small patch of saltier water within the 36.44 psu isohaline at 25 to 50 m deep. At the eastern extent (12.24°W) there is another patch of less saline water within the 36.36 psu isohaline at 20 to 30 m deep.

Density (Figure 30c) corresponds to temperature in its uniformity and slope of isopycnals. The pycnocline is centred around the 26.3 $kg.m^{-3}$ isopycnals. The density isopycnals are flat between 12.41°W and 12.3°W. Between 12.3°W and 12.23°W they have a slight positive slope towards the coast. The 26 $kg.m^{-3}$ isopycnal outcrops at 12.31°W and 12.26°W.

3.2.2.3. Velocity Field

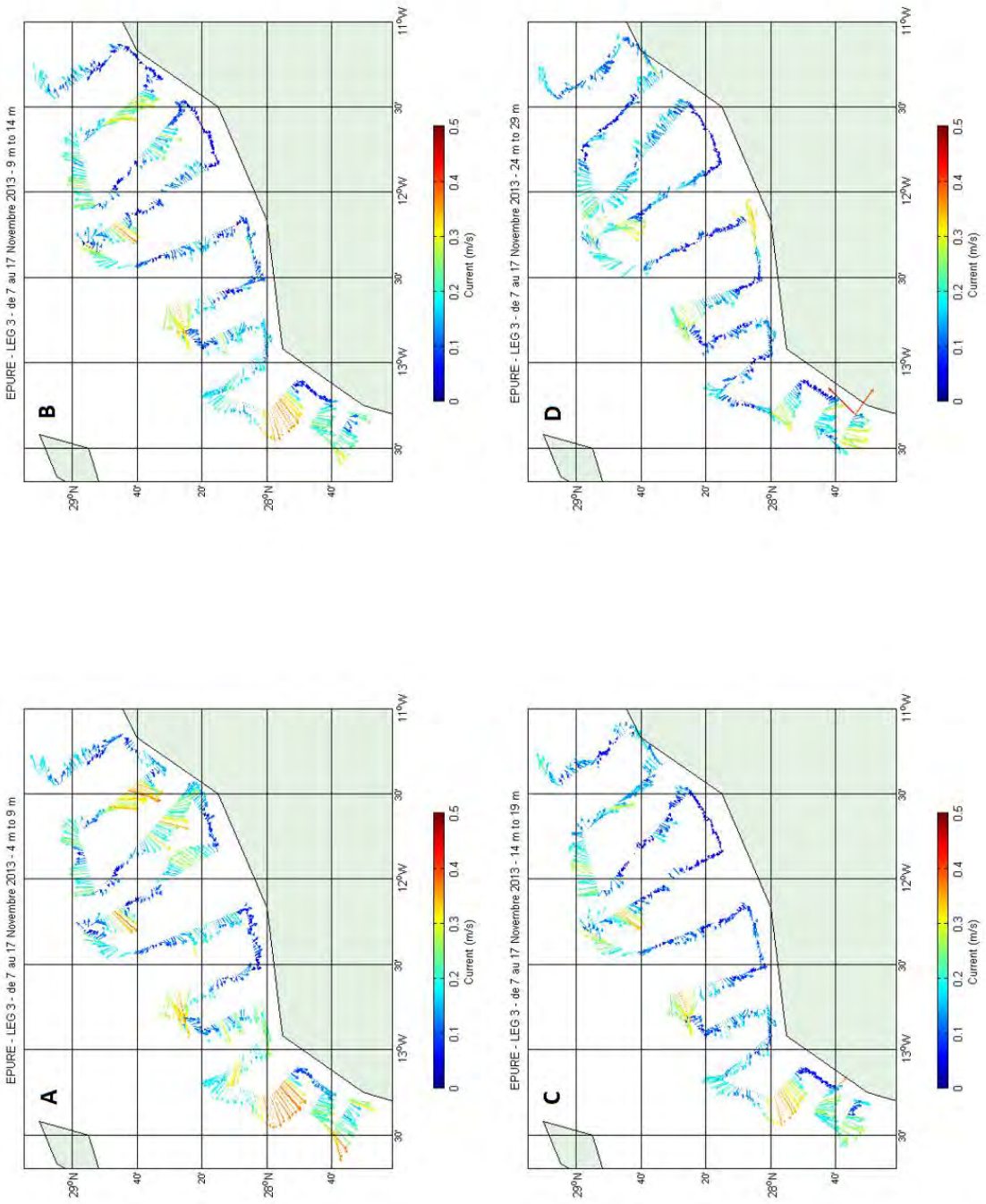

Figure 31: Velocity field for Epure 3

The detailed vertical structure of the current at locations I, G and E is shown on figures 28d, 29d and 30d respectively.

At location I, between 12.04°W and 11.98°W the alongshore current (Figure 28d) is almost barotropic with positive along shore velocities reaching over 0.4 $m.s^{-1}$ between 30 and 40 m. The most interesting point of this map lies between 11.8°W and 11.6°W where the current is vertically sheared with a positive along shore flow between 0 and 20 m, peaking at over 0.4 $m.s^{-1}$ near 11.65°W. Along the same transect (11.8°W and 11.6°W) between 25 and 40 m the current flows opposite to the surface in a negative (north east) direction with central velocities reaching 0.3 $m.s^{-1}$.

The along shore current at location G (Figure 29d) is very strong and jet-like between 12.24°W and 12.15°W where it flows in a positive along shore direction at velocities of up to 0.45 $m.s^{-1}$ between 0 and 40 m. Closer to the coast the current is vertically sheared between 11.95°W and 11.9°W where it flows at a speed of approximately 0.3 $m.s^{-1}$ in a north easterly (negative) direction. In the centre of the map, between 12.08°W and 12.035°W, the current flows in a southward along shore direction with speeds around 0.1$m.s^{-1}$ between depths of 0 and 30 m.

Location E shows along shore current (Figure 30d) that is vertically sheared from 12.32°W and 12.24°W between 0 and 30 m. At 12.3°W the current moves southward with along shore velocities of 0.4 $m.s^{-1}$. Between 12.41°W and 12.34°W the current is mostly barotropic with an average velocity of 0.1 $m.s^{-1}$. From 12.32°W to 12.25°W there appears to be a very slight counter current (northward) that is at 40 m deep at 12.32°W and shallower towards 12.25°W at 30 m. Overall the counter current is weak with speeds around 0.1 $m.s^{-1}$ and a small point of intensification of 0.25 $m.s^{-1}$ at 12.25°W at 20 m depth.

Figure 31 shows the velocity field at 4 depth ranges (a: 4 to 9 m, b: 9 to 14 m, c: 14 to 19 m, d: 24 to 29 m) from E3. Overall the currents have complex patterns, showing indications of mesoscale activity.

West of Cape Juby, there is a jet-like current that is surface intensified with velocities of 0.45 $m.s^{-1}$ at 4 to 9 m and decreasing to 0.25 $m.s^{-1}$ by 24 to 29 $m.s^{-1}$. This is the general pattern of sampled currents west of 13 °W. This pattern is most intense at 27.9°N 13.25°W.

At 28.9°N 12.25°W, an anticyclonic eddy is visible from 4 to 9 m and down to 24 to 29 m. Directly west, (28.9°N 12.1°W to 29°N 11.75°W) a strong current runs in a northerly direction with a velocity of approximately 0.25 $m.s^{-1}$ at all depth ranges.

Near 28.4°N 11.9°W the current flows north east with a velocity of almost 0.3 $m.s^{-1}$. At 28.58°N 11.7°W the velocity moves in a south westerly direction with a velocity of 0.3 $m.s^{-1}$. this structure is less obvious from 9 to 14 m is where the current at 28.4°N 11.9°W has reduced to less than 0.2 $m.s^{-1}$ and the current at 28.58°N 11.7°W is still strong (0.25 $m.s^{-1}$). At 14 to 19 m there is little activity for both of these currents. At 24 to 29 m the current at 28.58°N 11.7°W has reversed direction and now flows in a north easterly direction at 0.15 $m.s^{-1}$.

3.2.2.4. Internal Waves

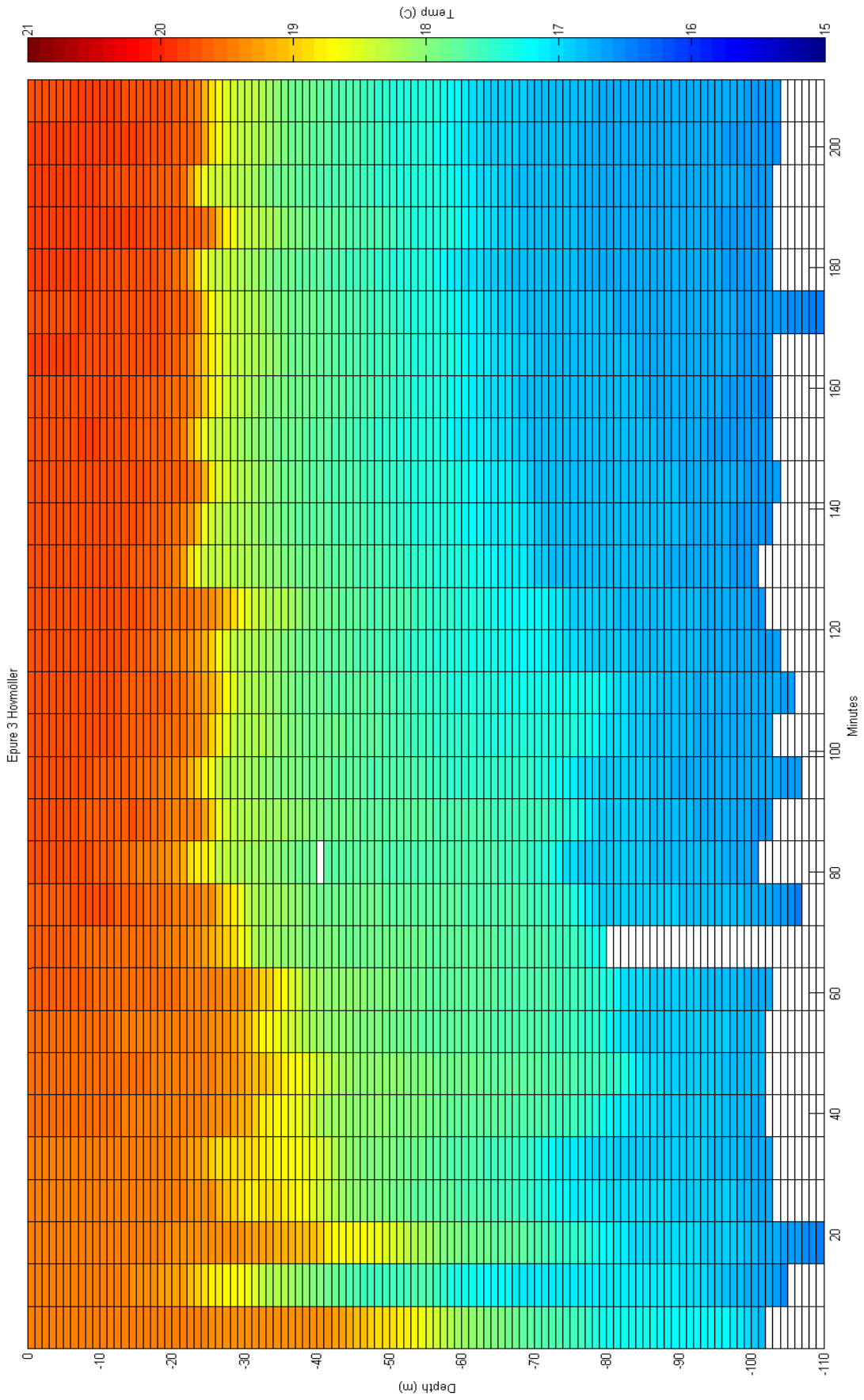

Figure 32: Hövmoller plot from 32 profiles at 28.888 °N 12.259 °W sampled on 12th November 2013 between 17h35 and 22h00 at location G.

Figure 32 is a hovmöller plot of repeated sampling at a fixed location which uses temperature as a proxy to detect perturbations of the thermocline that indicate the presence of internal waves or solitons.

The hovmöller plot shows a gradual sharpening of the thermocline from the first to the last of the 32 profiles. This is evident as the small yellow band (18.8 °C) decreases in size. At 200 minutes there is a shaper temperature gradient than at 20 minutes. The later profiles show a warmer surface temperature (20.5 °C) and cooler temperature at 90 m (16 °C). The first profile shows cooler temperatures at the surface (19.5 °C) and warmer temperatures at 90 m (17.5 °C)

The most striking feature occurs between 7 and 14 minutes (2^{nd} profile). Here the thermocline suddenly rises from 50 to 23 m and then drops back to 45 m in the 3^{rd} profile. This is possibly a sampling error but more likely to be a passing soliton or internal wave. The amplitude of the wave is roughly 25 m.

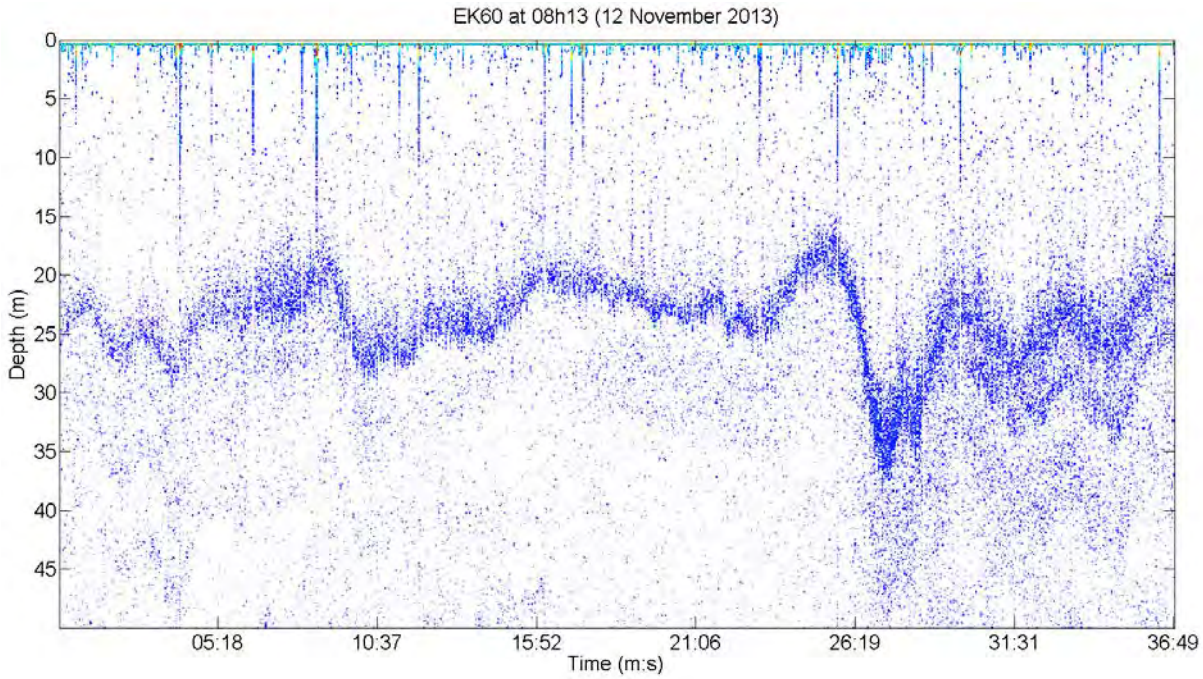

Figure 33: EK60 snapshot of Epure 3 Location E.

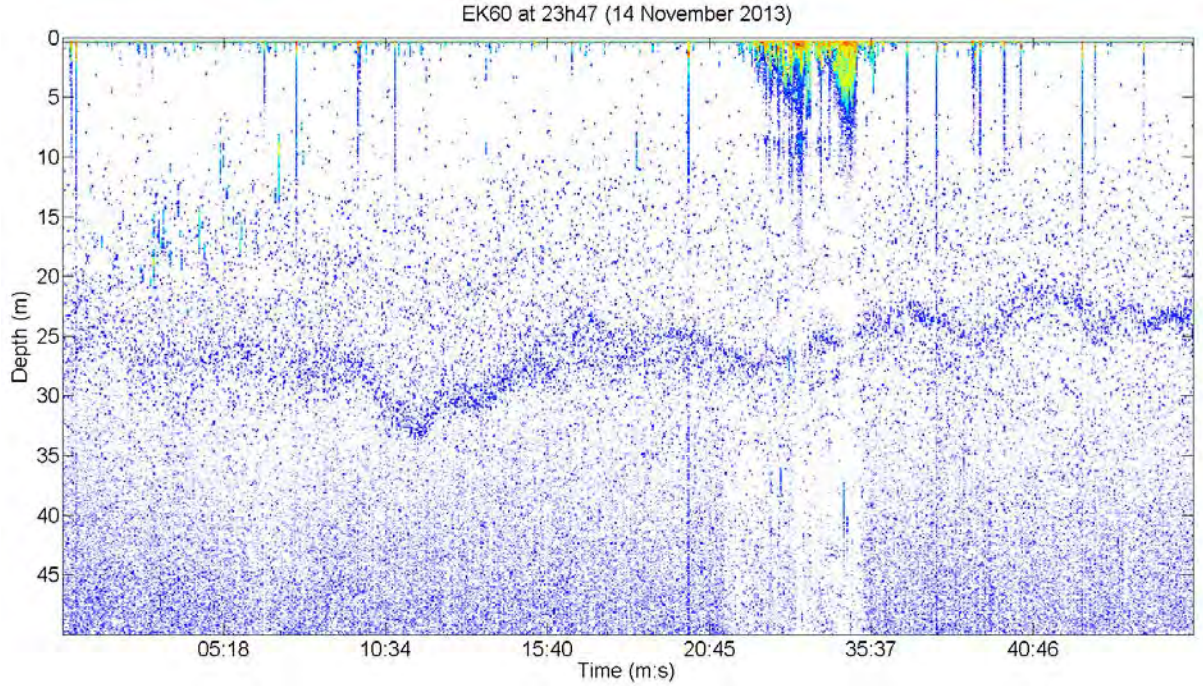

Figure 34: EK60 snapshot of Epure 3 Location I.

The acoustic data from the EK60 shows perturbations of the pycnocline (thick central line) for locations E and I in Figures 33 and 34 respectively.

Figure 33 at location E was recorded between 08:13 and 08:49 on 12 November 2013 for a duration of roughly 37 minutes. Between 22 min 30 s and 25 min there is a small rise in the pycnocline depth to 15 m and then a drop to 35 m at 27 min. The pycnocline then rises to 20 m at 29 min 30 s. There is also a drop in the pycnocline depth between 8 and 10 min where it falls from 18 to 28 m. These sharp fluctuations (especially after 27 min) indicate the presence of internal waves.

Figure 34 was recorded at location I between 23:47:33 (12th November) and 00:32:52 (13th November) over 45 min 19 s. The presence of bubbles between 22 and 35 minutes indicate that the vessel stopped over this time, possibly for brief CTD deployment. The pycnocline appears to be flat with minimal fluctuations. We observe a dip in the pycnocline after 09 min 47 s to 33 m and then an increase at 17 min 56 s to 25 m. Between 20 min 28 s and 36 min 14 s pings there is a rise in the pycnocline from 30 to 24 m. Between 39 min 49 s and 41 min 20 s there is a bubble shape in the pycnocline. In this figure the pycnocline is slightly harder to discern over the first 05 min 11 s (100 pings) indicating that there is potentially a low number of plankton to reflect the signal. Overall there is possibly evidence of internal waves. Evidence for internal waves is stronger in Figure 33.

3.2. Discussion

The hydrographic and velocity data show evidence of upwelling during both the E1 and E3 cruises. The situation was complicated by sub-meso to small scale patterns with intrusions of temperature and salinity inversions as well as convergence and divergence of the velocity field. Evidence of internal wave activity was also observed, which add a degree of complexity to the situation. However, the main patterns associated with the upwelling circulation were well identified and can be discussed and the physical processes responsible for the observed structure analysed.

3.2.1. Epure 1

There was evidence of coastal upwelling in SST, temperature and density, and little in salinity. This is supported in the vertical maps with rising isotherms and isopycnals towards the coast with no clear pattern observed with the isohalines. The horizontal maps showed evidence of upwelling that correspond to the SST. This pattern would be expected with the preceding days of strong, upwelling-favourable wind.

One of the striking features observed during Epure 1 was the absence of a strong upwelling front in the top 6 m while it remained defined at greater depths. This might be related to a combination of the wind variability and strong surface heat fluxes.

The most likely scenario is that the strong winds prior to field work drove strong coastal upwelling in the region. This winds then decreased prior to recording which would therefore decrease the following coastal upwelling. At the same time incoming solar radiation (insolation) warmed the surface of the water which would make the front difficult to discern at 6 m. We expect that between 6 and 21 m heat transfer declines and the temperature front corresponds to typical patterns of wind driven upwelling thereafter.

The presence of a surface jet that that entered the area with a south-westward direction, aligned with the coast and then meandered back offshore, was consistent with the density front patterns.

Another striking phenomenon was the presence of a shelf break upwelling, which is sometimes also known as a 'secondary upwelling', and has been previously observed in the MSR (Rossi *et al*., 2010). The shelf break upwelling is first observed in the SST and in the northern extents of the horizontal salinity maps. It is accompanied by a strong jet just offshore of the shelf break that meanders in a south-westerly direction.

The meandering coastal jet that seemed to exit the surveyed area might meander back toward the coast and merge into the strong current observed just off Cape Juby. The velocity data supports this hypothesis but it is not perfectly clear due to the influence of internal waves and sub-mesoscale variability which might account for the divergence of the current.

3.2.2. Epure 3

Epure 3 was surprising in that it mirrored Epure 1 in several ways yet still contained unique idiosyncrasies that could be attributable to seasonality or the apparent increase of sub-mesoscale and internal wave activity.

Evidence of coastal upwelling was present with the strongest upwelling occurring directly west of Cape Juby in a quasi-permanent upwelling cell. This pattern is reflected strongly in the temperature and density data, but little in the salinity data. In the vertical maps the isopycnals and isotherms rising towards the coast but did not outcrop. In the horizontal maps we observed a strong upwelling off Cape Juby at 6 m. The Cape Juby upwelling cell was much stronger because the coastline orientation changes south of Cape Juby to one more parallel to the predominant wind. Both the more upwelling favourable orientation of the coast at this location and the locally increased wind intensity might account for this enhanced upwelling cell.

The coastal upwelling front north of Cape Juby was also visible at 21 m but not at 6 m. Similar to Epure 1 this could be related to wind variability and surface heat fluxes. Along shore wind was strong for about three days until it suddenly decreased to almost 0 $m.s^{-1}$ 24 hours before field work began. The strong wind is expected to have driven strong coastal upwelling which would have slowed as the wind dropped. Furthermore we expect that as for E1, insolation caused strong heat fluxes, warming the surface water and preventing the outcropping of the isotherms and isopycnals closer to the coast.

The presence of a shelf break upwelling, detectable in the SST and the northern extent of the horizontal salinity maps is also an important feature of E3. At the shelf break upwelling there was an associated jet of water moving in a northerly direction at the northern extent of the velocity field which was not reflected in the density field. There was also a strong surface jet at Cape Juby that was flowing in a south westerly direction with an along shore orientation.

An increase in sub-meso to small scale patterns, in the form of eddies was obvious in the velocity field. Along with internal waves and the possibility of solitons in E3, they created further inconsistencies between the density and velocity fields but on the whole the hydrographic processes occurring during E3 are now clearer with further information on the presence of the Cape Juby upwelling cell.

3.2.3. Comparison of Epure 1 and Epure 3: The Seasonal Cycle

The most interesting similarity between the cruises is the presence of strong along shore winds that persist for several days and then suddenly decline 12 – 24 hours before recording. Surface heating from insolation (more in E3) has occurred in both cruises. The shelf break upwelling is only just observable in the northern extents of the salinity horizontal maps because the cruises use the continental margin as a turning point for each of the sections. If the cruise extended past the continental margin this could be further validated.

The existence of a shelf break upwelling is of particular interest because it can significantly enhance the production of a region and "directly influence waters exchange between the productive shelf and the open oligotrophic ocean" (Rossi *et al.,* 2010).

Figure 35 shows the position of the front for the cruises. Locations E to I are used for interpretation because they are juxtaposed and of similar orientation and length. The position of E1 is further from the coast than E3, this is because a larger amount of cooler water has upwelled and replaced the coastal water and therefore the front has moved further from the shore. Figure 35 also indicates that stronger upwelling was present for E1 however the impact of insolation may explain why the position of the front for E3 is closer to the shore. The wind prior to sampling was stronger in E3 than in E1 which would supposed upwelling to be stronger in E3. To further understand which upwelling event was stronger we recommend calculating the Ekman transport to elucidate this supposition.

The density horizontal maps are useful in explaining the velocity fields but can only partially explain the current processes. For example in E3 we clearly observe what appears to be an eddy

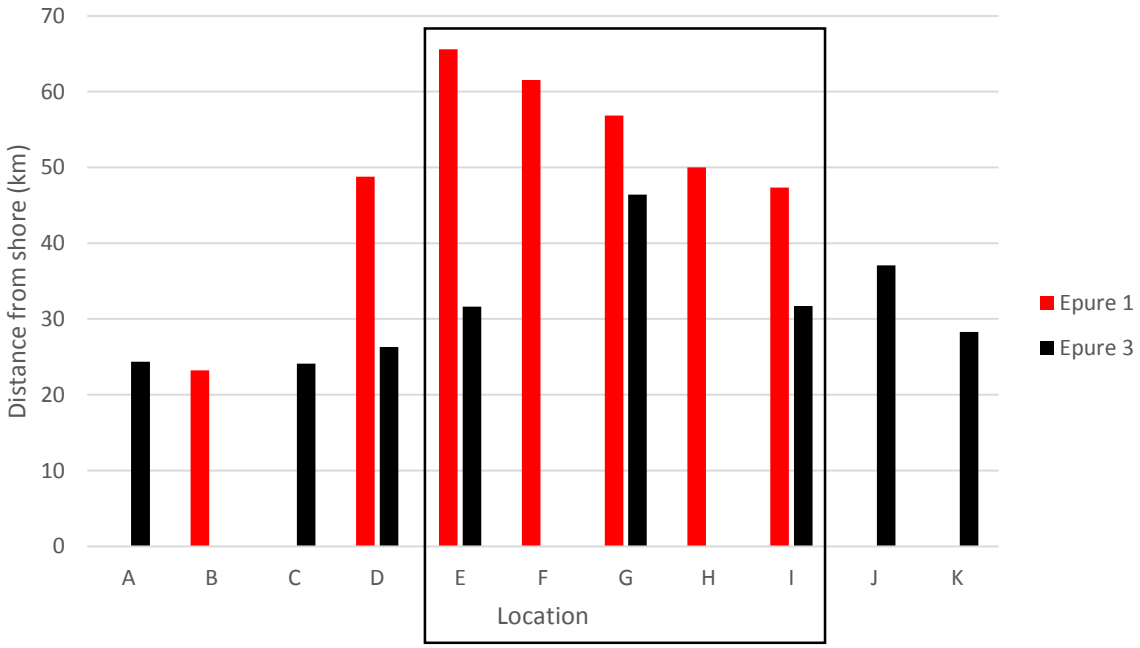

Figure 35: Position of the front for Epure 1 (red) and Epure 3 (black) for locations A to K. Locations E to I are used for interpretation.

at 28.9 °N 12.25°W in the velocity field (Figure 31) but on the density maps (Figure 27) there is no apparent evidence for this feature. However for both E1 and E3 the density maps correlate to the velocity fields and explain the jet like current just offshore of Cape Juby as well as the jet-like current in the northern extent of the sampled that connects to the Cape Juby jet (E1).

Both the SST maps show extensive evidence of sub-mesoscale to small-scale turbulence. There is also evidence of internal waves for both cruises (Figures 20, 21, 33 and 34). These waves are able to displace the pycnocline by up to 25 m within the space of 10 minutes. Furthermore the Hovmöller plot (Figure 32) shows a soliton passing a fixed point in less than 7 minutes with an amplitude of over 20 m.

The characteristics of internal waves are not fully resolved in this report. It is clear that they are present in the region and are able to strongly displace the pycnocline within a matter of minutes. Internal waves are likely to account for many of the anomalies observed. These include the temperature and salinity intrusions as well as non-corresponding regions between density and velocity.

Both cruises took several days to complete and therefore are aliased by spatial and temporal variability. The data at the western and eastern extents of the surveyed area was therefore small and sub-mesoscale activity could have a greater effect on the figures we generated.

Tidal current may also account for the possible zones of convergence and divergence in the velocity fields. The most notable zone of current convergence is in E3 (Figure 31) between 4 and 9 m at 28.5 °N 11.75 °W where adjacent transects show currents flowing directly against each other. The possibility of a tidal flow reversal between the two transect was taken in account. The strong baroclinity of the reversing current suggests that the barotropic tide cannot

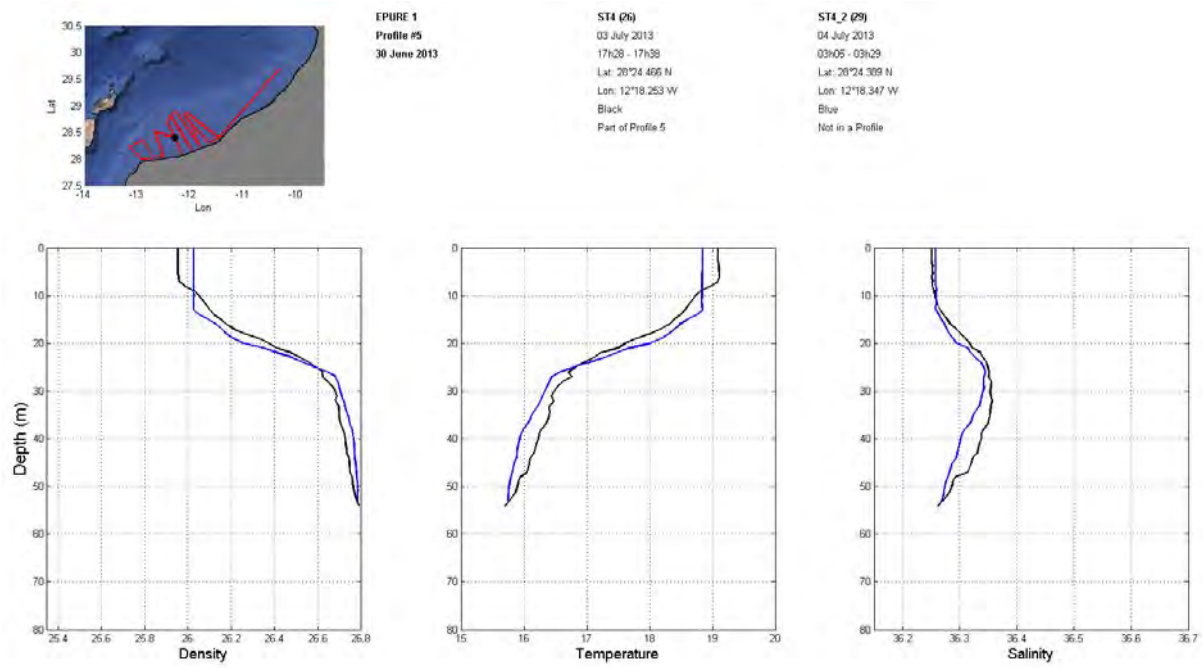

Figure 36: Vertical density, temperature and salinity profiles for CTD stations ST4 (day – black) and ST4_2 (night – blue) on Epure 1 Section 5 at location E.

be invoked to explain this phenomenon. Internal tide may however play an important role here. A more complete study of the internal wave field in the EPURE data could help to elucidate this matter.

Figure 36 shows one of the CTD stations (Location E) on E1 that was sampled twice to further understand the impact of temporal variability, especially day-night fluctuations. At 17h28 and then at 03h05 the next day the thermocline has increased in depth from 8 to 12 m in only 9 and a half hours. While the thermocline has changed position by approximately 4 m, the surface

and thermocline temperatures vary by 0.4 °C. There is little change in salinity within the first 25 m indicating that this cooling could be due to a decrease in solar radiation.

Data from World Ocean Atlas were downloaded was used to explore historical climatology. We must bear in mind that the cruises represent only a 'snapshot' of each season (E1 – summer, E3 – winter) and are too short to account for an entire season.

Figure 37 shows historical temperature patterns for the MSR. Upwelling is stronger in June, at the surface the 18.5 °C isotherm is visible between 29 and 31 °N. At 45 m in June the 17.5 °C isotherm is visible with an along shore orientations between 27 and 31 °N. In November upwelling is less intense where the 19.5 °C outcrops close to the coast between 29 and 31 °N (surface). At 45 the water is approximately 0.5 °C colder with upwelling centred north of 29 °N. This agrees with the literature where trade winds are said to be strongest in summer (Knoll

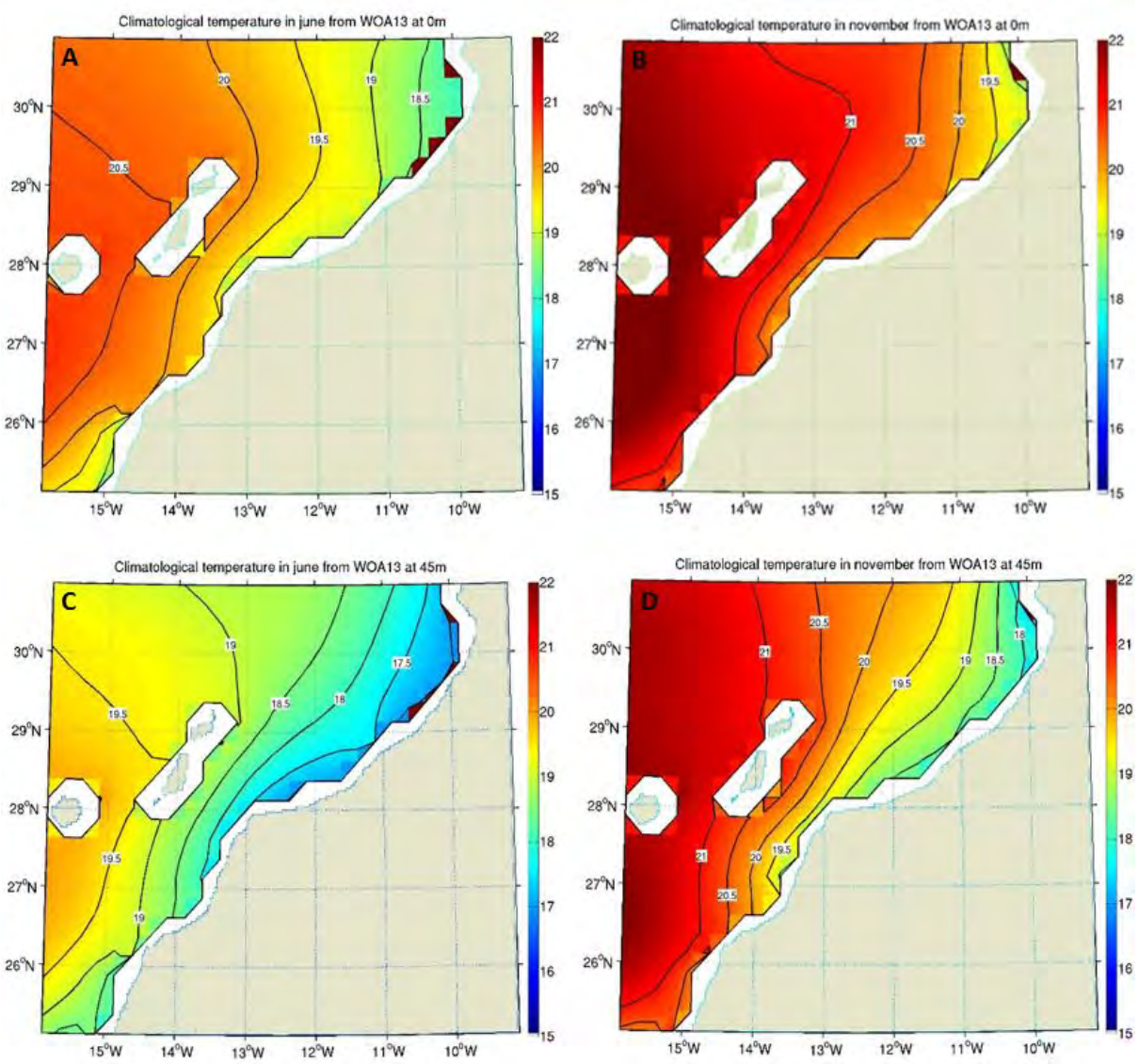

Figure 37: Horizontal maps for temperature from WOA13. (a) June surface, (b) November surface, (c) June at 45 m, (d) November at 45 m.

et al., 2002). The increased upwelling in the summer months corresponds to work by Arístegui et al. (2009) that shows Ekman transport to be strongest in the summer months for the MSR (Figure 4). The WOA13 data corresponds with the horizontal maps in this report where the surface temperature of the water is warmest in November (E3).

Figure 38 illustrates historical salinity patterns in June and November at 0 and 45 m. In June there is upwelling that shows similar patterns between 0 and 45 m where the 36.2 psu isohaline outcrops near the coast between 28 and 30 °N. In November the upwelling is less pronounced and the 38.3 psu isohaline outcrops close to the coast between 28.5 and 31 °N.

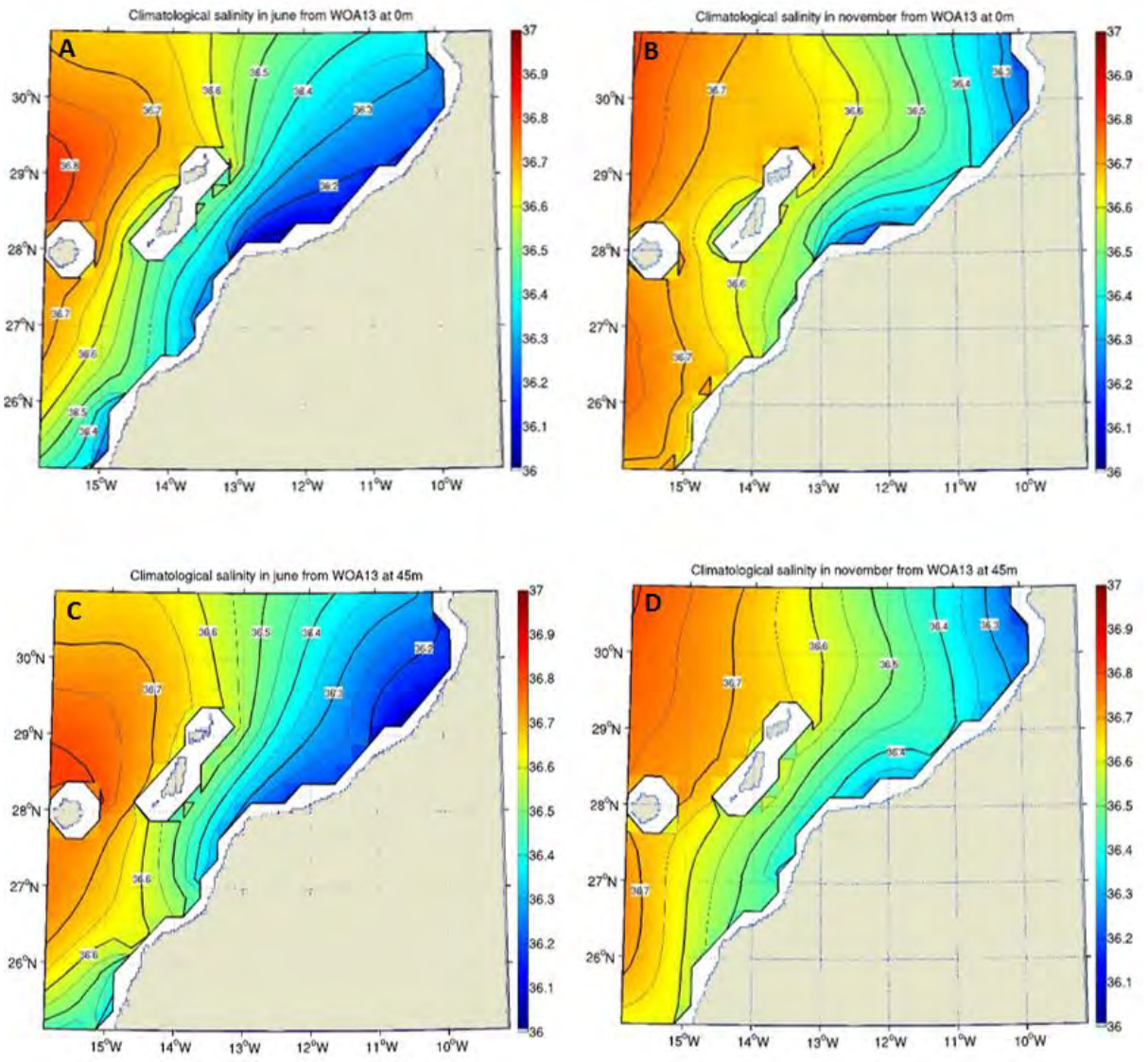

Figure 38: Horizontal maps for salinity from WOA13. (a) June surface, (b) November surface, (c) June at 45 m, (d) November at 45 m.

Temperature horizontal maps do not reflect upwelling near the surface because of insolation. With increasing depth the temperature front becomes increasingly along shore orientated in June and November. Salinity is not affected by insolation and we observe the salinity signature is largely unchanged.

Figure 39a shows WOA TS signatures for June in red and November in black. In June the data points are more widely distributed because less salty water is rapidly upwelled and then warmed via insolation. The stronger upwelling in June explains why there is a wide salinity

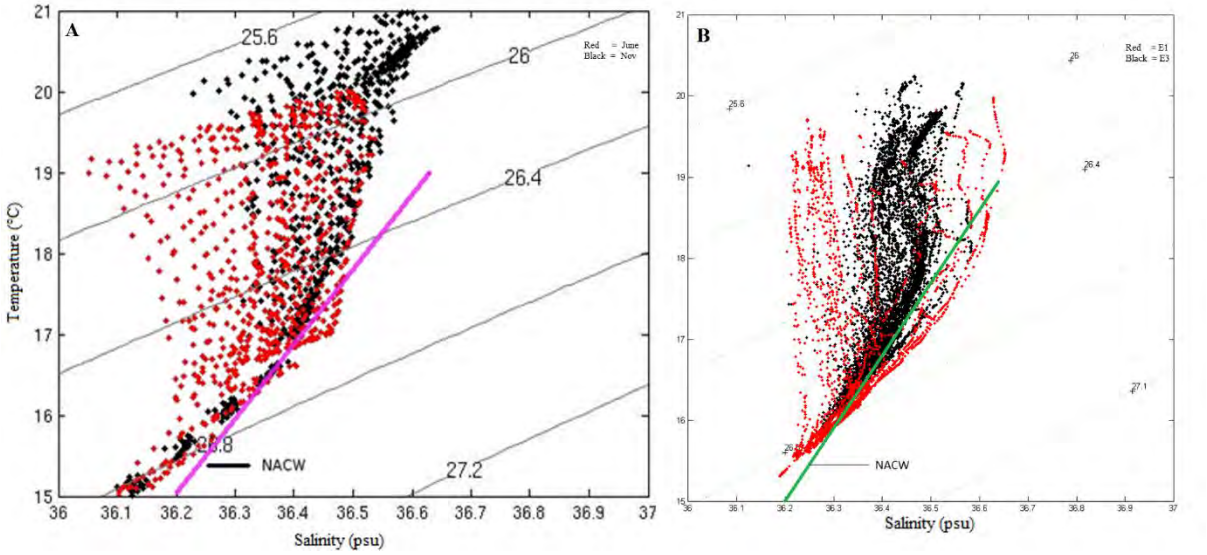

Figure 39: TS Plots. (a) WOA13 showing June in red and November in Black. (b) Epure cruises showing E1 in Red and E3 in Black.

distribution. In November the upwelling is weaker and so the water is slightly more saline. Insolation is stronger in November and we therefore observe higher temperatures in the plot.

The TS plot for the Epure cruises (Figure 39b) correspond to the WOA data. The data points in November are more saline due to weaker upwelling but of greater temperature due to insolation. Additionally the stronger upwelling in E1 shows less saline water that has been upwelled and warmed and therefore red data points are found to the left of the distribution. There are also some data points from June at the extreme right of the TS plot which can be attributed to cloud cover or insufficient insolation for those days which is consequence of the brief sampling period.

In both TS plots the upwelled water is NACW which is consistent with current literature and upwelling patterns for the MSR (Arísteguí *et al*., 2009).

Chapter Four: Conclusions and Future Outlook

4. Conclusion

The Epure mission showed coastal upwelling in both cruises with stronger upwelling in E1. The similar wind conditions prior to the cruises yielded similar coastal upwelling responses. The larger region sampled by E3 highlighted the enhanced upwelling off Cape Juby which is quasi-permanent due to the orientation of this portion of the coast which is aligned with the dominant wind direction. Furthermore, in both E1 and E3 insolation was hypothesized to explain why upwelling was not always clear closer to the surface.

The presence of a shelf break upwelling is exciting and sheds new light on the upwelling processes occurring in the MSR. In E1 the surface jet from the shelf break upwelling is hypothesized to connect with the jet at Cape Juby caused by the coastal upwelling. In E3 the surface jet associated with the shelf break upwelling was present but only just fell within the sampled region and therefore valid interpretations were not possible.

Hydrographic and velocity data can largely explain the processes occurring in the region but there are still small uncertainties in many of our interpretations. The presence of small and sub-mesoscale activity, presence of internal waves and temporal variation of the cruises made interpretations challenging but we feel our conclusions are strong despite these issues.

Considering that E1 and E3 offer only snapshots of summer and winter respectively we were still able to gain insights to seasonality. Climatological data showed stronger upwelling in summer (E1) and stronger insolation in winter (E3) which corresponded to our findings. Our TS plot also corresponds to climatological data where conditions in winter (E3) are slightly more saline due to weaker upwelling and warmer due to insolation.

To further understand the MSR future cruises should extend past the continental margin to capture data related to the shelf break upwelling. Additionally the characteristics of internal waves should be considered as they have the potential to increase mixing and spur productivity in the region.

References

Abbott, M. R. and Zion, P. M. 1985. Satellite observations of phytoplankton variability during an upwelling event. *Continental Shelf Research.* **4**(6): 661 – 680.

Alheit, J. and Bernal, P. 1993. Effects if physical and biological changes on the biomass yield of the Humbolt Current ecosystem. In: Large Marine Ecosystems, vol. V, *Stress, Mitigation and Sustainability.* (Eds) Sherman, K., Alexander, M and Gold, B. D. pp. 55 – 68. Am. Assoc. for the Adv. Of Science.

Arístegui, J., Tett, P., Hernández-Guerra, A., Basterretxea, G., Montero, M.F., Wild, K., Sangrá, P., Hernández-León, S., Cantón, J.A., García-Braun, Pacheco, M. and Barton, E.D. 1997. The influence of island-generated eddies on chlorophyll distribution: a study of mesoscale variation around Gran Canaria. *Deep-Sea Research Part I*. **44**: 71 – 96.

Arístegui, J., Barton, E.D., Tett, P., Montero, M.F., García-Munoz, M., Basterretxea, G., Cussatlegras, A.S., Ojeda, A. and de Armas, D. 2004. Variability in plankton community structure, metabolism, and vertical carbon fluxes along an upwelling filament (Cape Juby, NW Africa). *Process in Oceanography.* **62**: 95 – 113.

Arístegui, J., Barton, E.D., Álvarez-Salgado, X.A., Santos, A.M.P., Figueiras, F.G., Kifani, S., Hernández-León, S., Mason, E., Machú, E. and Demarq, H. 2009. Sub-regional ecosystem variability in the Canary Current upwelling. *Progress in Oceanography.* **83**: 33 – 48.

Bakun, A. 1990. Global climate change and the intensification of coastal upwelling. *Science*. **247**(4939): 198 – 201.

Barnes, S. L. 1973. Mesoscale objective map analysis using weighting time-series observations. NOAA Tech. Memo. ERL NSSL-62. U. S. Department of Commerc, pg. 60.

Barton, E.D. 1987. Meanders, eddies and intrusions in the thermohaline front off northwest Africa. *Oceanologica acta*. **10**(3): 267 – 283.

Barton, E.D. 1989. The Poleward undercurrent on the Eastern Boundary of the Subtropical North Atlantic. In: Neshyba, S.J., Mooers, C.N.K., Smith, R.L., Barber, R.T. (Eds). *Poleward Flows Along the Eastern Boundaries*. Springer: New York, pp. 82 – 95.

Barton, E.D., Arístegui, J., Tett, P., Cantón, M., García-Braun, J., Hernández-León, S., Nykjaer, L., Almeida, C., Almunia, J., Ballesteros, S., Basterretxea, G., Escánez, J., García-Weill, L., Hernández-Guerra, A., López-Laatzen, F., Molina, R., Montero, M.F., Navarro-Pérez, E., Rodríguez, J.M., van Lenning, K., Vélez, H. and Wild, K. 1998. The transition zone of the Canary Current upwelling Region. *Progress in Oceanography.* **41**(4): 455 – 504.

Barton, E.D., Arístegui, J., Tett, P. and Pérez, E.N. 2004. Variability in the Canary Islands area of filament-eddy exchanges. *Progress in Oceanography*. **62**: 71 – 94.

Barton, E.D., Field, D.B. and Roy, C. 2013. Canary current upwelling: More or less? *Progress in Oceanography*. **116**: 167 – 178.

Batteen, M. L. 1997. Wind-forced modeling studies of currents, meanders and eddies in the California Current System. *J. Geophys. Res.* **102**: 985 – 1009.

Batteen, M.L., Martinho, A.S., Miller, H.A. and McClean, J.L. 2007. A process-oriented modeling study of the coastal and Iberian Current system. *Ocean Modelling*. **18**: 1 -36.

Belkin, I.M. 2009. Rapid warming of large marine ecosystems. *Progress in Oceanography*. **81**: 207 – 213.

Brink, K. H. 1983. The near-surface dynamics of coastal upwelling. *Progress in Oceanography.* **12**(3): 223 – 257.

Charney, J. G. 1947. The dynamics of long waves in a baroclinic westerly current. *J. Meteor.* **4**: 1040 – 1053.

Chavez, F. P. and Messié, M. 2009. A comparison of Eastern Boundary Upwelling Ecosystems. *Progress in Oceanography*. **83**: 80 – 96.

Cruzado, A. and Salat, J. 1981. Interaction between the Canary Current and the bottom topograpgy. *Coastal Upwelling*. **1**: 167 – 175.

Djordjevic, V. D. and Redekopp. L. G. 1978. The fission disintegration of internal solitary waves moving over two-dimensional topography. **8**: 1016 – 1024.

Eady, E. T. 1949. Long waves and cyclone waves. *Tellus*. **1**: 33 – 52.

Ekman, V. W. 1905. On the influence of the earth's rotation on ocean currents. *Arkiv f. Matematik, Astronomi, och Fysik.* **2**(11): 1 – 52.

Epure. 2015. Élements trace métalliques, pollution, upwelling et ressources. [Online]. Available: http://www-iuem.univ-brest.fr/epure. Accessed: 20 February 2015.

Flament, P., Armi, L. and Washburn, L. 1985. The evolving structure of an upwelling filament. *Journal of Geophysical Research: Oceans (1978 – 2012).* **90**(C6): 11765 – 11778.

Garrett, C. J. R. and Munk, W. H. 1972. Ocean mixing by breaking internal waves. *Deep sea Research*. **19**: 823 – 832.

Gordon, H. R. and Clark, D. K. 1981. Clear water radiances for atmospheric correction of coastal zone color scanner imagery. *Applied Optics.* **20**(24): 4175 – 4180.

Gregg, M. C., D'Asaro, E. A., Shay, T. J. and Larson, N. 1985. Observations of Persistent Mixing and Near-Intertial Inernal Waves. *Journal of Physical Oceanography.* **16**: 856 – 885.

Haidvogel, D. B., Beckmann, A. and Hedström. K. S. 1991. Dynamic simulations of filament formation and evolution in the coastal transition zone. *Journal of Geophysical Research: Oceans (1978 – 2012).* **96**(C8): 15017 – 15040.

Hernández-Guerra, A., Machín, A., Antoranz, A., Cisneros-Aguirre, J., Gordo, C., Marrero-Díaz, A., Martínez, A., Ratismandresy, A.W., Rodríguez-Santana, A., Sangrá, P., López-Laatzen, F., Parrilla, G. and Pelegrí. 2002. Temporal variability of mass transport in the Canary Current. *Deep Sea Research II.* **49**: 3415 – 3426.

Hernández-León, S., Almeida, C., Portillo-Hahnefeld, Gómez, M., Rodríguez, J.M. and Arístegui, J. 2002. Zooplankton biomass and indices of feeding and metabolism in relation to an upwelling filament off northwest Africa. *Journal of Marine Research.* **60**: 346 – 327.

Huyer, A. 1976. A comparison of upwelling events in two locations: Oregon and North-West Africa. *Journal of Marine Research.* **34**: 531 – 546.

Ikeda, M., Johannessen, J. A., Lygre, K. and Sandven, S. 1989. A process study of mesoscale meanders and eddies in the Norwegian Coastal Current. *Journal of Physical Oceanography.* **19**(1): 20 – 35.

Ikeda, M. and Emery, W.J. 1984. Satellite observations and modeling of meanders in the California Current system off Oregon and Northern California. *Journal of Physical Oceanography.* **14**: 1434 – 1450.

Jackson, C. R., da Silva, J. C. B. and Jeans, G. 2012. The generation of nonlinear internal waves. *Oceanography.* **25**(2): 108 – 123.

James, I. N. 1987. Suppression of baroclinic instability in horizontally sheared flows. *Journal of the Atmospheric Sciences.* **44**(24): 3710 – 3720.

Knoll, M., Hernández-Guerra, A., Lenz, B., López Laatzen, F., Machín, F., Müller, T.J. and Siedler, G. 2002. The Eastern Boundary Current system betzeen the Canary Islands and the African Coast. *Deep Sea Research II*. **49**: 3427 – 3440.

Kelly, K. 1986. The influence of winds and topography on sea surface temperature patters over the northern California slope. *Journal of Geophysical Research.* **90**: 11783 – 11798.

Lathuiliére, C., Echevin, V. and Lévy, M. 2008. Seasonal and intraseasonal surface chlorophyll-a variability along the northwest African coast. *Journal of Geophysical Research: Oceans (1978 – 2012).* **113**(C5).

Lathuilière, C., Echevin, V., Lévy, M . and Madec, G. 2010. On the role of mesoscale circulation on an idealized coastal upwelling ecosystem. *Journal of Geophysical Research.* **115**(C9).

Levitus, S., Antonov, J. and Boyner, R. 2005. Warming of the world ocean. *Geophysical Research Letters.* **32**(2).

Levitus, S., Antonov, J. I., Boyer, T. P., Locarnini, R. A., Garcia, H. E., and Mishonov, A. V. 2009. Global ocean heat content 1955 – 2008 in light of recently revealed instrumentation problems. *Geophysical Research Letters.* **36**(7).

Lévy, M. 2008. The modulation of biological production by oceanic mesoscale turbulence. *Transport and Mixing in Geophysical Flows.* Springer Berlin Heidelberg: 219 – 261.

Mason, E., Colas, F., Molemaler, J., Shchepetkin, A.F., Troupin, C., McWilliams, J.C. and Sangrà, P. 2011. Seasonal variability of the Canary Current: A numerical study. *Journal of Geophysical Research: Oceans (1978 – 2012).* **116**(C6).

MATLAB 8.1.0.604. 2000. The Mathworks Inc. Natick, MA.

McEwen, G. F. 1912. The distribution of ocean temperatures along the west coast of north America deduced from Ekman's Theory of the upwelling of cold water from the adjacent ocean depths. With 21 Text-figures. *Internationale Revue der gesamten Hydrobiologie und Hydrograhpie*. **5**(2-3): 243 – 286.

McGregor, H., Fischer, H. and Mulitza, S. 2007. Rapid 20th-century increase in coastal upwelling off northwest Africa. *Science*. **315**: 637 – 639.

Meunier, T., Rossi, V., Morel, Y. and Carton, X. 2010. Influence of bottom topography on an upwelling current: Generation of long trapped filaments. *Ocean Modelling.* **35**(4): 277 – 303.

Meunier, T., Barton, E. D., Barreiro, B. and Torres, R. 2012. Upwelling filaments off Cap Blanc: Interaction of the NW African upwelling current and the Cape Verde frontal zone eddy field? *Journal of Geophysical Research*. **117**: C8.

Mittelstaedt, E. 1974. Some aspects of the circulation in the NW African upwelling area off Cap Blanc. *Tethys*. **6**: 89 – 92.

Mittelstadt, E., Pillsbury, D. and Smith, R. L. 1975. Flow patterns in the Northwest African upwelling area. *Deutsche Hydrografische Zeirschift.* **28**(4): 145 – 167.

Mittelstaedt, E. 1991. The ocean boundary along the African coast. Circulation and oceanographic properties at the sea surface. *Progress in Oceanography*. **26**(4): 307 – 455.

Mooers, C. N. K., Collins, C. A. and Smith, R. L. 1976. The dynamic structure of the frontal zone in the coastal upwelling region off Oregon. *Journal of Physical Oceanography.* **6**(1): 3 – 21.

Mooers, C.N.K. and Robinson, A.R. 1984. Turbulent jets and eddies in the California current and inferred cross-shore transports. *Science*. **223**: 51 – 53.

MyOcean. 2015. About MyOcean. [Online]. Available: http://www.myocean.eu/web/2-about-myocean.php. Accessed: 20 February 2015.

Narayan, N., Paul, A., Mulitza, S. and Schulz, M. 2010. Trends in coastal upwelling intensity during the late 20th century. *Ocean Sciences*. **6**: 815 – 823.

Navarro-Pérez and Barton, E.D. 2001. Seasonal and interannual variability of the Canary Current. *Scientia Marina*. **65**: 205 – 213.

Neshyba, S. J., Mooers, C. N K., Smith, R. L. Barber, R. T. (Eds.), 1989. Poleward Flows Along the Eastern Ocean Boundaries. Springer, New York.

Nieto, K., Demarq, H. and McClatchie, S. 2012. Mesoscale frontal structures in the Canary Upwelling System: New front and filament detection algorithms. *Remote Sensing of Environment*. **123**: 339 – 346.

Ocean Instruments. 2015. Acoustic Doppler Current Profiler (ADCP). [Online]. Available: http://www.whoi.edu/instruments/viewInstrument.do?id=819. Accessed: 20 February 2015.

Osborne, A. R. and Burch, T. L. 1980. Internal solitons in the Andaman sea. *Science.* **208**(4443): 451 – 460.

Pardo, P.D., Padín, X.A., Gilcoto, M., Farina-Busto, L. and Pérez, F.F. 2011. Evolution of upwelling sytems coupled to the long term variability in sea surface temperature and Ekman transport. *Climate Research*. **48**: 231 – 246.

Pelegrí, J.L., Marrero-Díaz, A., Ratsimandresy, A., Antoranz, A., Cisneros-Aguirre, J., Gordo, C., Grisolía, D., Hernándew-Guerra, A., Láiz, I., Martínez, A., Parilla, G., Pérez-Rodríguez, P., Rodríguez-Santana, A. and Sangrà, P. 2005. Hydrographic cruises off northwest Africa: the Canary Current and the Cape Ghir Region. *Journal of Marine Systems.* **54**: 39 – 63.

Quéro, J.C., Du Buit, M.H. and Vayne, J.J. 1998. Les observations de poisons tropicaux et le réchauffement des eaux dans l'Atlantique européen. *Ocenanologica Acta*. **21**(2) : 345 – 351.

Rattray, M. 1960. On the coastal generation of internal tides. *Tellus*. **12** : 54 – 62.

Reid, J.L. and Schwartzlose, R.A. 1962. Direct measurements of the Davidson Current of Central California. *Journal of Geophysicsal Research.* **67** : 2491 – 2497.

Rodríguez, J.M., Hernández-Leon, S. and Barton, E.D. 1999. Mesoscale distributions of fish larvae in relation to an upwelling filament off Northwest Africa. *Deep-Sea Research Part I.* **46**: 1969 – 1984.

Rossi, V., Morel, Y. and Garçon, V. 2010. Effect of the wind on the shelf dynamics : Formation of a secondary upwelling along the continental margin. *Ocean Modelling.* **31** : 51 – 79.

Ryther, J.H. 1969. Photosynthesis and fish production in the sea. *Science*. **166**: 72 – 76.

Salat, J. and Font, J. 1977. Internal waves off north-west Africa. In: Nihoul, J.C.J. (Ed). *Bottom Turbulence*. Amsterdam: Elsevier. 269 – 274.

Siesser, W. G. 1980. Late Miocene origin of the Benguela upwelling system off northern Namibia. *Science.* **208**(4441): 283 – 285.

Stark, J.D., Donlon, C. J., Martin, M. J., McColloch, M. E. 2007. OSTIA: An operational, high resolution,, real tile, global sea surface temperature analysis system. In: Oceans '07 IEEE Aberdeen, Conference Proceedings. Marine Challenges: Coastline to Deep Sea. Aberdeen, Scotland.

Stevens, I. and Johnson, J. 2003. A numerical modelling study of upwelling filaments off the NW African coast. *Oceanologica acta.* **26**: 549 – 564.

Stommel, H. and Fedorov, K. N. 1967. Small scale structure in temperature and salinity near Timor and Mindanao. *Tellus*. **19**: 306 – 325.

Stramma, L. and Siedler. 1988. Seasonal changes in the North Atlantic Subtropical Gyre. *Journal of Geophysical Research*. **93**(C7): 8111 – 8118.

Strub, P.T., Kosro, P.M. and Huyer, A. 1991. The nature of cold filaments in the California current system. *Jounral of Geophysical Research.* **96**: 14734 – 14768.

Strub, P.T., Combes, V., Shillington, F.A. and Pizarro, O. 2013. Currents and Processes along the Eastern Boundaries. In: Siedler, G., Griffies, S., Gould, J. and Church, J.A. (Eds). *Ocean Circulation and Climate – A 21st Century Perspect ive*. Oxford: Elsevier, Chapter 14: 33 - 374.

Thorade, H. 1909. Uber die Kalifornische Meeresströmung. *Hydrog. U. Marit. Met Ann.* **37**: 17 – 34.

Traganza, E. D., Nestor, D. A. and McDonald, A. K. 1980. Satelite observations of a nutrient upwelling off the coast of California. *Journal of Geographic Research: Oceans (1978 – 2012).* **85**(C7): 4101 – 4106.

Troupin, C., Mason, E., Beckers, J.M. and Sangrà, P. 2012. Generation of the Cape Ghir upwelling filament: A numerical study. *Ocean Modelling*. **41**: 1 – 15.

Warren, B. A. 1990. Book review of Poleward flows along eastern ocean boundaries. *Limnology and Oceanography.* **9**: 945 – 961.

Woods, J. D. 1968. Wave induced shear instability in the summer thermocline. *Journal of Fluid Mechanics.* **32**: 791 – 800.

Woods Hole Science Centre. 1998. Matlab Tools for Oceanographic Analysis. [Online]. Available: http://woodshole.er.usgs.gov/operations/sea-mat/. [Last Accessed: 9 February 2015].

Wooster, W.S., Bakun, A. and Mclain, D.R. 1976. The seasonal upwelling cycle along the eastern boundary of the North Atlantic. *Journal of Marine Research.* **34**: 131 – 140.

World Ocean Atlas. 2013. World Ocean Atlas 2013. [Online]. Available: https://www.nodc.noaa.gov/OC5/woa13/. Accessed: 20 February 2015.